

SESA 6071

Spacecraft Propulsion

Author: Yusaf Sultan
Lecturer: Charlie Ryan
Word Count: 17868

Contents

Definitions	10
1. Lecture 1	11
1.1. What is Rocket Propulsion ?	11
1.2. Rocket Propulsion Family Tree	11
1.2.1. Chemical Rockets	11
1.2.2. Electric Rockets	11
1.2.3. Nuclear Rockets	12
1.2.4. Solar and Laser Rockets	12
1.2.5. Solar Sails	12
1.3. Rocket Propulsion Applications	12
2. Lecture 2	13
2.1. Definitions and Fundamentals	13
2.2. Maximum Chemical Performance	14
2.3. Comparative Electric Performance	15
2.4. Nuclear Performance	16
2.5. Definitions and Fundamentals Cont.	16
2.6. Thrust Fundamentals	18
2.7. Tsiolkovsky Rocket Equation	19
3. Lecture 3	21
3.1. Rocket Staging	21
3.2. Launch Vehicle Dynamics	22
3.3. Converging Diverging Nozzle	23
3.4. Exit Velocity Equation	24
3.5. Mass Flow Rate Equation	26
4. Lecture 4	27
4.1. Nozzle Expansion Ratio Equation	27
4.2. Characteristic Velocity Equation	27
4.3. Thrust Equation	27
4.4. Coefficient of Thrust Equation	27
4.5. Summary of Equations	29
4.6. Equations Involving Mach Relations	29
4.7. Coefficient of Thrust for Converging Nozzles	30
4.8. Under, Ideal and Over Expanded Nozzles	31
4.8.1. Summerfield Criterion	32
5. Lecture 5	34
5.1. Nozzle Designs and the Perfect Nozzle	34
5.2. Conical Nozzles	34
5.3. Bell (Rao) Nozzles	35
5.4. Aerospike Nozzles	36
5.5. Expansion Deflection Nozzle	37
5.6. Intro to Liquid Propulsion	37
6. Lecture 6	38
6.1. Performance of Liquid Thrusters	38
6.2. Fuels	39
6.3. Overview of Monopropellant Thruster Systems	41
6.3.1. Decomposition of Hydrazine	41

6.3.2. Dangers of Hydrazine	43
6.3.3. Green Monopropellants: HAN	43
6.3.4. Green Monopropellants: ADN	43
6.3.5. Green Monopropellant: Hydrogen Peroxide	43
6.3.6. Comparison of Green Monopropellants and Downsides	44
6.4. Propellant Feed Mechanisms	44
6.4.1. Pump Driven Propellant Systems: Turbopumps	45
6.4.2. Pump Driven Propellant Systems: Open VS Closed Cycle	45
6.4.3. Open Cycle Pump Driven Propellant Systems: Gas Generator	46
6.4.4. Closed Cycle Pump Driven Propellant Systems: Staged Combustion ..	46
6.4.5. Closed Cycle Pump Driven Propellant Systems: Expander Cycle	47
6.4.6. Pump Driven Propellant Systems: Comparing cycles	47
6.4.7. Pump Driven Propellant Systems: Alternative Cycles	47
7. Lecture 7	49
7.1. Pressurized Propellant Feed Systems	49
7.1.1. Pressurized Propellant Feed Systems: Blow Down	49
7.1.2. Pressurized Propellant Feed Systems: Pressure Regulated	50
7.1.3. Pressurized Propellant Feed Systems: Bang Bang	50
7.2. Case Study: NASA Cassini Mission	50
7.3. Cold Gas Thrusters	52
8. Lecture 8	54
8.1. Intro to Solid Propulsion	54
8.2. Grain Shape and Thrust	54
8.3. Mass Flow and Burning Rates	55
8.3.1. Burning Effects: Burn Rate Exponent	55
8.3.2. Burning Effects: Plateau and Mesa Burning	55
8.3.3. Burning Effects: Ambient Temperature	56
8.3.4. Burning Effects: Erosive Burning	56
8.3.5. Burning Effects: Acceleration	57
8.3.6. Burning Effects: Metal Wires	57
8.4. Solid Propellants	58
8.4.1. Double Base	58
8.4.2. Composite	58
8.5. Solid Propellant Performance	59
8.6. Real Solid Propellant Makeup	60
8.7. Solid Propellant Flame Structure	60
8.8. Solid Rocket Ignition Systems	61
8.9. Hybrid rockets	61
8.9.1. Advantages of Hybrid Rockets	62
8.9.2. Disadvantages of Hybrid Rockets	62
9. Lecture 9	63
9.1. Hybrid Rocket Combustion	63
9.2. Hybrid Rocket Equations	64
9.3. Hybrid Rocket Propellents	64
9.4. Injectors	65
9.4.1. Orifice Injector	65
9.4.2. Spray Injectors	65
9.4.3. Pintle injectors	66

9.4.4. Orifice Pressure Drop	66
10. Lecture 10	67
10.1. Thrust Chambers	67
10.2. Thrust Chamber: Heat Transfer	67
10.2.1. Radiation Cooling	68
10.2.2. Regenerative Cooling	68
10.2.3. Film Cooling	69
10.2.4. Ablative cooling	69
10.3. Monopropellant Bed Loading	69
11. Lecture 11	71
11.1. Introduction to Electric Propulsion	71
11.1.1. Overview of Electrothermal Propulsion Systems	71
11.1.1.1. Overview of Resistojets	71
11.1.1.2. Overview of Arcjets	71
11.1.2. Overview of Electrostatic Propulsion Systems	72
11.1.2.1. Overview of Gridded Ion Thrusters	72
11.1.3. Overview of Electrospray Thrusters	72
11.1.4. Overview of Electromagnetic Propulsion Systems	72
11.1.4.1. Overview of Pulsed Plasma Thrusters	73
11.1.4.2. Overview of Magneto Plasma Thrusters (MPDs)	73
11.2. Overview of Hall Effect Thrusters	73
11.3. Electric Propulsion Performance	74
11.4. Why Electric Propulsion ?	75
11.5. Uses of Electric Propulsion	75
12. Lecture 12	76
12.1. History of Electric Propulsion	76
12.2. Use of EP in Spacecraft	76
12.3. EP Use-cases and Requirements	77
12.3.1. GEO Orbit Raising	77
12.3.2. LEO Orbit Raising	77
12.3.3. Applicable Thrusters for Orbit Raising	77
12.3.4. LEO and GEO Station Keeping	78
12.3.5. Applicable Thrusters for Station Keeping	79
12.3.6. Interplanetary Missions	79
12.3.7. Applicable Thrusters for Interplanetary Missions	80
12.4. Derivation of an Electric Thruster Rocket Equation	80
13. Lecture 13	82
13.1. Introduction to Plasma	82
13.2. Debye Length	82
14. Lecture 14	83
14.1. Charged Particle Motion in Magnetic Fields	83
14.2. Charged Particle Motion in Electric Fields	83
14.3. Charged Particle Motion in Magnetic and Electric Fields	84
14.4. Magnetic Mirroring	85
14.5. Working Principle Behind Hall Effect Thrusters	85
14.6. HET Performance and Improvement Areas	86
14.7. HET Lifetime and Magnetic Shielding	87
14.8. HET Propellants	87

15. Lecture 15	88
15.1. Calculating Larmor Radii in HETs	88
15.2. Hall Effect	88
16. Lecture 16	89
16.1. Electromagnetic and Electrostatic Thruster Thrust	89
16.1.1. Efficiency Parameters	89
16.2. Electromagnetic and Electrostatic Real Thruster Thrust	89
16.3. Electromagnetic and Electrostatic Thruster I_{sp} and Efficiency Terms	90
16.4. Electromagnetic and Electrostatic Thruster Efficiencies	90
16.5. Difficulties in Estimating HET Performance	91
16.6. Closing Remarks on HETs	92
16.7. Magnetoplasmadynamic (MPD) Thrusters	92
16.8. Pulsed Plasma Thrusters	94
16.9. Into to Electrostatic Propulsion	95
16.10. Radiofrequency Ion Thruster	95
16.11. Microwave Ion Thrusters	96
16.12. Electron Bombardment Ion Thruster	97
16.13. Ion Thruster Grids	97
17. Lecture 17	98
17.1. Ignition of Radiofrequency Ion thrusters	98
18. Lecture 18	99
18.1. Space Charge Limitations	99
18.2. Grid Erosion and Charge Exchange Ions	100
18.3. Closing Remarks on GITs	100
18.4. Heated Filament	101
18.5. Hollow Cathodes	101
18.6. Alternative Electron Sources	103
19. Lecture 19	104
19.1. FEEP and Electrospray Thrusters	104
19.1.1. Electrospray Thrusters	104
19.2. FEEP and Electrospray Onset Voltage	105
19.3. FEEP and Electrospray Performance, Uses and Drawbacks	106

List of Weeks

Week 1	11
Week 2	23
Week 3	37
Week 4	54
Week 5	65
Week 6	71
Week 7	82
Week 8	88
Week 9	95

List of Figures

Figure 1	Flowchart of the rocket propulsion family tree	11
Figure 2	Calculations for maximum chemical rocket engine performance	15
Figure 3	Basic principle of an electrostatic propulsion system.	15
Figure 4	Comparative electrical propulsion system voltage calculations.	16
Figure 5	Maximum nuclear thermal propulsive system performance.	16
Figure 6	Variation of spacecraft acceleration against performance.	18
Figure 7	Plot of ΔV against M_0/M_f	20
Figure 8	Plot depicting the effect of staging on the ΔV for a given payload fraction.	22
Figure 9	Plot illustrating the forces present on a launch vehicle.	22
Figure 10	Plot of pressure, temperature, velocity and Mach number over a De-Laval nozzle.	24
Figure 11	Plot of exit velocity for increasing P_e/P_c ratios [Left], Plot of exit velocity for increasing k ratios [Right]	25
Figure 12	Plot of C_F against area and pressure ratios	28
Figure 13	Plot of C_F against area ratio for varying pressure ratios	28
Figure 14	Plot of C_F against exit Mach number for varying pressure ratios	30
Figure 15	Plot of $C_F/C_F \text{Converging}$ against exit area ratio for varying pressure ratios	31
Figure 16	Under-expanded flow out of a nozzle	31
Figure 17	Over-expanded flow out of a nozzle	32
Figure 18	Plot of C_F against pressure ratio and area ratio	32
Figure 19	Plot of $C_F/C_F \text{Converging}$ against exit area ratio for varying pressure ratios with summerfield criterion and ideal expansion line.	33
Figure 20	Various nozzle designs.	34
Figure 21	Definitions for a conical nozzle	34
Figure 22	Bell nozzle dimensions.	35
Figure 23	Bell curves for various values of η_{Bell}	36
Figure 24	$\dot{m}_{\text{ox}}/\dot{m}_{\text{fuel}}$ against I_{sp} for different rocket engines.	38
Figure 25	System engineering diagram of a monopropellant thruster system [Left], real schematic of a monopropellant thruster [Right]	41
Figure 26	Decomposition reaction of hydrazine.	41
Figure 27	Thermal breakdown of ammonia.	42
Figure 28	Full decomposition reaction for hydrazine.	42
Figure 29	Performance parameters throughout a hydrazine decomposition reaction.	42
Figure 30	Hazard symbols associated with hydrazine (1.flammable 2.corrosive 3.acutely toxic 4.serious health hazard 5.hazardous to the environment)	43
Figure 31	Chemical formula [Left] and chemical structure [right] of HAN.	43
Figure 32	Chemical formula [Left] and chemical structure [right] of ADN.	43
Figure 33	Pressure driven feed system [Left], pump driven feed system [Right]	44
Figure 34	Spacecraft turbopump.	45
Figure 35	Open cycle propellant feed system [Left], closed cycle propellant feed system [Right].	45
Figure 36	A system level image of a open cycle, gas generator, pump driven propulsion system.	46
Figure 37	A system level image of a closed cycle, staged combustion, pump driven propulsion system.	46

Figure 38	A system level image of a closed cycle, expander cycle, pump driven propulsion system.	47
Figure 39	Comparison of different pump driven rocket engines.	47
Figure 40	Battery powered propellant feed system schematic [Left], Rutherford engine which uses batter powered propellant feed system [Right].	48
Figure 41	System level diagram of a pressure fed propellant system.	49
Figure 42	System level diagram of a blow down feed system [Left], thrust and pressure over time for a blow down system [Right].	49
Figure 43	System level diagram of a pressure regulated feed system [Left], thrust and pressure over time for a pressure regulated system [Right].	50
Figure 44	System level diagram of a bang bang feed system [Left], thrust and pressure over time for a bang bang system [Right].	50
Figure 45	Labelled diagram of the Cassini probe [Left], labelled diagram of the propellant tanks and thrusters for Cassini [Right]	51
Figure 46	Cassini propellent dellivery schematic.	51
Figure 47	Cassini propulsive events.	52
Figure 48	Constituent parts of a SRB.	54
Figure 49	Effect of grain shape on the thrust profile.	54
Figure 50	How changing n effects the burn rate.	55
Figure 51	Mesa and Plateau burning.	56
Figure 52	Effect of ambient temperature on thrust curve.	56
Figure 53	Diagram depicting erosive burning [Left], thrust graph overtime with and without erosive burning [Right].	57
Figure 54	Diagram depicting burning under rotational velocity [Left], thrust graph overtime at various angular velocities. [Right].	57
Figure 55	Diagram depicting the effect of lateral acceleration on a block grain.	57
Figure 56	Molecular structure and chemical formula for nitroglycerin [Left], molecular structure and chemical formula for nitrocellulose [Right].	58
Figure 57	Performance against burn rate for different solid rocket propellents [Left], solid composite fuel performance [Right].	59
Figure 58	Double base fuel flame structure [Top Left], Composite fuel flame structure [Top Right], Real double base flame [Bottom Left], Real composite flame structure [Bottom Right]	60
Figure 59	Pyrotechnic ignitor [Left], pyrogenic ignitor [Right]	61
Figure 60	System level diagram of a hybrid solid rocket motor.	62
Figure 61	Combustion for hybrid rockets.	63
Figure 62	Plot of oxidizer flow rate against fuel regression rate.	63
Figure 63	Image of an orifice injector.	65
Figure 64	Image of a spray injector.	65
Figure 65	Image of a pintle injector.	66
Figure 66	Thrust chamber dimensions.	67
Figure 67	Temperature variation over a nozzle.	68
Figure 68	Cross sectional schematic of a nozzle with regenerative cooling.	68
Figure 69	Temperature and stress variation across the nozzle wall of a regenerativly cooled engine.	68
Figure 70	Film cooling employed	69
Figure 71	Ablative cooling on a solid rocket motor's nozzle and thrust chamber	69
Figure 72	Schematic diagram of a Resistojet.	71

Figure 73	Schematic diagram of a Arcjet.	71
Figure 74	Schematic diagram of a gridded ion thruster.	72
Figure 75	Schematic diagram of a electrospray thruster.	72
Figure 76	Schematic diagram of a pulsed plasma thruster.	73
Figure 77	Schematic diagram of an MPD thruster.	73
Figure 78	Schematic diagram of a Hall effect thruster.	74
Figure 79	Cumulative number of satellites from 1964 - 2020.	76
Figure 80	Plot of thrust per power against impulse for different electric thrusters, including low TRL and envelope for orbit raising.	78
Figure 81	Plot showing which electric thrusters are used for orbit raising over time.	78
Figure 82	Plot of thrust per power against impulse for different electric thrusters, including low TRL and envelope for station keeping.	79
Figure 83	Plot of thrust per power against impulse for different electric thrusters, including low TRL and envelope for interplanetary missions.	80
Figure 84	Plot of normalized ΔV against normalized exhaust velocities.	81
Figure 85	Figure of potential applied across a plasma with a plot of teh potential difference against the distance away from the anode/cathode.	82
Figure 86	Path taken by an ion and electron in a magnetic and electric field.	84
Figure 87	Path taken by an ion and electron in a non-constant magnetic.	84
Figure 88	Magnetic mirroring.	85
Figure 89	Basic componenets of a Hall Effect thruster.	85
Figure 90	Simulated movement of electrons in a hall effect thruster.	86
Figure 91	Erosion rate of HET near at the mouth.	87
Figure 92	Magnetic shielding implemented on a HET with teh new and old erosion rates.	87
Figure 93	HET propellant performance	87
Figure 94	Plot of discharge loss against mass utilization efficiency.	91
Figure 95	Plot of voltage applied across a HET	91
Figure 96	Image of the anatomy of a MPD thruster.	92
Figure 97	Image of a self field MPD vs an applied field MPD.	93
Figure 98	Schematic image of a PPT.	94
Figure 99	Schematic image of a RIT.	95
Figure 100	Schematic image of a Microwave Ion Thruster.	96
Figure 101	Schematic image of an electron bombardment ion thruster.	97
Figure 102	Plot of electron collision probability against pressure.	98
Figure 103	Plot of voltage over distance for space charge limited case.	99
Figure 104	Image of barrel and pit and groove erosion.	100
Figure 105	Schematic image of a hollow cathode.	101
Figure 106	Work function vs temp for different hollow cathode insert materials.	102
Figure 107	Schematic diagram of a FEEP or electrospray type thruster.	104
Figure 108	Diagram of the formation of a Taylor cone.	104
Figure 109	Different types of electrospray thrusters.	105

List of Tables

Table 1	Typical values of I_{sp}	14
---------	----------------------------	----

Table 2	Respective bond energies of reactants and products in combustion.	14
Table 3	Typical ΔV values for different manoeuvre	21
Table 4	Typical liquid propellant parameters.	37
Table 5	Data on common liquid fuels and oxidizers	39
Table 6	Performance parameters for different fuel and oxidizer combinations.	41
Table 7	Performance of hydrazine vs green monopropellants	44
Table 8	Theoretical performance of different cold gas propellant	52
Table 9	Real performance of different cold gas propellant	53
Table 10	Common solid composite fuels, oxidizers and binders	58
Table 11	Makeup of different solid rocket fuels.	60
Table 12	Comparative performance of liquid bipropellant, solid and hybrid rockets.	62
Table 13	Comparative performance of different electrical propulsion systems.	74
Table 14	HET vs GIT performance.	86
Table 15	MPD vs HET vs GIT performance.	93
Table 16	PPT performance.	94
Table 17	PPT performance.	102
Table 18	Onset voltages for different fuel types.	106
Table 19	Onset voltages for different fuel types.	106

Definitions

I_t	Total Impulse (Ns)	I_{sp}	Specific Impulse (s)
F	Rocket Thrust (N)	g_0	Standard Gravitational Accel (m/s^2)
\dot{m}	Propellant mass flow rate (kg/s)	m_p	Expelled propellant mass (kg)
c	Effective exhaust velocity (m/s)	η_T	Power Conversion Efficiency
P_{in}	Input Power (W)	m	Spacecraft or launch vehicle mass (kg)
α	Specific power plant mass (kg/W)	M_{pow}	Power plant mass (kg)
v_e	Exhaust velocity (m/s)	P_e	Exhaust pressure (Pa)
P_a	Atmospheric pressure (Pa)	A_e	Exhaust area (m^2)
c^*	Characteristic velocity (m/s)	P_c	Chamber pressure (Pa)
A_t	Throat area (m^2)	M	Mass fraction
M_0	Initial mass (kg)	M_P	Propellant mass (kg)
M_f	Fuel mass (kg)	ΔV	Change in velocity (m/s)
α	Angle of attack ($^\circ$ or rad)	δ	Gimbal angle ($^\circ$ or rad)
γ	Flight path angle ($^\circ$ or rad)	θ	Pitch angle ($^\circ$ or rad)
D	Drag (N)	c_p	Specific heat at a constant pressure (J/kgK)
c_v	Specific heat at a constant volume (J/kgK)	θ	Pitch angle ($^\circ$ or rad)
D	Drag (N)	c_p	Specific heat at a constant pressure (J/kgK)
C_F	Coefficient of thrust	h	Enthalpy (J/ mol)
k	Ratio or specific heats		

1. Lecture 1

1.1. What is Rocket Propulsion ?

Propulsion itself is the **act of changing the motion of a body**, typically by using newtons third law and it can be classified in various types of ways. A more colloquial way of defining rocket propulsion is as **mass drivers**, throwing out mass one way to yield an acceleration in the other.

1.2. Rocket Propulsion Family Tree

In **Figure 1** the rocket propulsion types are grouped by the energy source.

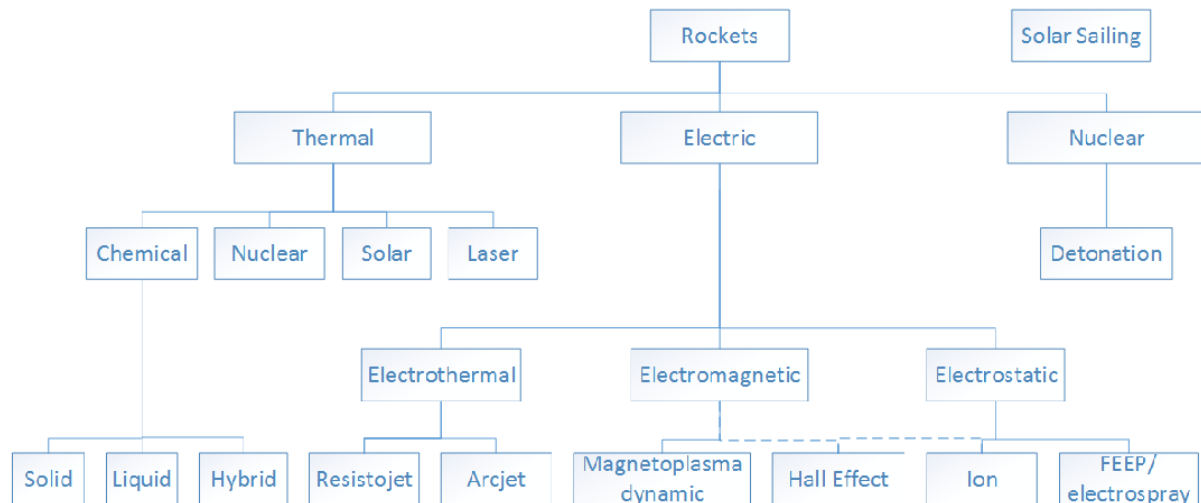


Figure 1: Flowchart of the rocket propulsion family tree

1.2.1. Chemical Rockets

These utilize either a chemical reaction or decomposition to generate energy. Gas is heated to between **700°C - 1300°C** and to speeds between **1.5 km/s - 4.5 km/s**. These require a **fuel and oxidizer** and come in the following types:

- **Solid:** Fuel and oxidizer mixed within into a solid grain which cannot stop burning once ignited. feature **high thrust with low performance**.
- **Liquid:** Burn a liquid fuel and oxidizer allowing for repeated firings and variable thrust. Feature **high performance and thrust with high complexity**.
- **Hybrid:** Have a liquid oxidizer but a solid fuel allowing for better performance than solid with lower complexity.

1.2.2. Electric Rockets

These use electrical energy to generate thrust without utilizing combustion. Typically have very high exhaust velocities ($\sim 60,000 \text{ m/s}$) and therefore **very high performance** at the costs of **high complexities and very low thrust**. The four distinct groups are:

- **Electrothermal:** Uses electrical energy to heat a propellant (Resistojet). Are **simple to build** at the cost of **low thrust**.
- **Electrostatic:** Uses electrical energy to accelerate ionized fuel across an electric fields. Feature **good performance** at the cost of **being expensive and low thrust**.
- **Electromagnetic:** Accelerates an ionized fuel using a magnetic field. Fall issue to **low efficiency unless power input is high**.
- **Hall Effect Thruster:** Uses a mixture of both electrostatic and electromagnetic propulsion methods to accelerate propellant. These are the most **commonly used**.

1.2.3. Nuclear Rockets

Broadly speaking there are two types of nuclear rockets, these are:

- **Nuclear Detonation:** Use the shockwave produced when nuclear bombs are detonated to produce thrust (Orion Drive). **High performance and thrust** but are **very dangerous and have limited testing**.
- **Nuclear Thermal:** Uses the heat energy produced during nuclear fission to heat a propellant (typically hydrogen) which is then exhausted. These have **high performance and thrust** but are **dangerous and have limited testing**.

1.2.4. Solar and Laser Rockets

These systems use large diameter telescopes to focus in a laser or solar radiation to heat up a propellant. These systems feature **high theoretical performance and moderate thrust** but are **very complex and lack any real testing**.

1.2.5. Solar Sails

These systems use no propellant at all and instead produce thrust through the momentum gained when a photon is incident on the sail. These systems feature **good performance with no fuel** but fall victim to **low thrust and engineering complexity**.

1.3. Rocket Propulsion Applications

Instead of grouping together rocket propulsion methods using the energy source, the rocket application can also be used, for example:

- **High Thrust/Maneuverability:** Typically have the cost of **low performance** and use **chemical or solid** propulsion methods.
- **High Performance:** Typically have the cost of **low thrust** and use **electrical** propulsion methods.
- **Balanced Thrust and Performance:** Typically the middle ground is **nuclear thermal**.

2. Lecture 2

2.1. Definitions and Fundamentals

To develop an empirical measure of performance we should first consider **Eq. 1**.

$$I_t = \int_0^t F \, dt \quad (1)$$

Where:

- I_t : Total Impulse (Ns)
- F : Thrust Force (N)
- t : Burn Duration (s)

Note that for **Eq. 1**, if F is constant then the equation simplified to $I_t = Ft$. A more useful measure of performance for rocket engines is shown in **Eq. 2**.

$$I_{sp} = \frac{\int_0^t F \, dt}{g_0 \int_0^t \dot{m} \, dt} = \frac{I_t}{g_0 \int_0^t \dot{m} \, dt} \quad (2)$$

Where:

- I_{sp} : Specific Impulse (s)
- g_0 : Standard Gravitational Accel (m/s^2) = $9.81 \, m/s^2$
- \dot{m} : Propellant mass flow rate (kg/s)

There is no concrete reason on why g_0 is present in this equation, however one common theory is that it allows I_{sp} to be in seconds instead of featuring a length unit which would eliminate any error in conversion from metric to imperial. If F and \dot{m} are both constant over the t then **Eq. 2** simplifies to **Eq. 3**.

$$I_{sp} = \frac{I_t}{g_0 m_p} \quad (3)$$

Where:

- m_p : Expelled propellant mass (kg) = $\dot{m}t$

Another useful parameter for defining engine performance is shown in **Eq. 4**.

$$c = \frac{F}{\dot{m}} \quad (4)$$

Where:

- c : Effective exhaust velocity (m/s)

The exhaust velocity is called as such as the **velocity profile of the exhaust is not uniform**, this is most seen in chemical rockets due to the **no slip condition** but is slightly seen in electrical rockets too. Rearranging all of the previous equations together yields a definition for I_{sp} in terms of c .

$$I_{sp} = \frac{c}{g_0} \quad (5)$$

Typical I_{sp} values for the rocket engine types defined in the previous lecture are shown in **Table 1**.

Rocket Engine Type	$I_{sp}(s)$	Thrust (N)	Efficiency	Propellant
Chemical bi-propellant	200 - 450	$\leq 10MN$	0.8	Liquid or Solid Propellents
Chemical mono-propellant	150 - 250	0.03 - 100	0.9	N_2H_4
Thermal Nuclear Fission	500 - 860	$\leq 10MN$	0.5	H_2
Resistojet - electrothermal	150 - 350	0.01 - 10	0.4	N_2H_4 , NH_3 , H_2
Ion Thruster - electrostatic	1500-8000	$10^{-5} - 0.5$	0.65	Xe
Hall Effect Thruster	1500-2000	$10^{-5} - 2$	0.55	Xe

Table 1: Typical values of I_{sp}

2.2. Maximum Chemical Performance

A typical chemical reaction used in chemical rockets is combustion shown in **Eq. 6**.



Combustion as shown in **Eq. 6** is an exothermic reaction as the energy of the reactants is more than the energy of the products, allowing for an excess of energy after the reaction. To estimate an effective upper limit to the energy released during combustion, the bond energies shown in **Table 2** can be used.

Chemical	Bond Energy (kJ/mol)
H_2	436
O_2	498
H_2O	428
	498.7

Table 2: Respective bond energies of reactants and products in combustion.

Note that there are two bond energies in **Table 2** due to the OH and the OH - H bonds. The maximum energy can be calculated and are shown in **Figure 2**.

Energy Per Kilogram Released During Combustion

$$M_{Water} := 18.01528 \frac{gm}{mol} \quad BE_{H2} := 436 \frac{kJ}{mol} \quad BE_{O2} := 498 \frac{kJ}{mol}$$

$$BE_{OH} := 428 \frac{kJ}{mol} \quad BE_{OHH} := 498.7 \frac{kJ}{mol}$$

$$E_{kg} := \frac{(BE_{OH} + BE_{OHH}) - \left(BE_{H2} + \frac{BE_{O2}}{2} \right)}{M_{Water}} = 13416388.75 \frac{J}{kg}$$

Maximum Chemical Performance

$$\eta := 0.9 \quad g_0 := 9.81 \frac{m}{s^2}$$

$$c := \sqrt{2 \eta \cdot E_{kg}} = 4914.21 \frac{m}{s} \quad I_{sp} := \frac{c}{g_0} = 500.94 \text{ s}$$

Figure 2: Calculations for maximum chemical rocket engine performance

Note that in this calculation, the bond energy of oxygen is halved as per [Eq. 6](#) and the equation for effective exhaust velocity comes from the kinetic energy equation and noting that $E_{kg} = Energy/mass$.

2.3. Comparative Electric Performance

To compare the efficiency of chemical propulsion to electric propulsion consider an electrostatic propulsion system shown in [Figure 3](#).

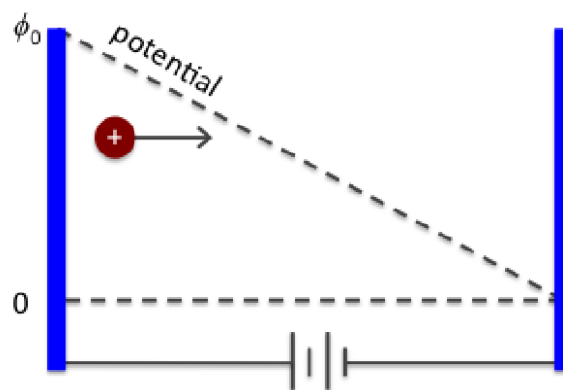


Figure 3: Basic principle of an electrostatic propulsion system.

A charged ion (assumed for these calculations to be a water ion) enters an electric field which causes it to be accelerated to the more negative (lower potential plate). By setting the electric potential energy gained by the ion equal to the kinetic energy ($\eta E_p = E_k$) then the I_{sp} can be calculated, shown in [Figure 4](#).

Voltage Required for an Isp of 500s Using Ionized Water

$$M_{Water} := 18.01528 \frac{gm}{mol} \quad \eta := 0.9 \quad g_0 := 9.81 \frac{m}{s^2} \quad N_a := 6.023 \cdot 10^{23} mol^{-1}$$

$$I_{sp} := 500 \text{ s} \quad q := 1.6 \cdot 10^{-19} C$$

$$V := \frac{\frac{1}{2} \frac{M_{Water}}{N_a} (I_{sp} \cdot g_0)^2}{\eta \cdot q} = 2.5 \text{ V}$$

Figure 4: Comparative electrical propulsion system voltage calculations.

As shown in **Figure 4** the voltage required to match the performance of a chemical system is very low and easily achievable, in reality electrostatic systems can achieve efficiencies in excess of 10,000s.

2.4. Nuclear Performance

To estimate the performance of a thermal nuclear rocket engine, Uranium-235 fission is considered, where the energy released in one fission event is immediately transferred to a water molecule, this calculation is shown in **Figure 5**.

Energy Transferred to One Water Molecule During One Nuclear Fission Event

$$E_{U235} := 180 \text{ MeV} = (2.88 \cdot 10^{-11}) J \quad M_{Water} := 18.01528 \frac{gm}{mol} \quad N_a := 6.023 \cdot 10^{23} mol^{-1}$$

$$m_{Water} := \frac{M_{Water}}{N_a} = 0 \text{ kg} \quad <- \text{ is } 2.99 \times 10^{-26} \text{ but is too small for mathcad to show}$$

$$E_{kg} := \frac{E_{U235}}{m_{Water}} = (9.63 \cdot 10^{14}) \frac{J}{kg}$$

Performance of a Nuclear Thermal System

$$\eta := 0.9 \quad g_0 := 9.81 \frac{m}{s^2}$$

$$c := \sqrt[2]{2 \eta \cdot E_{kg}} = 41631151.15 \frac{m}{s}$$

$$I_{sp} := \frac{c}{g_0} = (4.24 \cdot 10^6) \text{ s}$$

Figure 5: Maximum nuclear thermal propulsive system performance.

Note that this I_{sp} is a theoretical upper limit and in reality the true performance is much lower and is limited by material limits due to heat.

2.5. Definitions and Fundamentals Cont.

For propulsion systems, efficiency can be defined in terms of the fraction of source power that is converted to jet power, this efficiency is shown in **Eq. 7**.

$$\eta_T = \frac{\dot{m}c^2}{2P_{in}} \quad (7.1)$$

$$P_{in} = \frac{\dot{m}c^2}{2\eta_T} = \frac{Fc}{2\eta_T} \quad (7.2)$$

$$\frac{P_{in}}{m} = \frac{F}{m} \frac{c}{2\eta_T} = a \frac{c}{2\eta_T} \quad (7.3)$$

Where:

- η_T : Power conversion efficiency
- a : Acceleration (m/s^2)
- P_{in} : Input or Source power (W)
- m : Spacecraft mass (kg)

Note that for electrical systems P_{in} , the power must come from a source e.g., solar panel array. **Eq. 7** Also shows that **for a fixed specific power: ($\frac{P_{in}}{m}$) a high effective exhaust speed (c) means a low acceleration.** It is also useful to define a specific power plant mass as shown in **Eq. 8**.

$$\alpha = \frac{M_{pow}}{P_{in}} \quad (8)$$

Where:

- α : Specific power plant mass (kg/W)
- M_{pow} : Power plant mass (kg)

By manipulating equations **Eq. 8** and **Eq. 7**, as well as assuming that $\eta_T \approx 1$ and $M_{pow} \approx 0.1m$ then the acceleration can be written as **Eq. 9**.

$$a = \frac{0.2}{\alpha c} \quad \begin{cases} M_{pow} \approx 0.1m \\ \eta_T \approx 1 \end{cases} \quad (9)$$

Eq. 9 shows that a and c are inversely proportional from one another, meaning a high acceleration will typically mean a low effective exhaust velocity and vice versa. A showing how performance varies with acceleration is shown in **Figure 6**.

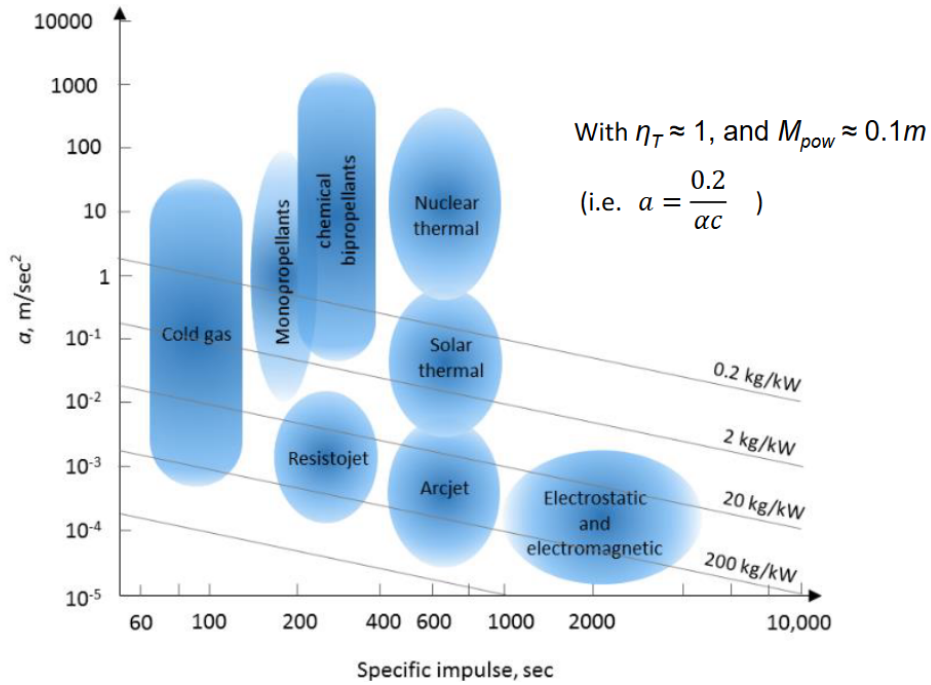


Figure 6: Variation of spacecraft acceleration against performance.

Note that for electrical propulsion systems shown in **Figure 6** a higher I_{sp} means a lower acceleration as $I_{sp} \propto c \propto \frac{1}{a}$. Different power sources have different values of α , for example:

- Nuclear Reactors $\Rightarrow 2\text{kg}/\text{kW}$
- Solar Panels $\Rightarrow 20\text{kg}/\text{kW}$
- RTGs $\Rightarrow 200\text{kg}/\text{kW}$

2.6. Thrust Fundamentals

By applying Newton's second law to a rocket nozzle, considering the difference in atmospheric and exhaust pressure as well as using the equations derived in the previous sections, **Eq. 10** can be derived.

$$F = \dot{m}v_e + (P_e - P_a)A_e \quad (10.1)$$

$$c = v_e + \frac{(P_e - P_a)A_e}{\dot{m}} \quad (10.2)$$

$$I_{sp} = \frac{1}{g_0} \left(v_e + \frac{(P_e - P_a)A_e}{\dot{m}} \right) \quad (10.3)$$

Where:

- v_e : Exhaust velocity (m/s)
- A_e : Exhaust Area (m^2)
- P_e : Exhaust Pressure (Pa)
- P_a : Atmospheric Pressure (Pa)

One key thing to note about **Eq. 10** is that the thrust is made up of two parts, the first part being the **momentum thrust** accounting for the majority of the thrust (90-70%) and the second part is the **pressure thrust** (10-30%).

Crucially, as $P_a(h)$ then the I_{sp} and c vary with the height, typically being lower at lower altitudes and increasing up and reaching their maximums in the thinner sections of the atmosphere.

Another impartial performance parameter for chemical rockets which does not depend on the altitude is shown in **Eq. 11**.

$$c^* = \frac{P_c A_t}{\dot{m}} \quad (11)$$

Where:

- c^* : Characteristic velocity (m/s)
- P_c : Chamber pressure (Pa)
- A_t : Throat area (m^2)

Typical values of c^* are 1500 m/s for a solid rocket and 2500 for H_2/O_2 liquid bi-propelled rocket.

2.7. Tsiolkovsky Rocket Equation

One way to represent the quantity of propellant to the structure of the rocket is by using the **propellant mass fraction** shown in **Eq. 12**.

$$\mu = \frac{M_P}{M_0} \quad (12)$$

Where:

- μ : Mass fraction
- M_P : Propellant mass (kg)
- M_0 : Structure Mass (kg)

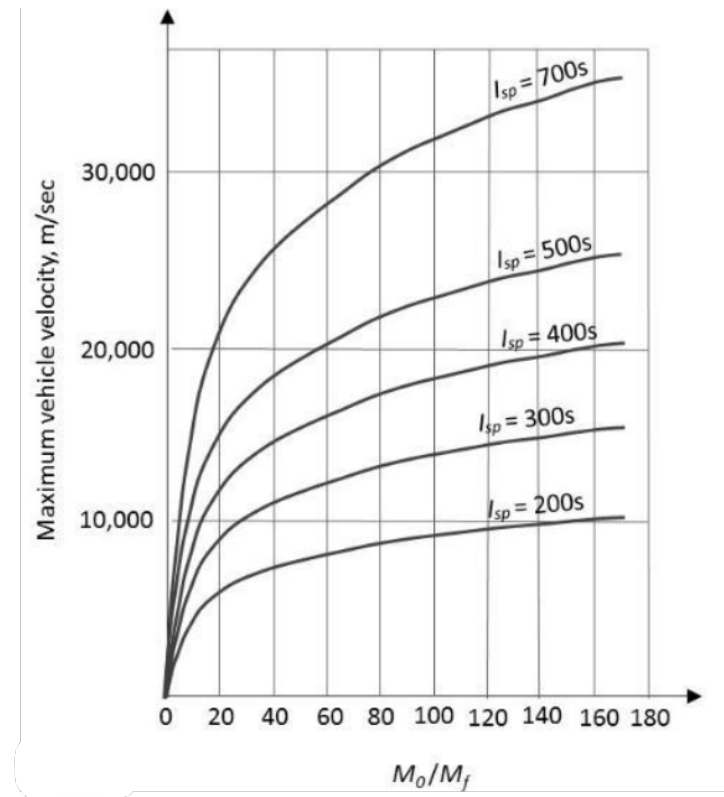
For a well designed rocket $\mu \approx 0.8 - 0.85$. The famous rocket equation is derived by starting with Newtons second law and considering the momentum of the fuel leaving the engine and integrating that equation, this yields .

$$\Delta V = c \ln \left(\frac{M_0}{M_f} \right) = I_{sp} g_0 \ln \left(\frac{M_0}{M_f} \right) \quad (13)$$

Where:

- ΔV : Change in velocity (m/s)
- M_f : Final mass (kg)

The ΔV and the M_0/M_f are plotted against one another in **Figure 7**. Note that for a single stage rocket $M_0/M_f \approx 20$ and the ΔV required to reach LEO is 9.5 km/s and so a single stage to rocket is on the boundary of being possible using a chemical bi-propellant rocket.

Figure 7: Plot of ΔV against M_0/M_f

3. Lecture 3

3.1. Rocket Staging

The typical ΔV s required for different manoeuvre are shown in **Table 3**.

Manoeuvre	Req ΔV (km/s)
Surface of Earth to LEO (inc drag and grav losses)	9.5
LEO to GEO (impulsive no plane change)	3.95
LEO to GEO (low thrust no plane change)	4.71
LEO to Lunar (impulsive)	3.9
LEO to Lunar (low thrust)	8
LEO to Mars (impulsive)	5.7
GEO station keeping	50 m/s /year
LEO station keeping	< 25 m/s /year

Table 3: Typical ΔV values for different manoeuvre

For a conventional chemical rocket, to reach LEO from the surface of the Earth, assuming an ideal mass ratio ($I_{sp} \approx 450s$, $\Delta V \approx 9.5km/s$, $M_o/M_f \approx 8.6$) then the mass fraction μ would have to be $\approx 90\%$, leaving 10% for the payload itself. This is mitigated through using **rocket staging**. Stages offer various benefits, the most prominent of which is the gain in ΔV when compared with one stage. The expression of the ΔV of a multistage rocket is shown in **Eq. 14**.

$$\Delta V_{\text{Total}} = \Delta V_{\text{Stage 1}} + \Delta V_{\text{Stage 2}} + \dots + \Delta V_{\text{Stage } n} \quad (14.1)$$

$$\Delta V_{\text{Total}} = I_{sp \text{ Stage 1}} g_0 \left(\frac{M_0 \text{ Stage 1}}{M_1 \text{ Stage 1}} \right) \quad (14.2)$$

$$+ I_{sp \text{ Stage 2}} g_0 \left(\frac{M_0 \text{ Stage 2}}{M_1 \text{ Stage 2}} \right) \quad (14.3)$$

$$+ \dots \quad (14.4)$$

$$+ I_{sp \text{ Stage } n} g_0 \left(\frac{M_0 \text{ Stage } n}{M_1 \text{ Stage } n} \right) \quad (14.5)$$

An image depicting the payload fraction against delta V is shown in **Figure 8**.

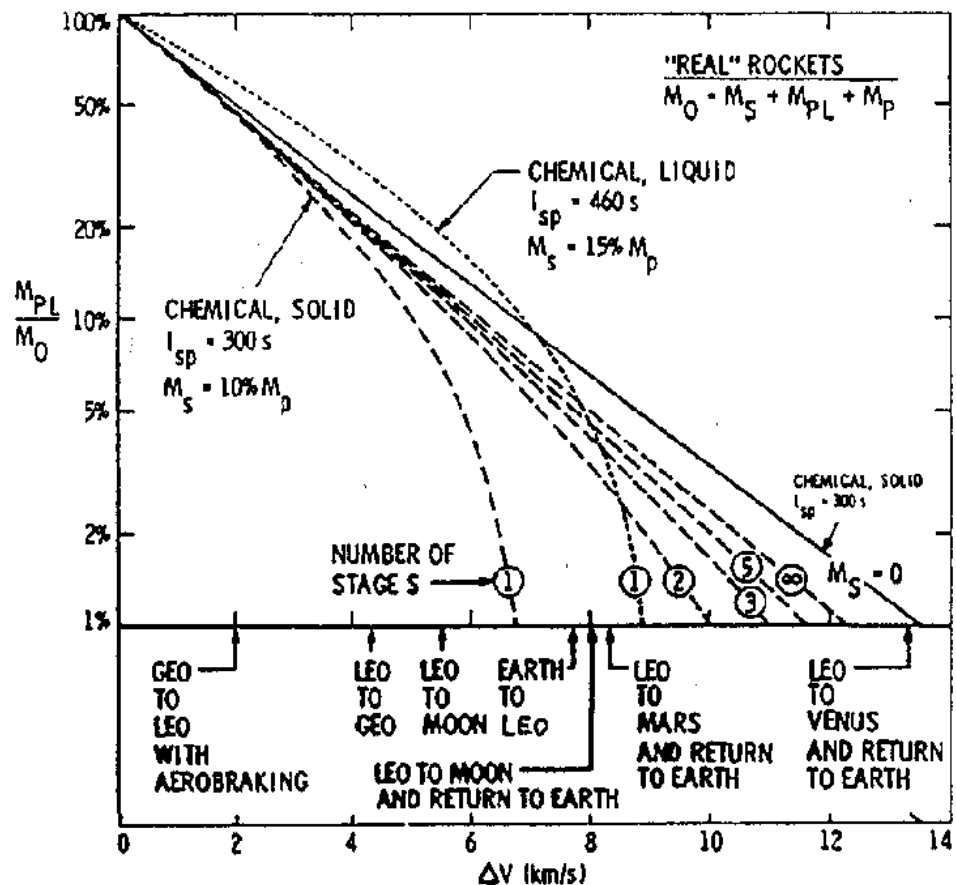


Figure 8: Plot depicting the effect of staging on the ΔV for a given payload fraction.

3.2. Launch Vehicle Dynamics

The key forces acting on a launch vehicle during launch are shown in **Figure 9**.

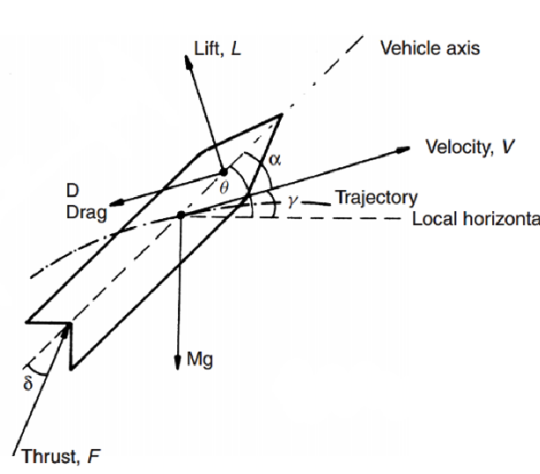


Figure 9: Plot illustrating the forces present on a launch vehicle.

Taking the forces shown in **Figure 9**, a differential expression can be generated for the motion of the craft, using Newton's second law, this is shown in

$$M \left(\frac{dV}{dt} \right) = F \cos(\alpha - \delta) - Mg \sin(\gamma) - D \quad (15)$$

Where:

- M : Total launch vehicle mass (kg)
- V : Spacecraft velocity (m/s)
- F : Thrust (N)
- α : Angle of attack ($^{\circ}$ or rad)
- δ : Gimbal angle ($^{\circ}$ or rad)
- γ : Flight path angle ($^{\circ}$ or rad)
- θ : Pitch angle ($^{\circ}$ or rad) = $\gamma + \alpha$
- D : Drag (N)

Note that within **Eq. 15**, many of the terms depend on the time as well as on one another. These equations can be rearranged and manipulated to yield **Eq. 16** (assuming $V_0 \approx 0, \alpha \approx 0, \delta \approx 0$).

$$\Delta V = \Delta V_{\text{ideal}} - \Delta V_g - \Delta V_D \quad (16.1)$$

$$\Delta V_{\text{ideal}} = \bar{c} \ln \left(\frac{M_0}{M_f} \right) \quad (16.2)$$

$$\Delta V_g = \int_0^{t_b} g \sin(\gamma) dt \quad (16.3)$$

$$\Delta V_D = \int_0^{t_b} \frac{D/M_0}{1 - \mu t/t_p} dt \quad (16.4)$$

Note that for **Eq. 16**, $\Delta V_g \approx 1.1 \text{ km/s}$, $\Delta V_D \approx 0.2 \text{ km/s}$. Additionally a boost of 0.5 km/s can be gained by launching at the equator. Note that \bar{c} is an averaged effective exhaust velocity.

3.3. Converging Diverging Nozzle

START OF WEEK 2

All of the thermal rockets that were shown in **Figure 1** will most likely use a converging diverging nozzle (De-Laval nozzle) to accelerate the hot exhaust gas and increase the thrust of the engine. They effectively **convert the gases thermal energy to kinetic energy**. Note that when considering gaseous or liquid flow in this module, the following assumptions will be made:

- The fluid used are homogeneous.
- The species are gaseous.
- No heat transfer across the rocket walls (adiabatic assumption).
- No friction and all boundary layer effects effects negligible
- No shock waves or discontinuities in the nozzle
- Gas composition does not change in the nozzle (frozen flow) (not necessarily true but will assume for simplification that all reactions occur in the combustion chamber)

A plot of how the temperature, pressure, velocity and Mach number change over the nozzle is shown in **Figure 10**.

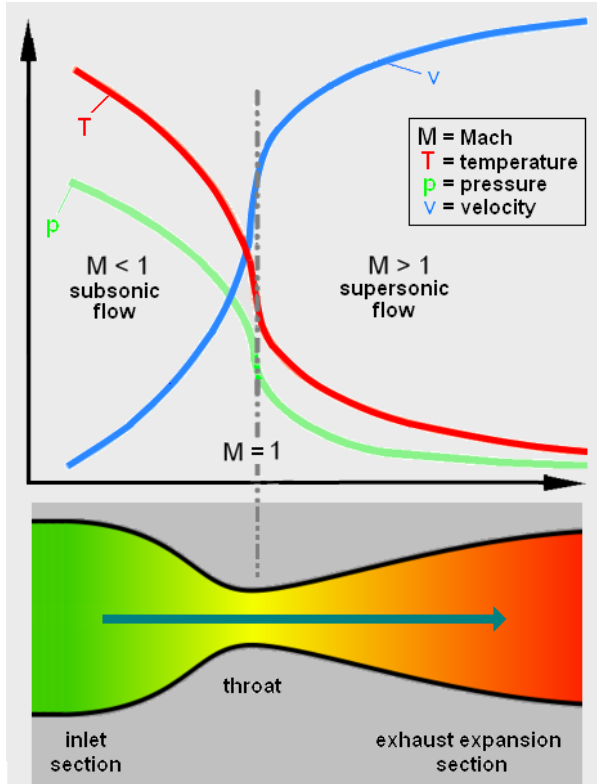


Figure 10: Plot of pressure, temperature, velocity and Mach number over a De-Laval nozzle.

3.4. Exit Velocity Equation

Utilizing the isentropic flow equations it is possible to derive equations for many of the nozzle and engine parameters that have been previously stated. To derive an expression for the **exit velocity** v_e from isentropic flow equations, we first start with the expression for stagnation enthalpy and apply the following criteria shown in **Eq. 17**.

$$h_0 = h_e + \frac{v_e^2}{2} \quad (17.1)$$

$$c_p T_0 = c_p T_e + \frac{v_e^2}{2} \quad \begin{cases} 1. \text{ Ideal gas} \\ 2. c_p \text{ is constant at a given } T \end{cases} \quad (17.2)$$

Where:

- h_0 : Stagnation enthalpy (J/mol).
- h_e : Enthalpy at nozzle exit (J/mol).
- c_p : Specific heat at a constant pressure ($J/mol \cdot K$).
- T_0 : Stagnation temperature (T).
- T_e : Temperature at nozzle exit (T).

This equation can be further developed by **assuming isentropic flow** from the stagnation point to the exhaust point. This allows for the isentropic flow equations to apply, which are shown in **Eq. 18**.

$$\frac{T_0}{T_e} = \left(\frac{P_0}{P_e} \right)^{\frac{k-1}{k}} = \left(\frac{\rho_0}{\rho_e} \right)^{k-1} \quad (18)$$

Where:

- P_0 : Stagnation pressure (pa).
- ρ_0 : Stagnation density (kg/m^3).
- k : Ratio of specific heats.
- P_e : Pressure at nozzle exit (pa).
- ρ_e : Density at nozzle exit (kg/m^3).

Finally the last equation that is needed for a useful expression for v_e is the equation for the specific heat capacity at a constant pressure c_p , this is shown in **Eq. 19**.

$$c_p = \frac{R}{W} \frac{k}{k-1} \quad (19)$$

Where:

- R : Molar gas constant ($J/(mol K)$).
- W : Molecular weight (kg/mol).

Using **Eq. 19**, **Eq. 18** and **Eq. 17**, a useful expression for the exhaust velocity v_e can be derived, this is shown in **Eq. 20**.

$$v_e = \sqrt{\frac{R}{W} \frac{2k}{k-1} T_0 \left(1 - \left(\frac{P_e}{P_0} \right)^{\frac{k-1}{k}} \right)} \quad (20)$$

Where T_0, P_0 can be assumed to be the combustion conditions. Alternatively, **Eq. 20** can also be used to define the I_{sp} , shown in **Eq. 21** (assuming ideal expansion).

$$I_{sp} = \frac{1}{g_0} \sqrt{\frac{R}{W} \frac{2k}{k-1} T_0 \left(1 - \left(\frac{P_e}{P_0} \right)^{\frac{k-1}{k}} \right)} \quad (21)$$

To see what parameters effect the value of v_e and what need sto be maximized, various plots are shown in **Figure 11**.

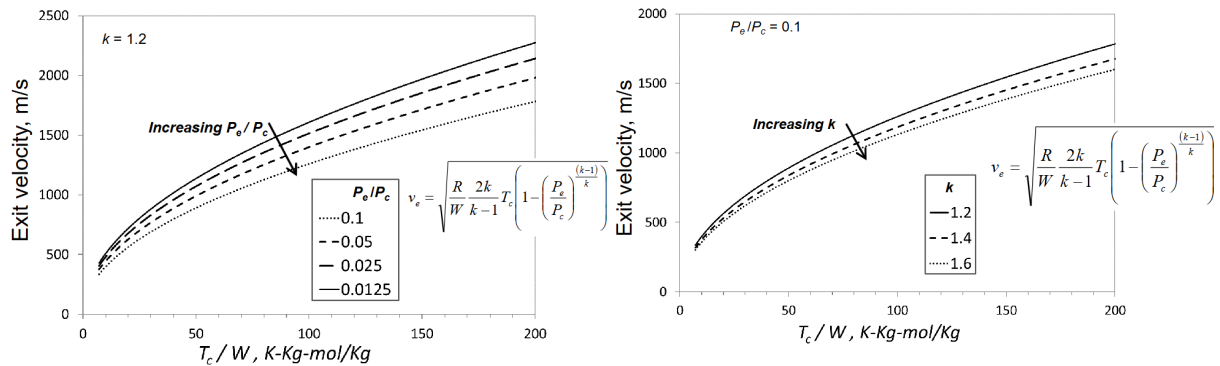


Figure 11: Plot of exit velocity for increasing P_e/P_c ratios [Left], Plot of exit velocity for increasing k ratios [Right]

From **Figure 11** it is clear to see that to maximize the value of v_e the following optimizations of parameters must occur:

- **Minimizing the molecular weight M of the reactants** will have a substantial effect on v_e .

- **Maximizing the combustion temperature** T_c will have a substantial effect on v_e .
- **Decreasing the ratio of P_e/P_c** will have a small impact on v_e .
- **Decreasing the ratio of k** will have a small impact on v_e .

3.5. Mass Flow Rate Equation

Assuming chocked flow ($M_a @ \text{Throat} \approx 1$), the mass flow rate \dot{m} is given by the expression shown in **Eq. 22**.

$$\dot{m} = \rho_t A_t v_t \quad (22)$$

Where:

- ρ_t : Density at the throat (kg/m^3)
- A_t : Area of the throat (m^2)
- v_t : Velocity at the throat (m/s).

Ideally **Eq. 22** should be expressed in terms of chamber parameters. The first substitution that can be made is an expression for the velocity at the throat v_t using the speed of sound equation, this equation is shown in **Eq. 23**. **Eq. 17** can then be used to yield an expression for the stagnation/chamber pressure, shown again in **Eq. 23**.

$$v_t = a = \sqrt{\frac{kRT_t}{W}} \quad (23.1)$$

$$T_0 = T_t + \frac{v_t^2}{2c_p} = T_t + \frac{\left(M_a \sqrt{\frac{kRT_t}{W}}\right)^2}{2c_p} \quad (23.2)$$

Where:

- a : Speed of sound (m/s)
- M_a : Mach number

The next goal is to find expressions for the throat temperature and densities as this will then eliminate them from the equation. By using **Eq. 19**, **Eq. 18** and assuming that $M_t \approx 1$ **Eq. 24** can be derived for T_t as well as for ρ_t .

$$T_t = \frac{2T_c}{k+1} \quad \rho_t = \rho_c \left(\frac{2}{k+1} \right)^{\frac{1}{k-1}} \quad (24)$$

Finally, **Eq. 24** and **Eq. 23** can be substituted into **Eq. 22** to yield **Eq. 25**.

$$\dot{m} = \frac{A_t \rho_c k}{\sqrt{\frac{kRT_c}{W}}} \sqrt{\left(\frac{2}{k+1} \right)^{\frac{k+1}{k-1}}} \quad (25)$$

4. Lecture 4

4.1. Nozzle Expansion Ratio Equation

Momentum conservation can be applied between the exhaust and the throat to yield an expression including A_t and A_e , this expression is shown in **Eq. 26**.

$$\dot{m} = \rho_t A_t v_t = \rho_e A_e v_e \rightarrow \frac{A_t}{A_e} = \frac{\rho_e v_e}{\rho_t v_t} \quad (26)$$

Equations for v_e , v_t and ρ_e/ρ_t have already been defined and so by substituting **Eq. 23**, **Eq. 20** and **Eq. 18** into **Eq. 26** will yield **Eq. 27**.

$$\frac{A_t}{A_e} = \left(\frac{k+1}{2}\right)^{\frac{1}{k-1}} \left(\frac{P_e}{P_c}\right)^{\frac{1}{k}} \sqrt{\frac{k+1}{k-1} \left(1 - \frac{P_e}{P_c}\right)^{\frac{k-1}{k}}} \quad (27)$$

Note that for low altitude rockets $\frac{A_e}{A_t} \approx 3 - 25$ and for high altitude rockets $\frac{A_e}{A_t} \approx 40 - 200$.

4.2. Characteristic Velocity Equation

The characteristic velocity was first defined in **Eq. 11**. It can be rewritten in terms of the equations that have been previously defined to yield **Eq. 28**.

$$c^* = \frac{P_c A_t}{\dot{m}} = \frac{\sqrt{\frac{kRT_c}{W}}}{k \sqrt{\frac{2}{k+1}}^{\frac{k+1}{k-1}}} \quad (28)$$

Note that for a liquid oxygen, liquid hydrogen bipropellant rocket, $c^* \approx 2300m/s$ and for an ammonium perchlorate + polymer + Al solid rocket, $c^* \approx 1590m/s$.

4.3. Thrust Equation

Similarly to characteristic velocity, the thrust can be written in terms of the equations that have just been derived, mainly **Eq. 20** and **Eq. 25** to yield **Eq. 29**.

$$F = \dot{m} v_e + (P_e - P_a) A_e = A_t P_c \sqrt{\frac{2k^2}{k-1} \left(\frac{2}{k+1}\right)^{\frac{k+1}{k-1}} \left(1 - \left(\frac{P_e}{P_c}\right)^{\frac{k-1}{k}}\right)} + (P_e - P_a) A_e \quad (29)$$

4.4. Coefficient of Thrust Equation

A useful parameter when quantifying the performance of a nozzle is the coefficient of thrust C_F . The definition of C_F as well as the equation after substituting **Eq. 29** into it are shown in **Eq. 30**.

$$C_F = \frac{F}{P_c A_t} = \sqrt{\frac{2k^2}{k-1} \left(\frac{2}{k+1}\right)^{\frac{k+1}{k-1}} \left(1 - \left(\frac{P_e}{P_c}\right)^{\frac{k-1}{k}}\right)} + \frac{(P_e - P_a) A_e}{P_c A_t} \quad (30)$$

Values of $C_F \approx 0.8 - 1.9$ with a higher value meaning better thrust amplification. C_F is a peak when there is ideal expansion ($P_e = P_a$) at a constant P_a/P_c . Note that the equation

has a **momentum part** and a **pressure part** similar to the thrust itself. The behavior of the C_F against the area and pressure ratios is shown in **Figure 12**

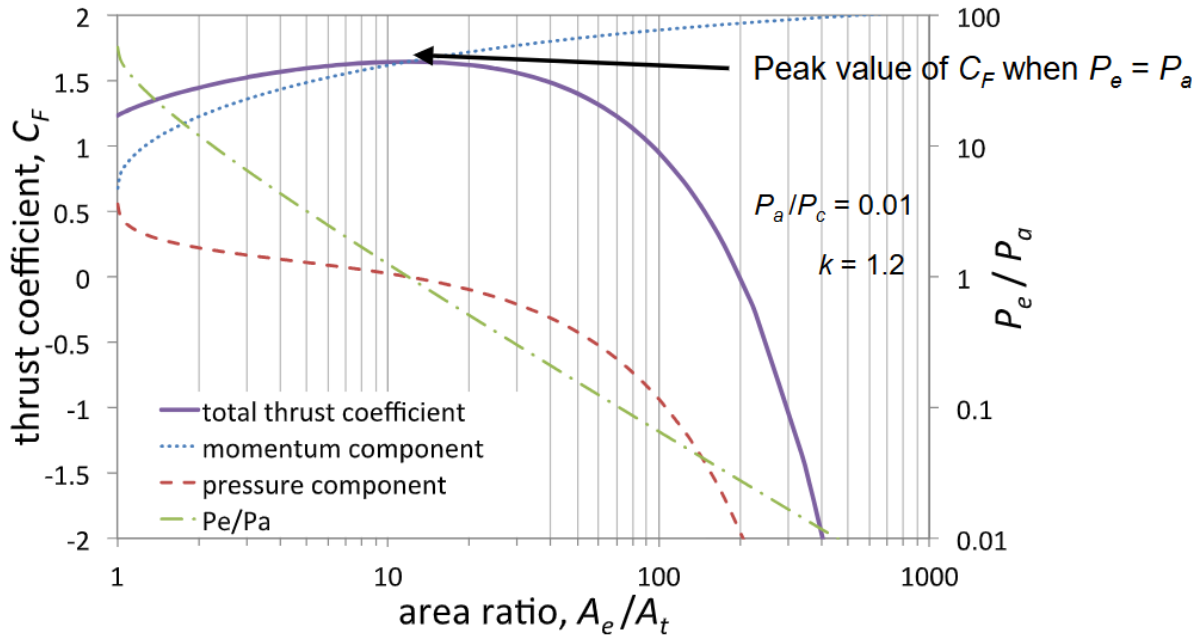


Figure 12: Plot of C_F against area and pressure ratios

Note that as the area ratio increases the momentum component increases but the pressure component decreases. This is interesting as the area ratio **does not appear in the momentum section of the equation**. In reality there is still a dependency as area ratio depends on pressure ratio which is present in the area ratio equation. Another plot is shown in **Figure 13**.

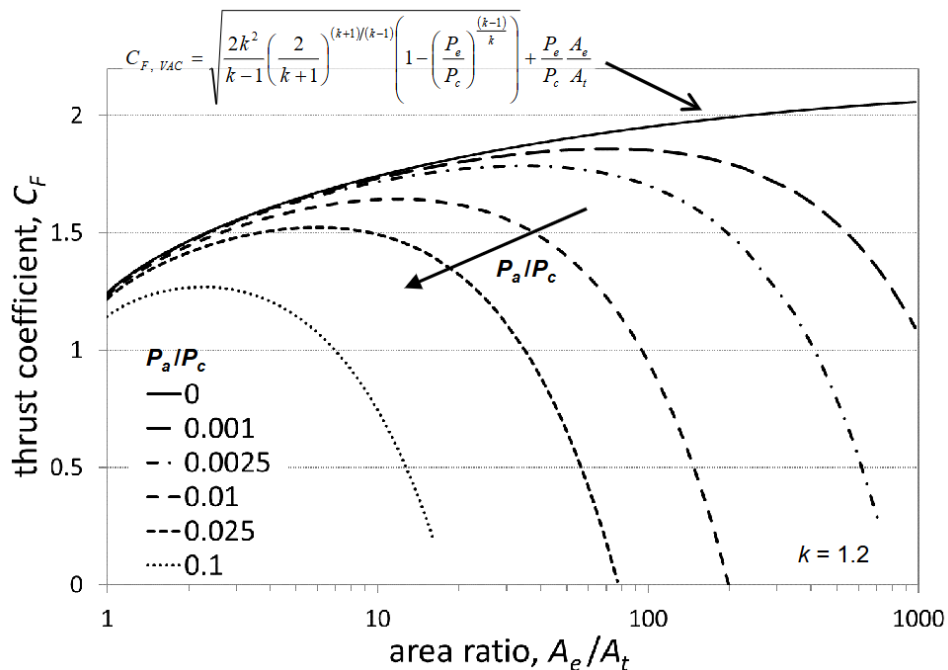


Figure 13: Plot of C_F against area ratio for varying pressure ratios

Note that in **Figure 13**, increasing the pressure ratio will decrease the thrust coefficient. The highest possible thrust coefficient is given when the pressure ratio is zero such as in a vacuum.

4.5. Summary of Equations

$$v_e(R, W, k, T_0, P_e, P_0) = \sqrt{\left(\frac{R}{W}\right) \frac{2k}{k-1} T_0 \left(1 - \left(\frac{P_e}{P_0}\right)^{\frac{k-1}{k}}\right)} \quad (31.1)$$

$$\dot{m}(A_t, \rho_c, k, R, T_c, W) = \frac{A_t \rho_c k}{\sqrt{\frac{kRT_c}{W}}} \sqrt{\left(\frac{2}{k+1}\right)^{\frac{k+1}{k-1}}} \quad (31.2)$$

$$\frac{A_t}{A_e}(k, P_e, P_c) = \left(\frac{k+1}{2}\right)^{\frac{1}{k-1}} \left(\frac{P_e}{P_c}\right)^{\frac{1}{k}} \sqrt{\frac{k+1}{k-1} \left(1 - \left(\frac{P_e}{P_c}\right)^{\frac{k-1}{k}}\right)} \quad (31.3)$$

$$c^*(T_c, k, R, W) = \frac{\sqrt{\frac{kRT_c}{W}}}{k \sqrt{\left(\frac{2}{k+1}\right)^{\frac{k+1}{k-1}}}} \quad (31.4)$$

$$F(A_t, P_c, k, P_e, A_e, P_a) = A_t P_c \sqrt{\frac{2k^2}{k-1} \left(\frac{2}{k+1}\right)^{\frac{k+1}{k-1}} \left(1 - \left(\frac{P_e}{P_c}\right)^{\frac{k-1}{k}}\right)} + (P_e - P_a) A_e \quad (31.5)$$

$$C_{F(k, P_e, P_a, A_e, P_c, A_t)} = \sqrt{\frac{2k^2}{k-1} \left(\frac{2}{k+1}\right)^{\frac{k+1}{k-1}} \left(1 - \left(\frac{P_e}{P_c}\right)^{\frac{k-1}{k}}\right)} + \frac{(P_e - P_a) A_e}{P_c A_t} \quad (31.6)$$

4.6. Equations Involving Mach Relations

Many of the previous equations can be represented in terms of mach number, namely **Eq. 18**, which are shown in **Eq. 32**.

$$T_0 = T \left(1 + \frac{1}{2}(k-1)M^2\right) \quad P_0 = P \left(1 + \frac{1}{2}(k-1)M^2\right)^{\frac{k}{k-1}} \quad \rho_0 = \rho \left(1 + \frac{1}{2}(k-1)M^2\right)^{\frac{1}{k-1}} \quad (32)$$

The Mach relations can be applied to **Eq. 27** to yield an expression for the area ratio in terms of Mach number shown in **Eq. 33**.

$$\frac{A_y}{A_x} = \frac{M_x}{M_y} \sqrt{\left(\frac{1 + \frac{1}{2}(k-1)M_y^2}{1 + \frac{1}{2}(k-1)M_x^2}\right)^{\frac{k+1}{k-1}}} \quad (33)$$

Eq. 33 shows that area ratio is directly proportional to the Mach ratio. Furthermore this equation is also proportional to coefficient of thrust as was previously stated, and this relation is also shown in **Figure 14**.

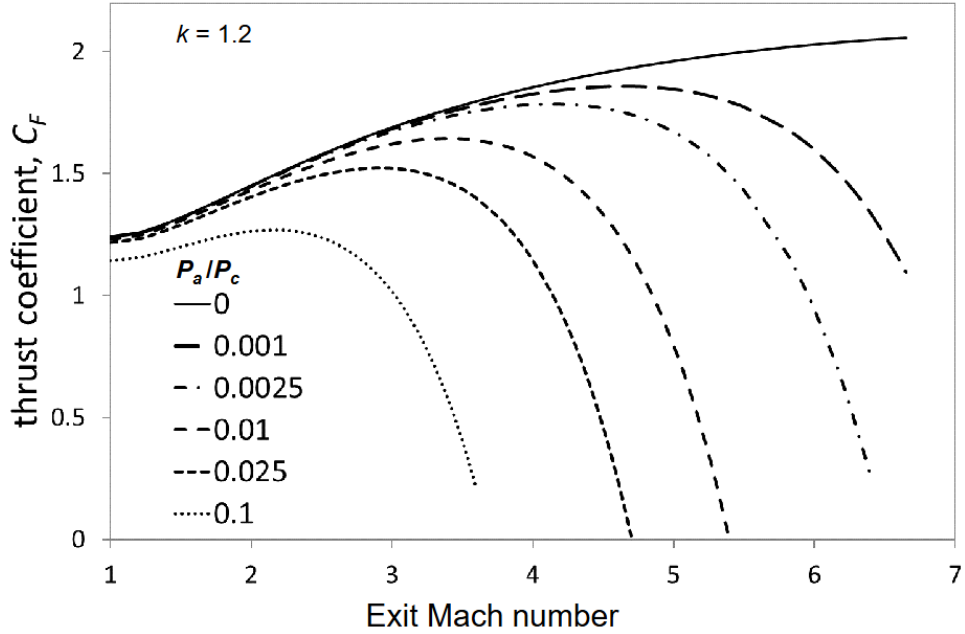


Figure 14: Plot of C_F against exit Mach number for varying pressure ratios

Figure 14 is effectively the same as **Figure 13** apart from altering the x-axis. A larger mach number will require a larger area ratio which will drive up the C_F as it depends on the pressure ratio which is proportional.

4.7. Coefficient of Thrust for Converging Nozzles

Figure 14 can be further edited to yield a neater plot. To get to this, consider the pressure equation in **Eq. 32** when there is no diverging nozzle. This would mean that $M_e = 1$ and **Eq. 32** can therefore be then written as **Eq. 34**.

$$\frac{P_c}{P_e} = \left(1 + \frac{1}{2}(k-1)M_e^2\right)^{\frac{k}{k-1}} \quad \text{If } M_e = 1 \rightarrow \frac{P_e}{P_c} = \left(\frac{2}{k+1}\right)^{\frac{k}{k-1}} \quad (34)$$

Eq. 34 can be substituted into **Eq. 30** to yield an equation for C_F for the converging section of the nozzle, this is shown in **Eq. 35**.

$$C_F \text{ Converging} = (k+1) \left(\frac{2}{k+1}\right)^{\frac{k}{k-1}} - \frac{P_a}{P_c} \quad (35)$$

Using **Eq. 35** a modified version of **Figure 14** can be plotted, this plot is shown in **Figure 15**. This plot now has a point where all lines roginiate, when the ratio of $C_F/C_F \text{ Converging} = 1$ and $A_e/A_t = 1$ when there is no diverging section at all.

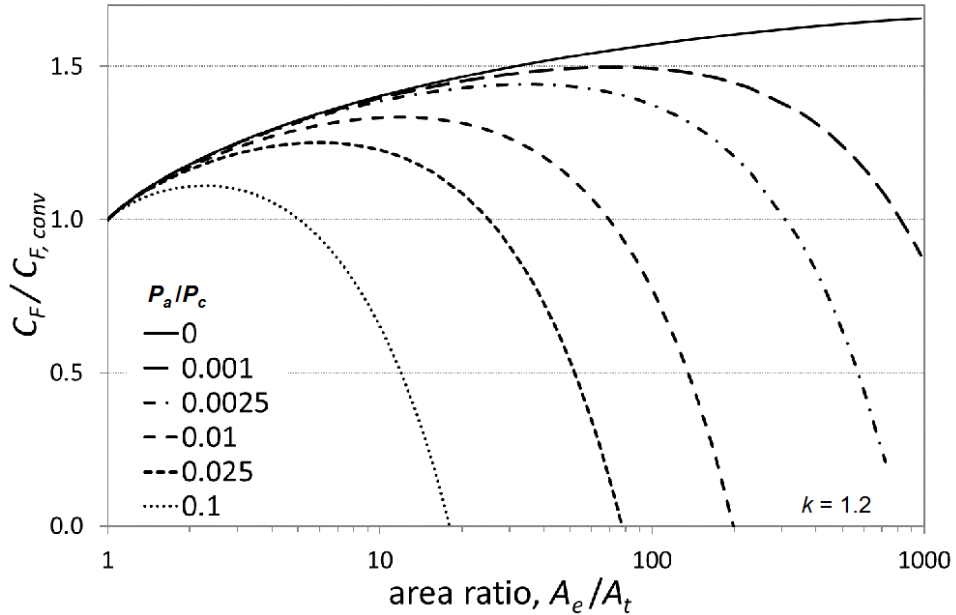


Figure 15: Plot of $C_F / C_{F,conv}$ against exit area ratio for varying pressure ratios

4.8. Under, Ideal and Over Expanded Nozzles

Depending on the relationship between the exit pressure P_e and the ambient pressure P_a , there are three cases of nozzle exhaust flow, these are:

- **Under-expanded ($P_e > P_a$):**
 - ▶ Typically occurs at **high altitudes** and happens when the **nozzle is too short**. Exhaust wasn't expanded enough and so expands out the back of the nozzle via expansion waves.
 - ▶ C_F and thrust are **below maximum**.

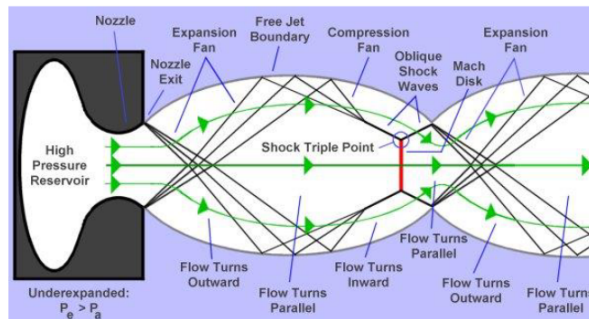


Figure 16: Under-expanded flow out of a nozzle

- **Ideally Expanded ($P_e \approx P_a$):**
 - ▶ **Nozzle is perfect length** and exhaust exits in a perfect rectangular plume with no losses or shocks.
 - ▶ C_F and thrust are **maximized**.
 - ▶ $v_e = c$, exhaust velocity is equal to effective exhaust velocity.

- **Over-expanded ($P_e < P_a$):**

- Typically occurs at **low altitudes** and happens when the **nozzle is too long**. Exhaust is at a lower pressure than ambient causing shocks and possible flow separation within the nozzle.
- C_F and thrust are **below maximum**.

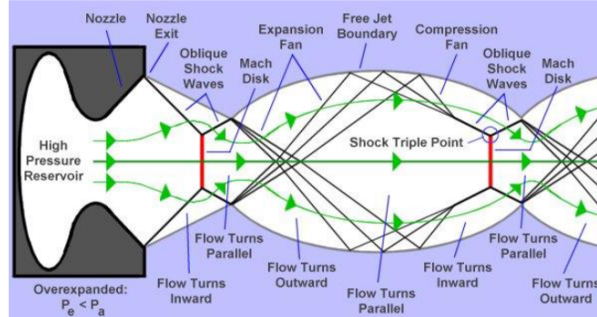
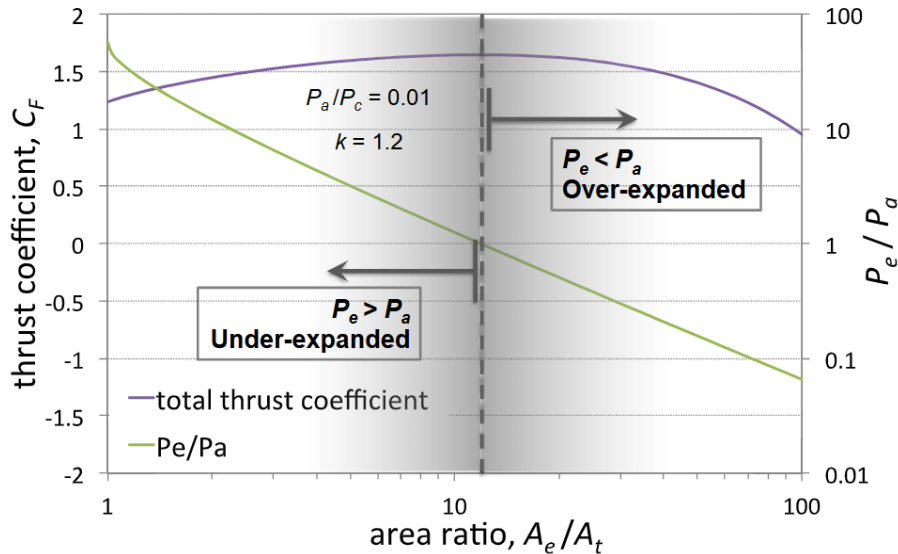


Figure 17: Over-expanded flow out of a nozzle

Plotting the behavior of the thrust coefficient against pressure ratio and the area ratio yields **Figure 18**. Note that the value of C_F is maximized when $P_e = P_a$ and $P_e/P_a = 1$.

Figure 18: Plot of C_F against pressure ratio and area ratio

4.8.1. Summerfield Criterion

The Summerfield criterion applies to heavily over-expanded nozzles and describes when the flow is likely to separate from inside of the nozzle and create shocks. The criterion is shown in **Eq. 36**.

$$P_e < (0.25 \text{ to } 0.4)P_a \quad (36)$$

Eq. 36 as well as the line of ideal expansion can be applied to **Figure 15** to produce **Figure 19**.

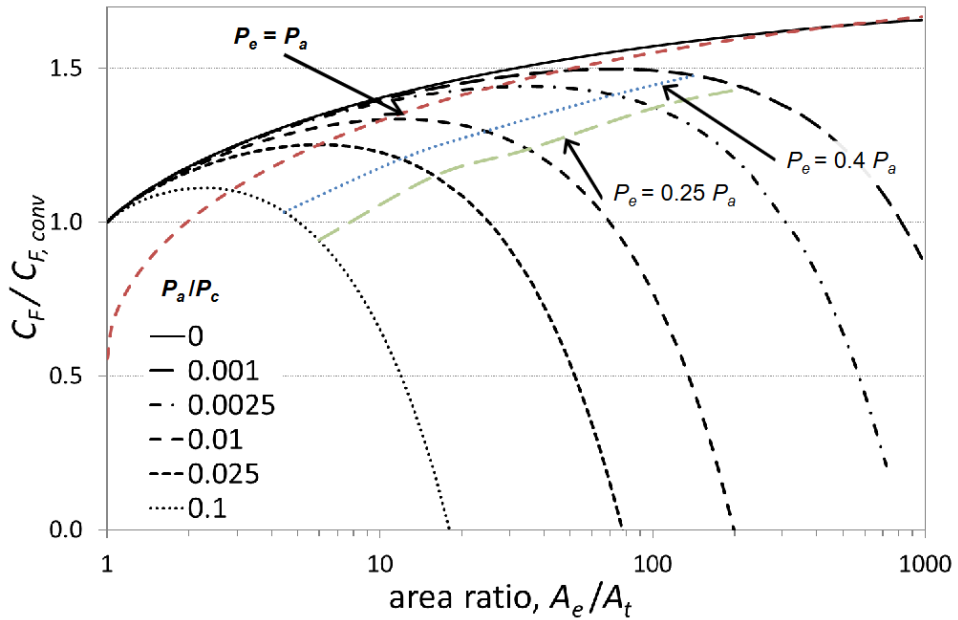


Figure 19: Plot of $C_F/C_{F, \text{conv}}$ against exit area ratio for varying pressure ratios with summerfield criterion and ideal expansion line.

On **Figure 19**, the red dotted line represents ideal expansion. **Below this line** sits **over-expanded flow**. **Above this line** sits **under-expanded flow**. **Below the yellow and blue lines** sits **super over-expansion** when the Summerfield criterion applies. Note that a typical rocket fired at sea level will undergo the following movements through this graph:

1. Initially **over-expanded** at sea level.
2. As the altitudes rises the rocket engine moves vertically upwards on the graph and the engine becomes less and less over-expanded until it is **ideally-expanded**.
3. As the rocket ascends further, the engine starts to become **under-expanded** and thrust and C_F start to decrease.

5. Lecture 5

5.1. Nozzle Designs and the Perfect Nozzle

Ideally a nozzle's expansion ratio A_e/A_t should increase as the rocket increases in altitude so that the flow is constantly ideally expanded. Some rockets achieve this using a skirt which drops down at higher altitudes to increase A_e/A_t . Some nozzle designs are shown in **Figure 20**

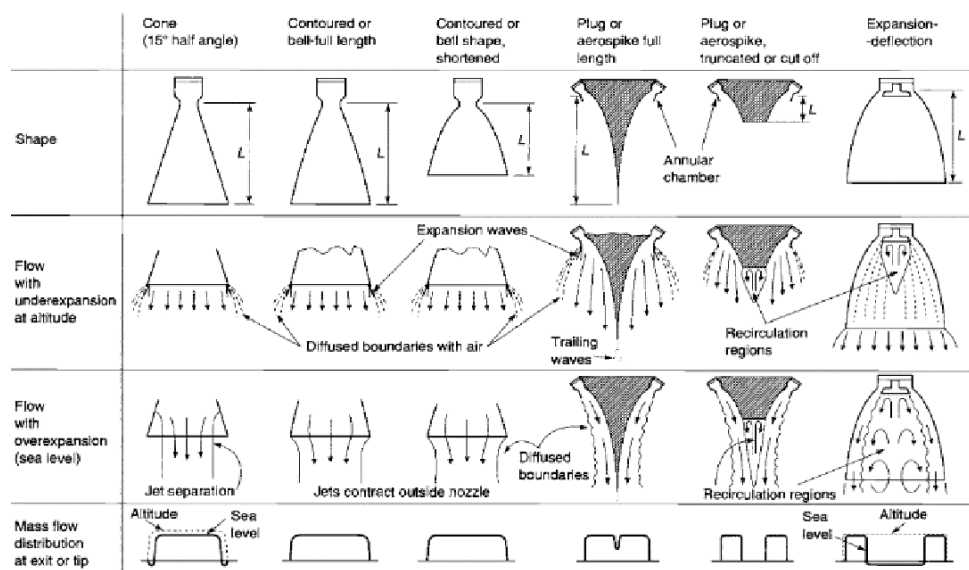


Figure 20: Various nozzle designs.

5.2. Conical Nozzles

Conical nozzles are a relatively simple nozzle design that is also easy to manufacture. There are various parameters that control the shape of a conical nozzle, these are depicted within **Figure 21**.

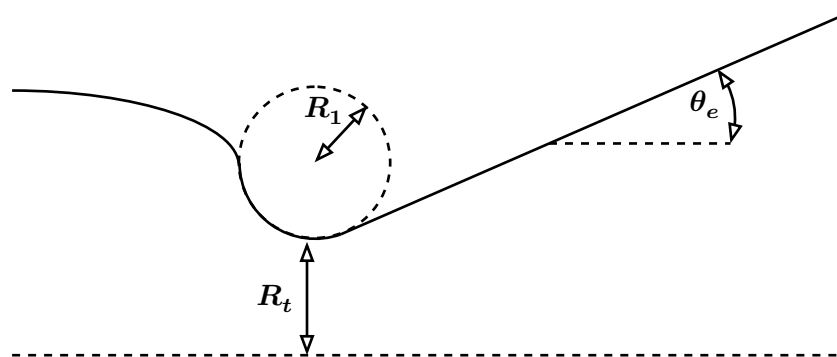


Figure 21: Definitions for a conical nozzle

Where:

- R_t : Throat radius (m).
- R_1 : Throat radius of curvature (m) $\approx 1.5 \times R_t$
- θ_e : Cone divergence half angle (° or Rad)

Ideally $\theta_e \approx 12^\circ - 18^\circ$ with:

- **Smaller angles** constituting a larger I_{sp} but higher mass and more complexity
- **Larger angles** constituting a lower I_{sp} but lower mass.

One issue with conical nozzles is that the flow does not all go directly straight out of the nozzle, it is instead directed outwards slightly at the edges. This introduces losses which are characterized by **Eq. 37** and are only applied to the **momentum term**. This is then applied to C_F .

$$\lambda = \frac{1}{2}(1 + \cos \theta_e) \quad (37.1)$$

$$C_{F(\lambda, k, P_e, P_a, A_e, P_c, A_t)} = \lambda \sqrt{\frac{2k^2}{k-1} \left(\frac{2}{k+1} \right)^{\frac{k+1}{k-1}} \left(1 - \left(\frac{P_e}{P_c} \right)^{\frac{k-1}{k}} \right)} + \frac{(P_e - P_a) A_e}{P_c A_t} \quad (37.2)$$

5.3. Bell (Rao) Nozzles

Bell nozzles have typically higher efficiency than conical by allowing the flow to quickly expand whilst it has high pressure and then slowly redirecting the flow to be as axial as possible by the end. An image showing the key dimensions for a bell nozzle are shown in.

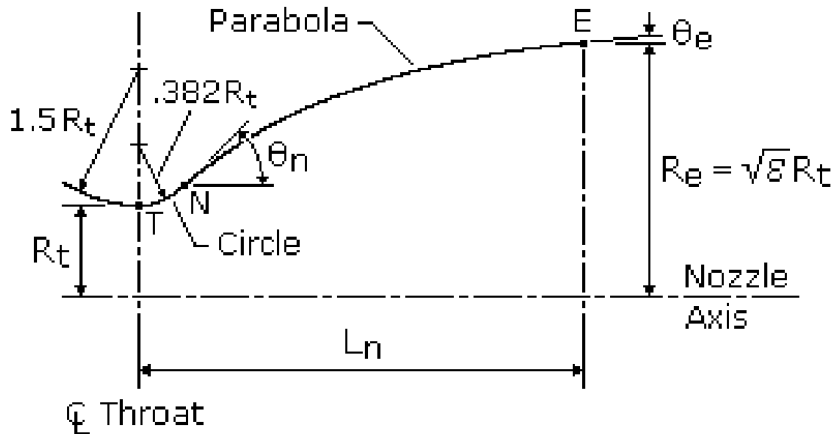


Figure 22: Bell nozzle dimensions.

Note that the bell curve will have a **point of inflection** along it. The coordinates of the inflection point are given by **Eq. 38** the following coordinates relative to the center of the throat (where R_t is measured from).

$$X_n = R_t \sin \theta_N \quad Y_n = R_t + R_1(1 - \cos \theta_e) \quad (38)$$

Note that θ_N here is the angle that the line at the inflection point makes with the horizontal datum (initial large divergence angle). If the initial diverging section of the nozzle is conical then this would be the cone angle for that portion. The equation for the parabolic low divergence angle section is shown in **Eq. 39**.

$$y' = Px' + Q + (Sx' + T)^{0.5} \quad (39.1)$$

$$P = \frac{y'_E \tan \theta_N + y'_E \tan \theta_E - 2x'_E \tan \theta_E \tan \theta_N}{2y'_E - x'_E \tan \theta_M - x'_E \tan \theta_E} \quad S = \frac{(y'_E - Px'_E)^2 (\tan \theta_N - P)}{x'_E \tan \theta_N - y'_E} \quad (39.2)$$

$$Q = \frac{S}{2(\tan \theta_N - P)} \quad T = Q^2 \quad (39.3)$$

Note that in **Eq. 39** any terms with a subscript of E are the coordinates and angles relating to the exit of the nozzle and the coordinates themselves are relative to the inflection point. Typically $\theta_E \approx 2^\circ - 8^\circ$. The length of a bell nozzle is compared to a 15° conical nozzle using **Eq. 40**.

$$L_{15} = \eta_{\text{Bell}} \frac{R_T(\sqrt{\varepsilon} - 1) + R_1 \left(\frac{1}{\cos \theta_e} - 1 \right)}{\tan \theta_e} \quad (40)$$

Where:

- L_{15} : Length of a 15° conical nozzle (m).
- ε : Expansion ratio $= A_e/A_t$
- θ_e : Divergence angle at exit ($^\circ$ or Rad)
- η_{Bell} : Percentage of full bell.

To obtain an values for θ_E, θ_N and ε for a given value of η_{Bell} then **Figure 23** can be used.

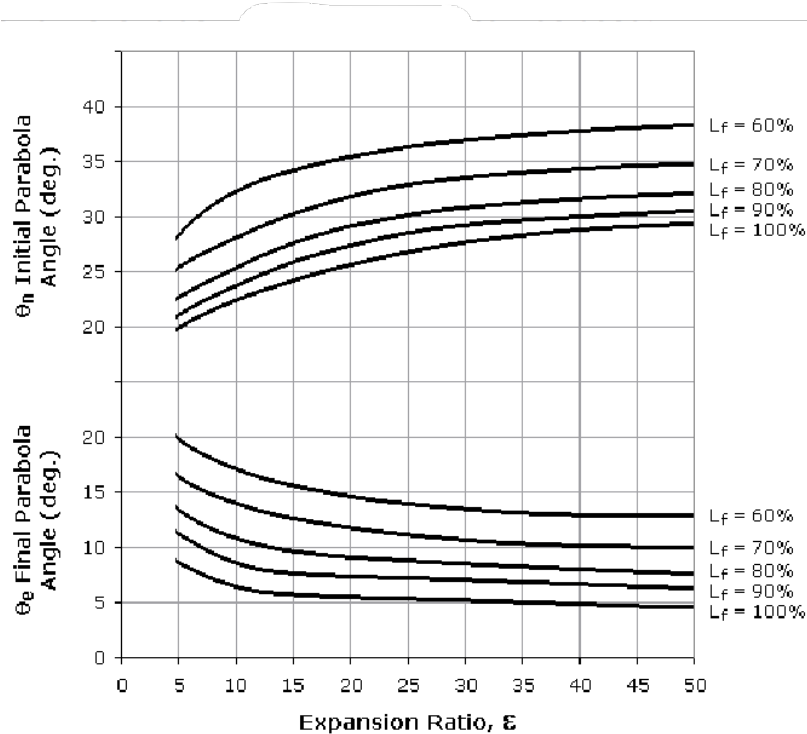


Figure 23: Bell curves for various values of η_{Bell} .

5.4. Aerospike Nozzles

Aerospike nozzles are a version of altitude compensating engine where the external air pressure changes the value of A_e Effective as it rises in altitude. They commonly feature many smaller combustion chambers which then have their exhausts directed onto a spike. The two main types of aerospike engines (shown in **Figure 20**) are:

- **Full Aerospike:** Feature a full length spike where there is no recirculation region, however the end of the spike is typically difficult to cool.
- **Truncated Aerospike:** The end of the spike is missing which allows for better cooling at penalty of lower performance.

Aerospikes can come in linear and annular forms. They are typically smaller than typical bell nozzles and can still vector thrust by controlling the thrust coming from individual combustion chambers. They haven't yet had much proven flight experience and lack any larger surface area examples.

5.5. Expansion Deflection Nozzle

Make use of a pintle at the center of the nozzle which redirects the flow along the walls of the nozzle (again shown in **Figure 20**). At low altitudes a large recirculation area caused by the high ambient pressure causes a smaller value of A_e . At higher altitudes the lower ambient pressure means the recirculation area is much smaller and the value of A_e is bigger. These engines haven't seen much use with one issue being keeping the pintle itself cool.

5.6. Intro to Liquid Propulsion

START OF WEEK 3

There are three main sub categories within liquid propulsion, these are shown in the bullet pointed list below. The relative performance of these liquid propulsion methods is shown in **Table 4:**

Type	$I_{sp}(s)$	$T_{max}(^{\circ}C)$	Thrust (N)	Propellants
Monopropellant	200 - 250	600 - 800	0.03 - 100	N_2H_4 , H_2O_2
Bipropellant	200 - 468	2500 - 4100	≤ 10 MN	N_2H_4 , H_2 , Kerosene, N_2O_4
Cold Gas	50 - 100	N/A	0.01 - 270	He, H_2 , Kr, N_2

Table 4: Typical liquid propellant parameters.

- **Bipropellant:** Mix together a liquid fuel and liquid oxidizer and combust them to produce thrust.
- **Monopropellant:** Flow a liquid fuel over a catalyst bed where it undergoes a exothermic decomposition reaction.
- **Cold Gas:** A gas is stored at pressure where it is released and flows through a nozzle to accelerate it.

From **Eq. 20**, a good rocket engine will maximize and minimize the following parameters:

- **Low molecular weight of combustion products W .** This is also why typically rocket engines operate fuel rich as the low molecular weight fuel dominates the reaction.
- **High combustion temperature T_c .**
- **High combustion pressure P_c ,** though there is a smaller gain from this parameter.
- **Low ratio of specific heats k ,** though there is a smaller gain from this parameter. Typically k sits at about one anyways.

6. Lecture 6

6.1. Performance of Liquid Thrusters

There are many engine parameters which can be calculated using the equations in [Eq. 31](#), however there are many parameters, mainly the combustion parameters (W and k) which cannot be calculated as easily. A **chemical reaction simulator** such as NASA's Glenn Chemical Equilibrium with Applications simulator can be used ([Press to go to link](#)). One useful parameter is the **oxidizer to fuel ratio**, shown in [Eq. 41](#).

$$r = \frac{\dot{m}_{\text{ox}}}{\dot{m}_{\text{fuel}}} \quad (41)$$

Typically, rocket engines **burn fuel rich** and not purely stoichiometric. This is to decrease W as lighter molecules make up more of the exhaust. An example of this is shown in [Figure 24](#).

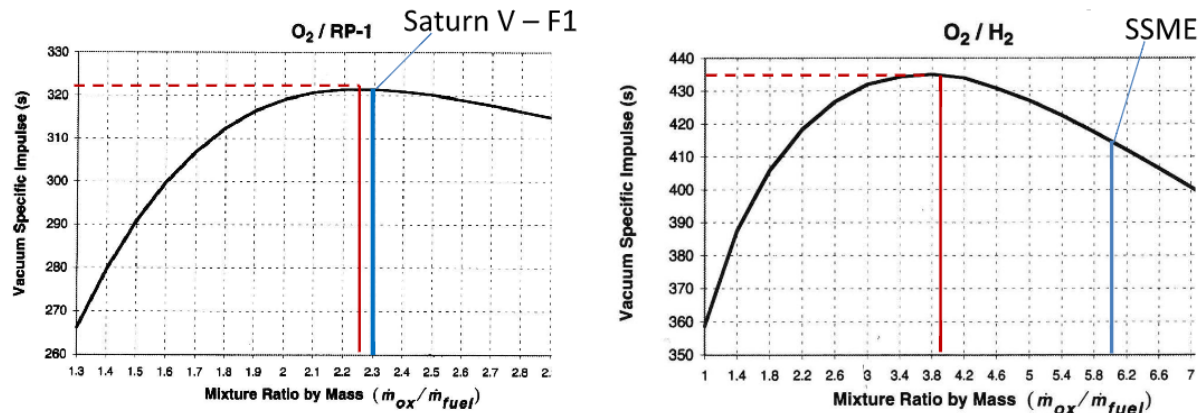


Figure 24: $\dot{m}_{\text{ox}}/\dot{m}_{\text{fuel}}$ against I_{sp} for different rocket engines.

Note that the stoichiometric ratio for r for the Saturn V F1 engines was 3.4 and for the Space Shuttle Main Engines (SSME) it was 8. Note that the Space shuttle couldn't reach r_{optimum} due to the low density of hydrogen and the lack of anymore space in the main fuel tanks for any more fuel.

6.2. Fuels

Name	Chemical Formula	Chemical Structure	Type	Toxicity	Corrosivity	Flammability	Hypergolic?	Molecular Weight (g/mol)	Density (kg/m ³)	Boiling and Freezing Temp (°C)
Fuels										
Liquid Hydrogen (LH ₂)	H ₂	H — H	Bi	None	None	High	No	2.016	70.85	Boil: -253 Freeze: -259
RP-1 (Rocket Propellant Group 1)	C _n H _{1.97n}		Bi	Moderate	None	High	No	170	810	Boil: 277 Freeze: -40
Hydrazine	N ₂ H ₄		Mono	High	Moderate	Spontaneous	N/A	32.05	1021	Boil: 113.5 Freeze: 2
Monomethylhydrazine (MMH)	CH ₃ NHNH ₂		Bi	High	High	High	Yes	46.07	880	Boil: 87.5 Freeze: -52.4
Unsymmetrical Dimethylhydrazine (UDMH)	(CH ₃) ₂ NNH ₂		Bi	High	High	High	Yes	60.1	793	Boil: 63 Freeze: -58
Methane	C ₂ H ₄		Bi	None	None	High	No	16.04	422.6	Boil: -162 Freeze: -183
Ethanol	C ₂ H ₅ OH		Bi	High	Moderate	High	No	46.07	789	Boil: 78.37 Freeze: -114
Pentaborane	B ₅ H ₉		Bi	Extremely	Extremely	Pyrophoric	Yes	63.13	618	Boil: 58.4 Freeze: -46.8

Name	Chemical Formula	Chemical Structure	Type	Toxicity	Corrosivity	Flammability	Hypergolic?	Molecular Weight (g/mol)	Density (kg/m ³)	Boiling and Freezing Temp (°C)
Oxidizers										
Liquid Oxygen (LOX)	O ₂	O = O	Bi	None	None	N/A	No	32	1141	Boil: -182 Freeze: -218
Dinitrogen Tetroxide	N ₂ O ₄		Bi	Extremely	High	N/A	Yes	92.01	1440	Boil: 21.2 Freeze: -11.2
Hydrogen Peroxide	H ₂ O ₂		Bi	High	High	N/A	No	34.014	1450	Boil: 150.2 Freeze: -0.43
Nitric Acid	HNO ₃		Bi	High	High	N/A	No	63.012	1510	Boil: 83 Freeze: -42
Chlorine Trifluoride	ClF ₃		Bi	Extreme	Extreme	N/A	Yes	92.45	1800	Boil: 11.75 Freeze: -76.34
Oxygen Difluoride	OF ₂		Bi	Extreme	Extreme	N/A	No	54	1880	Boil: -144.75 Freeze: -223.8
Fluorine	F ₂	F — F	Bi	Extreme	Extreme	N/A	Yes	38	1513	Boil: -188.1 Freeze: -219.6

Table 5: Data on common liquid fuels and oxidizers

Note that nitrogen tetroxide shown in **Table 5** is usually mixed with nitric oxide NO to increase the temperature range over which it is liquid, this mixture is called **Mixed Oxides of Nitrogen** (MON). To compare different fuel and oxidizer ratios, **Table 6** can be used.

Oxidizer	Fuel	Mass Mixture Ratio	ρ (g/cm ³)	c^* (m/s)	Sea Level I_{sp} (s)
O_2	Methane	3.20	0.81	1.84	296
	Hydrazine	0.74	1.06	1.87	301
	Hydrogen	3.40	0.26	2.43	386
	RP-1	2.24	1.01	1.77	300
	UDMH	1.39	0.96	1.84	295
F_2	Hydrazine	2.30	1.31	2.21	365
	Hydrogen	4.54	0.33	2.53	389
N_2O_4	Hydrazine	1.08	1.20	1.77	283
	RP-1	3.4	1.23		297
	MMH	1.65	1.16	1.59	278
H_2O_2	RP-1	7.0	1.29		297

Table 6: Performance parameters for different fuel and oxidizer combinations.

One new area of interest is **green hypergolic fuels** such as Dimethylthioformamide. These are safer and more environmentally friendly alternatives to traditional rocket fuels.

6.3. Overview of Monopropellant Thruster Systems

These systems generate thrust by flowing a propellant over/through a catalyst bed, where it endothermically decomposes, generating a hot, high velocity exhaust gas. The performance of such systems is shown in **Table 4** with a top level systems drawing of a thruster shown in **Figure 25**.

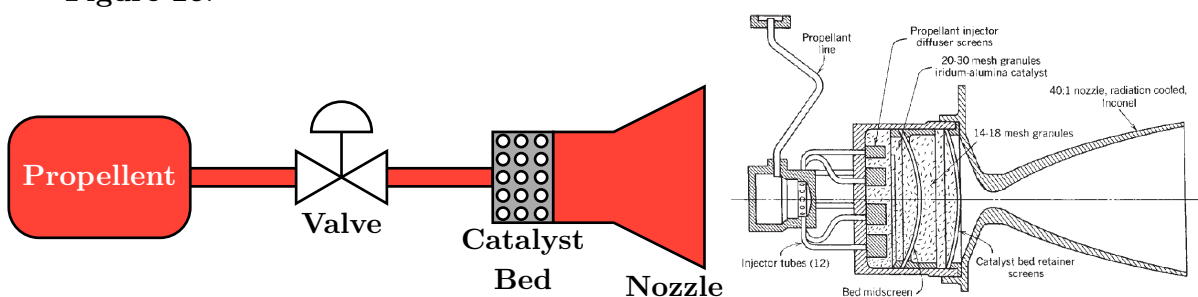


Figure 25: System engineering diagram of a monopropellant thruster system [Left], real schematic of a monopropellant thruster [Right]

6.3.1. Decomposition of Hydrazine

Hydrazine is the most common monopropellant fuel used in rockets. It decomposes over a catalyst bed following the reaction detailed in **Figure 26**.

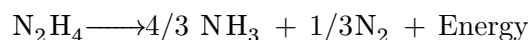


Figure 26: Decomposition reaction of hydrazine.

This exothermic decomposition reaction has a equilibrium temperature of 1650K and releases a large amount of energy ($\approx 111.7\text{ kJ/mol}$ of hydrazine). One issue is that at this temperature, the ammonia produced is unstable and itself decays via the reaction shown in **Figure 27**.

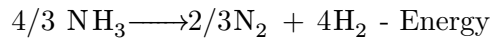


Figure 27: Thermal breakdown of ammonia.

This reaction is **slow and endothermic**, reducing the energy released in the decomposition reaction and subsequently reducing thrust. As this reaction is slow, the **dwell time** (the amount of time the fuel remains in the combustor), plays a large roll in the energy released. The full decomposition reaction for hydrazine can therefore be written as **Figure 28**.

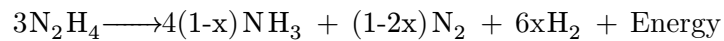


Figure 28: Full decomposition reaction for hydrazine.

Where x is the degree of ammonia dissociation. This parameter depends on the:

- Catalyst type
- Geometry
- Dwell time
- Size of chamber
- Chamber pressure

Note that the real schematic shown in the right of **Figure 25** has a very small combustor section, to ensure a low dwell time and thus increase thrust by reducing energy losses through the endothermic reaction of ammonia breakdown. Some key performance parameters for a hydrazine thruster are plotted in **Figure 29**.

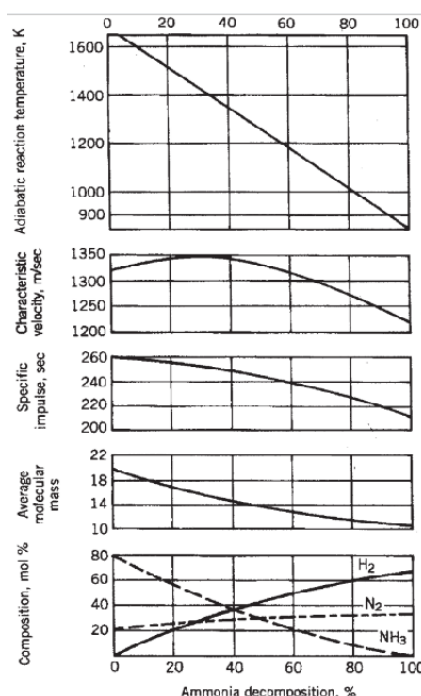


Figure 29: Performance parameters throughout a hydrazine decomposition reaction.

Note that the main parameter effecting the performance of the hydrazine thruster is the percentage of ammonia decomposition, meaning that dwell time is therefore one of the main contributing factors for engine performance.

6.3.2. Dangers of Hydrazine

Hydrazine is highly toxic, corrosive and flammable, meaning that working with this propellant is dangerous and costly. Some of the warning symbols related to hydrazine are shown in **Figure 30**.



Figure 30: Hazard symbols associated with hydrazine (1.flammable 2.corrosive 3.acutely toxic 4.serious health hazard 5.hazardous to the environment)

This provides motivation for the development of **green monopropellants** to decrease costs, allow for in-house refueling and ease of use.

6.3.3. Green Monopropellants: HAN

HAN or hydroxylammonium nitrate is an ionic liquid based compound which is solid at room temperature and often used in solid rocket motors. If mixed with water alcohol it becomes a monopropellant, the chemical formula as well as chemical structure are shown in **Figure 31**.

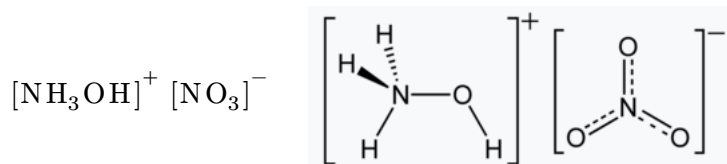


Figure 31: Chemical formula [Left] and chemical structure [right] of HAN.

6.3.4. Green Monopropellants: ADN

ADN or ammonium dinitramide is another ionic liquid based compound which is mixed with methanol, water and ammonia to yield a usable monopropellant. The chemical formula as well as the chemical structure are shown in **Figure 32**.

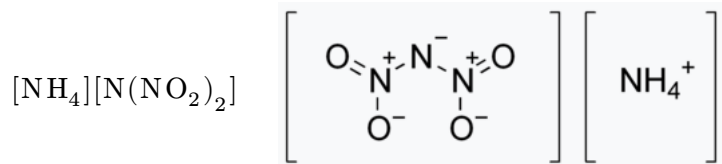


Figure 32: Chemical formula [Left] and chemical structure [right] of ADN.

6.3.5. Green Monopropellant: Hydrogen Peroxide

Hydrogen peroxide (H_2O_2) can also be used as a monopropellant where it decomposes over a catalyst bed into oxygen and water, however the efficiency of hydrogen peroxide as a monopropellant has a lower I_{sp} than the other monopropellant options.

6.3.6. Comparison of Green Monopropellants and Downsides

A table showing the performance of green monopropellents in comparison with traditional monopropellants (hydrazine) is shown in **Table 7**.

Name	Density g/m^3	Specific Impulse s	Temperature $^{\circ}C$	Density Specific Impulse $s \cdot g/m^3$
Hydrazine	1.01	230	1120	232
ADN-based LMP-103S	1.24	244	1600	302
HAN-based AF-M315E	1.46	248	1900	362
98% Hydrogen Peroxide	1.439	198	955	285

Table 7: Performance of hydrazine vs green monopropellants

Some of the main downsides or caveats of green monopropellants are:

- **High temperatures** which require more exotic materials or active cooling.
- **Pre-heating of thruster** up to high temperatures to reach equilibrium temperature of reaction.
- Exact compositions are **owned by companies**.

6.4. Propellant Feed Mechanisms

There exist two main propellant feed mechanisms, these are **pressure driven** and **pump driven**. A system level image for both methods is shown in **Figure 33**.

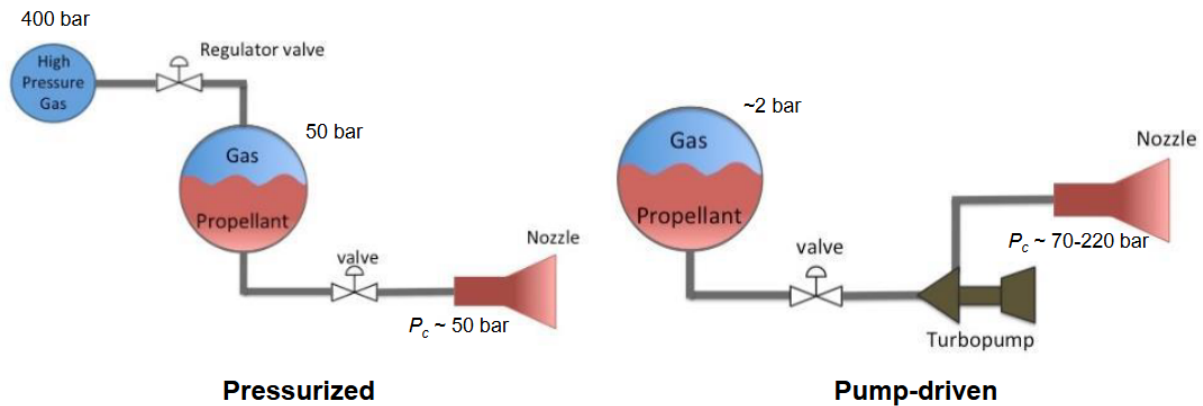


Figure 33: Pressure driven feed system [Left], pump driven feed system [Right]

For launch vehicles which require higher I_{sp} , higher thrust, higher pressures and higher flow rates a **pump driven** system is usually chosen. For spacecraft which require less weight, lower pressures and volume, a **pressure driven** system is chosen.

6.4.1. Pump Driven Propellant Systems: Turbopumps

Turbopumps pressurize the propellant before it enters the combustor, allowing for much higher pressures and flow rates. An example of a turbopump is shown in **Figure 34**.

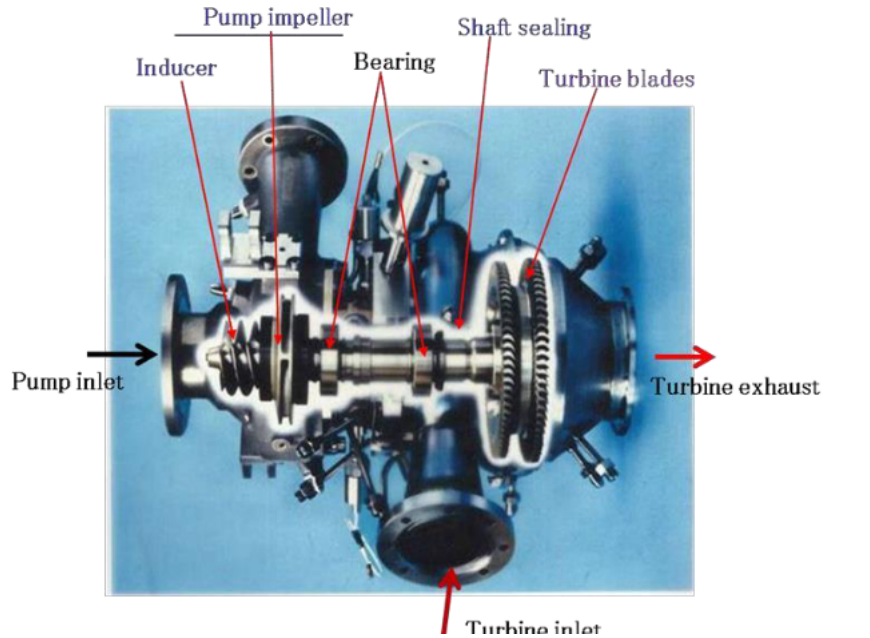


Figure 34: Spacecraft turbopump.

The working principle of a turbopump is that:

1. Propellant enters through the **propellant inlet**.
2. The **inducer** gradually increases the propellant pressure by a small bit, decreasing the chance of cavitation (like pre-stage fan in a jet engine).
3. **Impeller** increases the pressure and kinetic energy of the flow by rotating it axially out of the turbopump.
4. A **diffuser/volute** is placed at the exit of the impeller and converts any kinetic energy the flow has into static pressure.
5. This system is all driven by the **turbine** which is connected on the same shaft as the inducer and impeller. It takes hot energetic flow from the **combustor** and extracts work from it to drive the pump.

6.4.2. Pump Driven Propellant Systems: Open VS Closed Cycle

A pump driven propellant system can be categorized on whether the exhaust from the turbopumps is fed back into the main combustion chamber (**closed cycle**) or if it is dumped externally (**open cycle**). System level diagrams of these are shown in **Figure 35**.

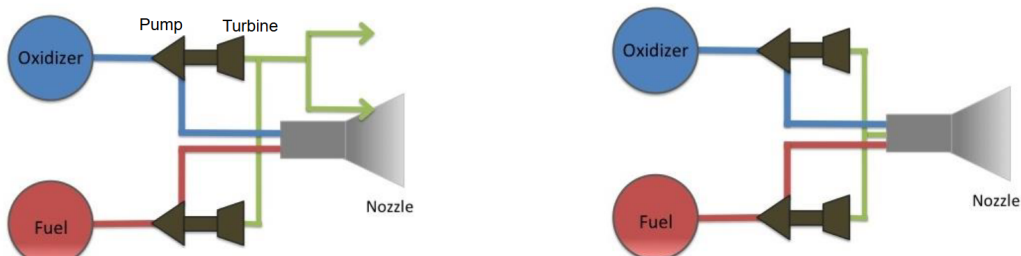


Figure 35: Open cycle propellant feed system [Left], closed cycle propellant feed system [Right].

While open cycle systems are simpler as the turbine's of the turbopump are operated at a lower relative pressure, the closed cycle systems offer higher efficiency (I_{sp}) at the cost of added complexity due to a much higher turbine pressure (turbine pressure must be close to or match combustion pressure.)

6.4.3. Open Cycle Pump Driven Propellant Systems: Gas Generator

In this system, a small amount of fuel and oxidizer are burnt in a **gas generator** (burnt **fuel rich**, keeping temperature low). The exhaust of the gas generator then powers the turbopumps. These systems are **simpler** and have a **lower mass** but have a **lower efficiency** (due to wasting fuel) than closed cycle systems by a few percent. An image of such a systems is shown in **Figure 36**.

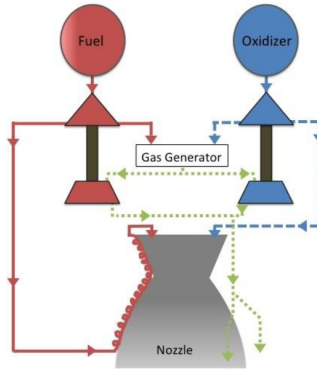


Figure 36: A system level image of a open cycle, gas generator, pump driven propulsion system.

6.4.4. Closed Cycle Pump Driven Propellant Systems: Staged Combustion

Similar to the gas generator system, some fuel and oxidizer are burnt in a **pre-combustor** which drives the turbines. The difference here, is that the exhaust is then piped into the main combustor. This system allows for **higher efficiencies** at the cost of **higher pre-combustor temperatures and pressures**. Note that the pre-combustor is less fuel rich than before, allowing for higher pressures. The pressure in the pre-combustor **must be higher** than the main combustor to avoid backflow, increasing complexity. An image of such a systems is shown in **Figure 37**.

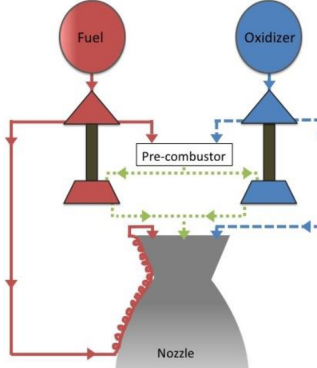


Figure 37: A system level image of a closed cycle, staged combustion, pump driven propulsion system.

6.4.5. Closed Cycle Pump Driven Propellant Systems: Expander Cycle

In this cycle, the turbines are driven by the fuel which is used to cool the nozzle. During the cooling process, the fuel is heated into a gas which is used to drive the turbines. Note that for this system, an initial starter or ignition is required in order to start the system. An image of such a systems is shown in **Figure 38**.

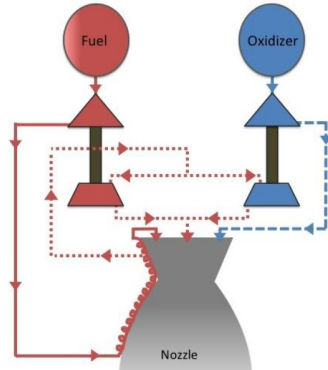


Figure 38: A system level image of a closed cycle, expander cycle, pump driven propulsion system.

6.4.6. Pump Driven Propellant Systems: Comparing cycles

	Merlin	RD-180	F-1	Raptor	BE-4	RS-25
Cycle	Open	Closed (LOX rich)	Open	Closed (Full Flow)	Closed (LOX rich)	Closed (Fuel Rich)
Fuel Type	RP-1	RP-1	RP-1	Methane	Methane	Hydrogen
Total Thrust	0.84 MN	3.83 MN	6.77 MN	2.00 MN	~2.40 MN	1.86 MN
Thrust : Weight	198 : 1	78 : 1	94 : 1	107 : 1	~80 : 1	73 : 1
Specific Impulse (ISP)	282 sl 311 vac	311 sl 338 vac	263 sl 304 vac	330 sl ~350 vac	~310 sl ~340 vac	366 sl 452 vac
Chamber Pressure	97 bar	257 bar	70 bar	270 bar	~135 bar	206 bar

Figure 39: Comparison of different pump driven rocket engines.

6.4.7. Pump Driven Propellant Systems: Alternative Cycles

One alternative cycle used in pump driven systems is **battery powered**. In this system, batteries drive the turbopumps instead of combustion of the propellant and oxidizer, saving on complexity. An example of this cycle is shown in **Figure 40**.

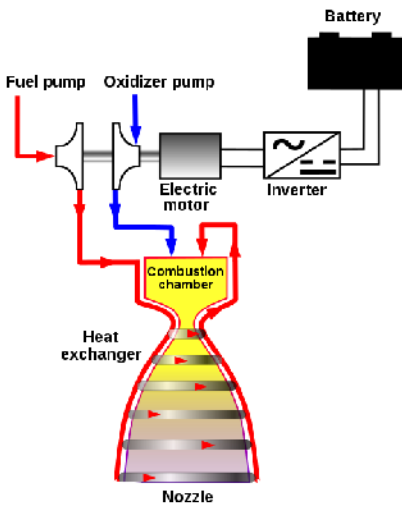


Figure 40: Battery powered propellant feed system schematic [Left], Rutherford engine which uses battery powered propellant feed system [Right].

7. Lecture 7

7.1. Pressurized Propellant Feed Systems

In pressurized propellant feed systems, a high pressure inert gas (such as helium) is fed into the tanks which pushes out the propellant. This means that the **propellant tanks need to have thick walls**, which means that the majority of the system mass is the propellant walls not the engine. Typically these systems are **used in space and yield lower thrusts, chamber pressures and performances**. A system level diagram of a pressure fed system is shown in **Figure 41**.

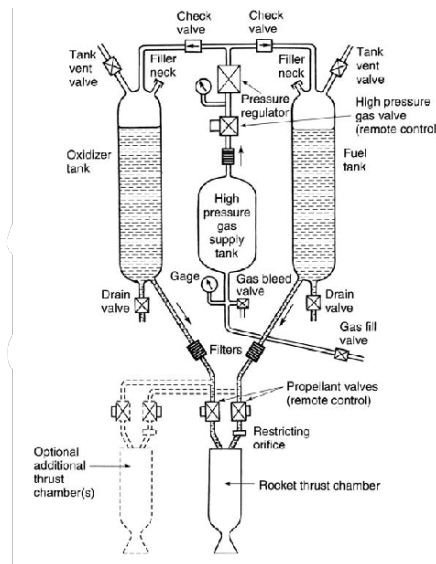


Figure 41: System level diagram of a pressure fed propellant system.

7.1.1. Pressurized Propellant Feed Systems: Blow Down

A **blow down** feed system is the most simple propellant feed system possible where the propellant tank is kept at a high pressure (30 - 40 Bar) which then decreases overtime as the propellant is used up (pressure is not topped up). These systems lead to a drop of pressure and therefore thrust over the lifetime of the engine. A system level image of this system as well as the pressure and thrust overtime are shown in **Figure 42**.

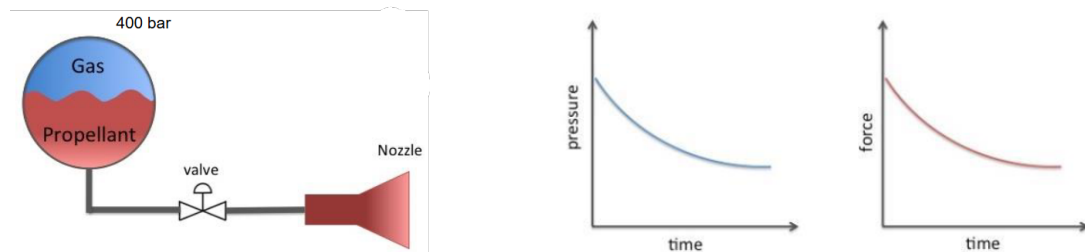


Figure 42: System level diagram of a blow down feed system [Left], thrust and pressure over time for a blow down system [Right].

7.1.2. Pressurized Propellant Feed Systems: Pressure Regulated

A **pressure regulated** system ensures that the pressure in the tanks remains the same over time by topping up the tanks with an inert high pressure gas. These systems ensure optimal thrust over the lifetime of the engine at the cost of **complexity** as the **regulator valve** is complex and is needed to allow for the small opening of the valve to ensure constant pressure. A system level image of this system as well as the pressure and thrust overtime are shown in **Figure 43**.

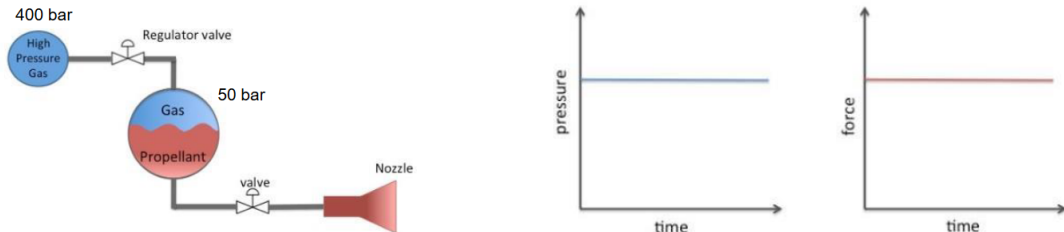


Figure 43: System level diagram of a pressure regulated feed system [Left], thrust and pressure over time for a pressure regulated system [Right].

7.1.3. Pressurized Propellant Feed Systems: Bang Bang

Bang bang systems are a variant of the **pressure regulated** system where instead of a regulator valve, a solenoid valve (bang bang valve) is used which can either be opened or closed. When the pressure in the propellant tank is below a certain value, the valve opens adding pressure until it reaches the cutoff pressure when the valve closes. This allows for a **simpler system** at the cost of a **jagged thrust profile**. A system level image of this system as well as the pressure and thrust overtime are shown in **Figure 44**.

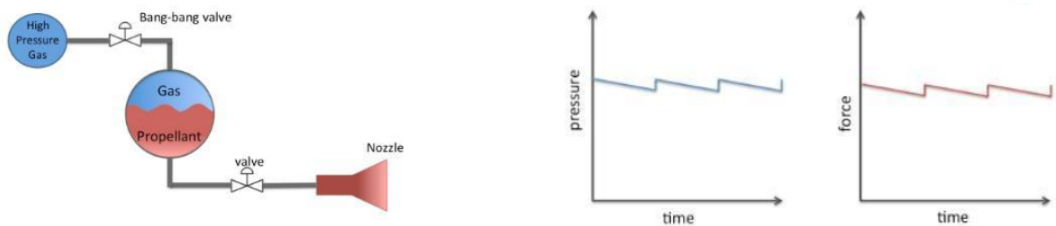


Figure 44: System level diagram of a bang bang feed system [Left], thrust and pressure over time for a bang bang system [Right].

7.2. Case Study: NASA Cassini Mission

The Cassini mission was a joint NASA ESA mission to investigate Saturn and its moon. The spacecraft was launched in 1997 by a Titan IV rocket and arrived at Saturn in 2004. The mission consisting of fly bys as well as the landing of a probe on Titan concluded in 2017. An image of the spacecraft is shown in **Figure 45**.

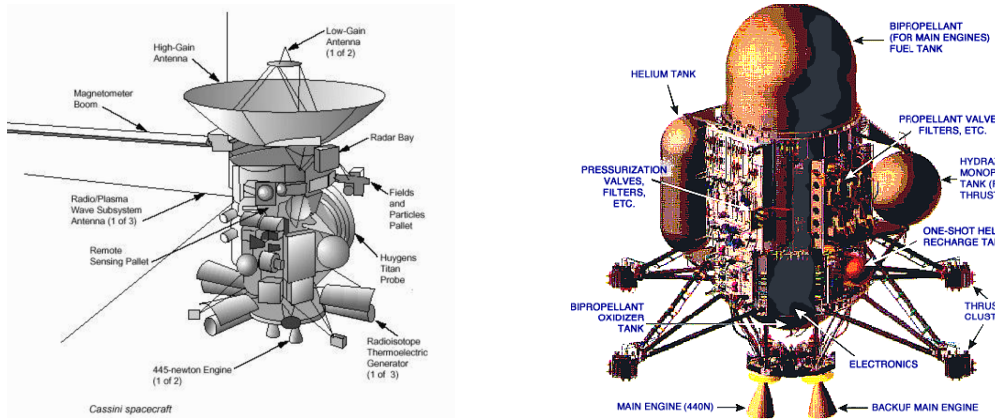


Figure 45: Labelled diagram of the Cassini probe [Left], labelled diagram of the propellant tanks and thrusters for Cassini [Right]

In terms of the propulsion system, the spacecraft used **MMH** for the fuel and **nitrogen tetroxide** for the oxidizer for the main engines whereas for the four attitude control thrusters, **hydrazine** was used. Both systems would have their pressure replenished by a high pressure helium tank. The propellant delivery schematic for the Cassini probe is shown in **Figure 46**.

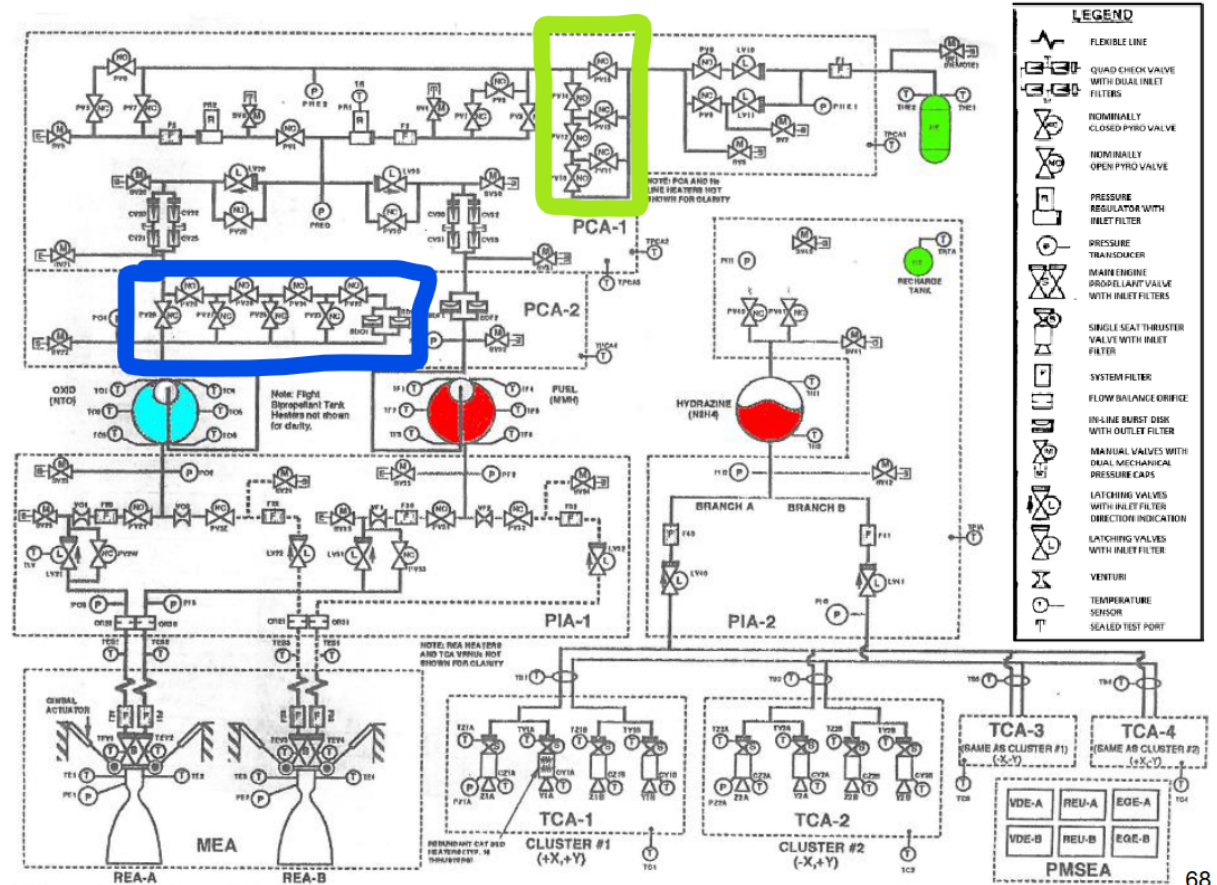


Figure 46: Cassini propellant delivery schematic.

In the bottom right of **Figure 46**, the attitude control thrusters as well as the hydrazine tank are shown. On the left side of **Figure 46** shows the **pressure fed bipropellant engine**

($T \approx 400N$) with the MMH tank shown as light blue and the nitrogen textroroxide tank in red. The blue labelled section was a system of **pyro ladders** which controlled the pressure-regulated side of the system. The green was the redundant blow down system. Finally, every component had at least two levels of redundancy to the point that there were even two engines. A table detailing the different propulsion events for the mission is shown in **Figure 47**.

Event	Event or Phase End Date	Days From Launch	High ΔV (mps)	Pre-Maneuver Pressure (psia)	Pre-Maneuver Mass (kg)	Pyro Isolation Status
Launch	10/22/97	0	0	100	5609	Isolated
Press'n	11/13/97	22	0	250	5609	0-1
TCM-1	11/16/97	25	24	250	5609	Regulated
Post Sat	12/15/97	55	0	250	5564	c-1
TCM-2	3/3/98	132	3.5	250	5564	Blowdown
TCM-3	4/12/98	172	0.3	243	5557	Blowdown
Venus-1	5/2/98	192	0	243	5557	-
TCM-4	5/22/98	212	25.6	205	5557	Blowdown
Repress	11/30/98	404	0	205	5509	0-2
DSM-1	12/2/98	406	435.4	25 L..	5509	Regulated
Isolate	12/3/98	407	0	250	4760	c-2
TCM-5	1/5/99	440	13.8	250	4760	Blowdown
TCM-6	4/25/99	550	0.6	245	4738	Blowdown
TCM-7	6/4/99	590	0.1	245	4737	Blowdown
Venus-2	6/24/99	610	0	245	4737	Blowdown
TCM-8	7/4/99	620	82.7	245	4737	Blowdown
TCM-9	7/19/99	635	6.8	218	4607	Blowdown
TCM-10	8/8/99	655	3.8	216	4597	Blowdown
Earth	8/18/99	665	0	215	4591	-
TCM-11	9/7/99	685	45.7	204	4591	Blowdown
TCM-12	6/12/00	964	2.2	203	4521	Blowdown
TCM-13	10/10/00	1084	0.7	203	4518	Blowdown
TCM-14	12/9/00	1144	1	203	4517	Blowdown
Repress	6/1/04	2414	0	203	4515	0-3
SCI	7/1/04	2444	594	250	4515	Regulated
PRM	9/16/04	2521	264	25 Q..	3701	Regulated
Isolate	9/17/04	2522	0	250	3387	c-3
ODM	12/3/04	2599	3.8	250	3387	Blowdown
Tour	7/1/08	3905	497	246	3344	Blowdown
EOM	7/1/08	3905	0	203	2830	-

Figure 47: Cassini propulsive events.

Note that for important manuevers such as flybys the pressure regulated section of the system is used whereas for general manuevers the blow down section of the system is used.

7.3. Cold Gas Thrusters

These are the most basic thruster systems often used in **attitude control systems**, **micro or nano** satellites. These systems consis of a **high pressure gaseous propellant** is fed into a nozzle (flow controlled via valve) without any heating or reactions. Typically these systems are pressurized from **30 to 100 MPa** with **nitrogen being commonly used** due to its **inertness** as well as **low molecular mass** and relatively **high density**. The performance of different propellents is shown in **Table 8**.

Propellant	Molecular Mass (W)	Density (g/cm ³))	Ratio Specific Heats (k)	Theoretical (I _{sp})
Hydrogen	2.0	0.028	1.40	284
Helium	4.0	0.057	1.67	179
Methane	16.0	0.23	1.30	114
Nitrogen	28.0	0.39	1.40	76
Air	28.9	0.41	1.40	74

Propellant	Molecular Mass (W)	Density (g/cm^3)	Ratio Specific Heats (k)	Theoretical (I_{sp})
Argon	39.9	0.57	1.67	57
Krypton	83.8	1.19	1.63	50

Table 8: Theoretical performance of different cold gas propellant

However, the performances detailed in **Table 8** are only theoretical and in reality there are several losses in cold gas thrusters such as:

- Many molecules are very small meaning that the thrust produced by exhausting them is low.
- Over the nozzle, the temperature of the exhaust decreases which can go below the boiling temperature. This phase change sucks out energy, further decreasing performance.

In reality therefore, the thrust and performance of these engines is much lower, some real world cold gas thrusters are shown in

Thruster	Max Thrust (N)	Chamber Pressure (MPa)	$I_{sp}(s)$
Bradford Engineering PMT	0.002	0.25	60
Moog 58-118	3.6	1.59	65
RDMT-5	5		70
Vacco MIPS	55		65

Table 9: Real performance of different cold gas propellant

8. Lecture 8

8.1. Intro to Solid Propulsion

In their most primitive form, solid rocket boosters consist of a fuel and oxidizer that are bound together using a binder and are located within the combustion chamber itself. When ignited via an ignitor the mixture burns in place and is accelerated through a nozzle to produce thrust. Note that once ignited, solid rocket boosters cannot be stopped. They are used in two main scenarios, shown below. Note that the basic constituent parts of a SRB are shown in **Figure 48**.

- **Launch Vehicles:** The total required impulse is already known before launch and doesn't change so SRBs can be used.
- **When restarts are not needed**

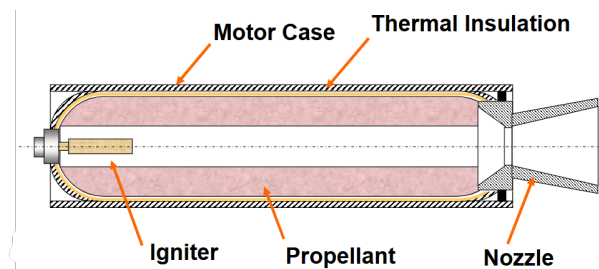


Figure 48: Constituent parts of a SRB.

8.2. Grain Shape and Thrust

Depending on the shape of the grain within the solid rocket motor, the thrust produced by the engine can vary. Various grain shapes and their associated thrust curves are shown in **Figure 49**.

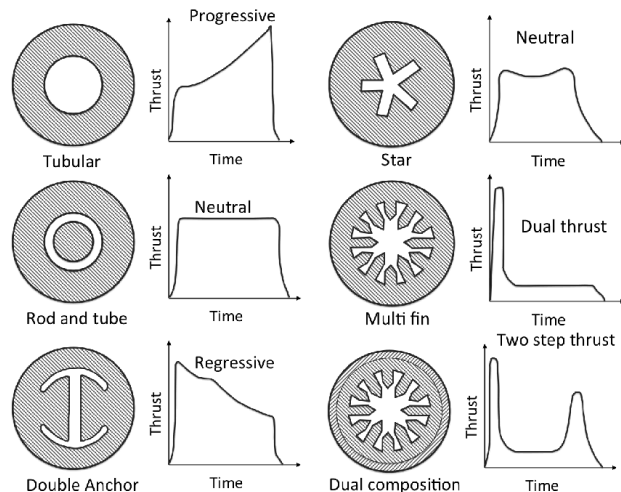


Figure 49: Effect of grain shape on the thrust profile..

The most common grain shape used is the **star** shape as this gives a quasi-constant thrust profile over the burn time. Note that for the **rod and tube** design, the tube can become

easily dis-logged and cause issues. Typically SRBs will have a star grain pattern at the top with a tubular pattern below.

8.3. Mass Flow and Burning Rates

The equation for the mass flow rate of the exhaust of the solid propellant is given by **Eq. 42**

$$\dot{m} = A_b \dot{r} \rho_p \quad (42)$$

Where:

- \dot{m} : Mass flow rate (kg/s)
- \dot{r} : Burn rate (m/s)
- A_b : Burn area (m^2)
- ρ_p : Propellant density (kg/m^3)

The burn rate shown in **Eq. 42** is given by the empirical formula detailed in **Eq. 43**.

$$\dot{r} = a P_c^n \quad (43)$$

Where:

- P_c : Chamber pressure (Pa)
- a : Burn rate Coefficient,
- n : Burn rate exponent

The burn rate typically varies from 0.6 - 1.3 cm/s but can reach values of 5 cm/s in extreme cases. n typically varies from 0.2 - 0.6 with $n > 1$ leading to combustion instabilities.

8.3.1. Burning Effects: Burn Rate Exponent

The value of n controls how quickly the reaction flattens at a fixed burn rate, as shown in **Figure 50**.

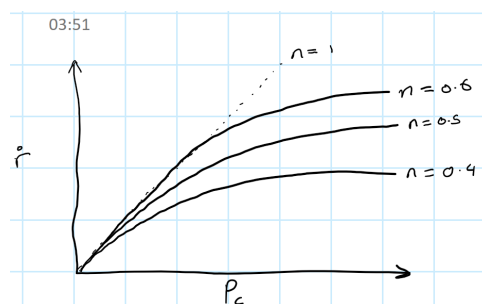


Figure 50: How changing n effects the burn rate.

Larger values of n mean an eventual higher burn rate and vice versa. Note that the value of $n = 1$ acts as an upper limit.

8.3.2. Burning Effects: Plateau and Mesa Burning

Plotting the burn rate on a log plot yields **Figure 51**. **Plateau** burning occurs when the binding material begins to breakdown and **Mesa** burning is another burning phenomena.

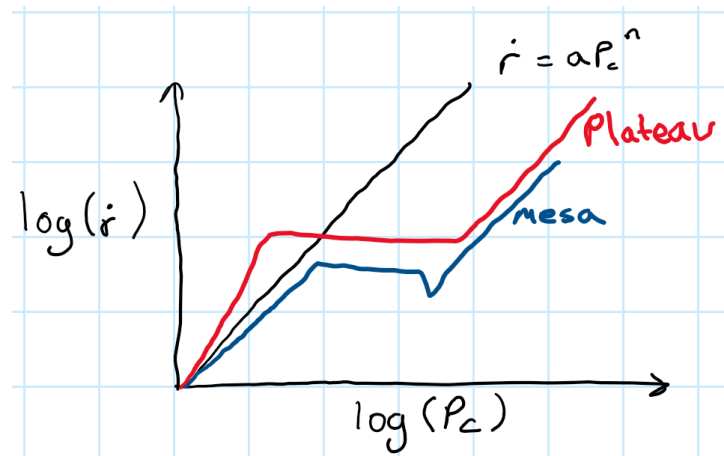


Figure 51: Mesa and Plateau burning.

8.3.3. Burning Effects: Ambient Temperature

Ambient temperature also has an effect on the performance as shown in **Figure 52**.

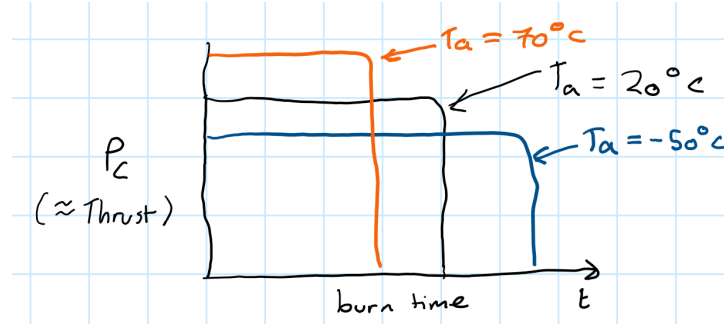


Figure 52: Effect of ambient temperature on thrust curve.

Note that higher ambient temperatures yield shorter burn times and vice versa. Note that the area under the graphs must remain constant as the amount of propellant doesn't change. The degree with which the temperature or pressure change with a given change in ambient temperature are given by the equations shown in **Eq. 44**.

$$\sigma_p = \left(\frac{\partial \ln(r)}{\partial T_b} \right)_{P_c} = \frac{1}{r} \left(\frac{\partial r}{\partial T_b} \right)_{P_c} \quad (44.1)$$

$$\pi_K = \left(\frac{\partial \ln(P_c)}{\partial T_b} \right)_K = \frac{1}{P_c} \left(\frac{\partial P_c}{\partial T_b} \right)_K \quad \text{Where } K = \frac{A_b}{A_t} \quad (44.2)$$

8.3.4. Burning Effects: Erosive Burning

Another parameter which effects the burning behavior is **erosive burning**, which occurs when high speed combustion products flow over the burning surface. An example where this can occur is if the inner radius of a tubular grain is similar to the throat area, this mean the edges of the grain near the throat see a non-zero velocity flow and so are burnt away quicker. An image depicting this example as well as the effect it has on the thrust curve is shown in **Figure 53**.

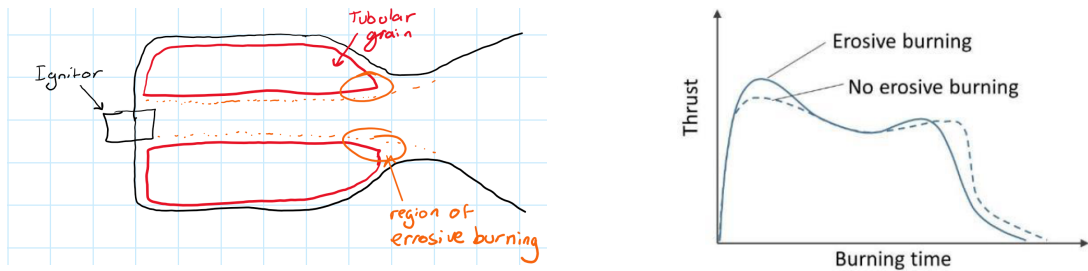


Figure 53: Diagram depicting erosive burning [Left], thrust graph overtime with and without erosive burning [Right].

8.3.5. Burning Effects: Acceleration

For an annular (or similar) grain where the burning occurs along the center of the rocket, spinning the rocket will **increase** the peak thrust whilst **reducing** the burn time, this is shown in **Figure 54**.

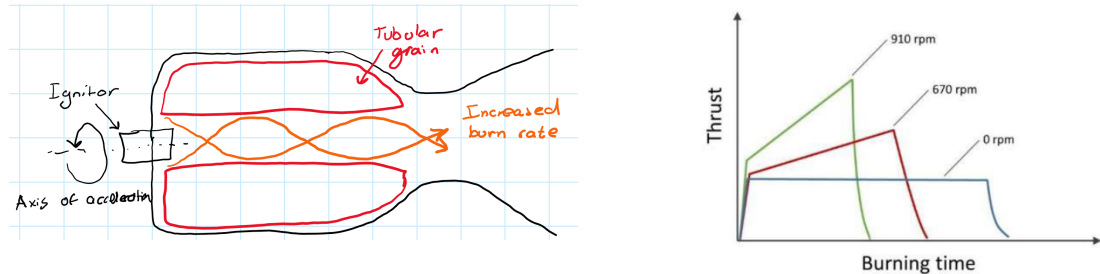


Figure 54: Diagram depicting burning under rotational velocity [Left], thrust graph overtime at various angular velocities. [Right].

In contrast, for a simple block of grain which is burning from the bottom, a lateral velocity will see a decrease in the peak thrust, this is shown in **Figure 55**.

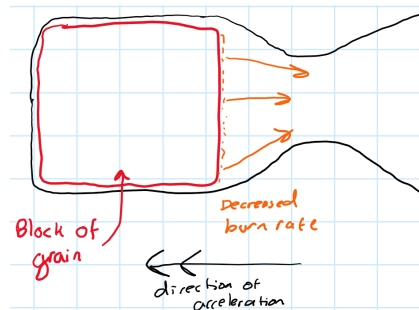


Figure 55: Diagram depicting the effect of lateral acceleration on a block grain.

8.3.6. Burning Effects: Metal Wires

The burning behavior can also be controlled through the embedding of metal wires, typically of silver or aluminum.

8.4. Solid Propellants

8.4.1. Double Base

A double base propellant consists of two monopropellant molecules where one is a **high energy** unstable molecule and the other is a **low energy** more stable gelling molecule. The most common double base propellant is nitroglycerin and nitrocellulose, shown in **Figure 56**.



Figure 56: Molecular structure and chemical formula for nitroglycerin [Left], molecular structure and chemical formula for nitrocellulose [Right].

When nitroglycerin and nitrocellulose are burnt together, the nitroglycerin acts as the high-energy component and nitrocellulose acts as the stabilizer. When burnt together, these two monopropellents **burn smokeless**, have an $I_{sp} \approx 210$ and have a **low density**.

8.4.2. Composite

Composite propellents have a better performance than double base propellents and consist of multiple constituent parts which are:

- **Fuel:** Typically a metal powder (normally Aluminum).
- **Oxidizer:** Typically an inorganic salt (ammonium perchlorate).
- **Binder:** Forms the fuel and oxidizer into a rubber/cement like grain.

Some common fuels and oxidizers are shown in **Table 10**.

Name	Chemical Formula	Molecular Mass (W)	Density (kg/m^3)	Notes
Fuels				
Aluminium (powder)	Al	26.98	2.70	Widely used, good performance
Boron (powder)	B	10.81	2.34	High gravimetric and volumetric energy.
Magnesium (powder)	Mg	24.31	1.74	Easy ignition and high temp burning.
Oxidizers				
Ammonium Perchlorate	NH_4CIO_4	59.5	1950	High performance, low cost
Ammonium Nitrate	NH_4NO_3	60	1730	Smokeless, moderate performance, low cost
Sodium Nitrate	NaNO_3	56.4	2170	Moderate performance

Name	Chemical Formula	Molecular Mass (W)	Density (kg/m ³)	Notes
Potassium Perchlorate	KC ₁ O ₄	46.2	2520	Moderate performance, low regression rate
Potassium nitrate	KNO ₃	47.5	21120	Low cost, low performance
Binders				
Hydroxyl-Terminated Polybutadiene (HTPB)	(C ₄ H ₆) _n (OH) ₂	54.09	0.90-0.92	Industry-standard inert binder but has a decent fuel contribution.
Glycidyl Azide Polymer (GAP)	(C ₃ H ₅ N ₃ O) _n	99.09	1.10-1.30	Energetic binder with higher performance than inert binders, more expensive, more sensitive.

Table 10: Common solid composite fuels, oxidizers and binders

8.5. Solid Propellant Performance

Plotting the performance of different solid propellant fuels against their burn rates yields **Figure 57**. Note that the maximum I_{sp} of a solid rocket motor is only 250s which is less much less than a chemical rocket. Also the method of by which the solid grain is form (extrusion or casting) further effects the performance. Finally their are hybrid grains which are both double base and composite as is shown in the figure.

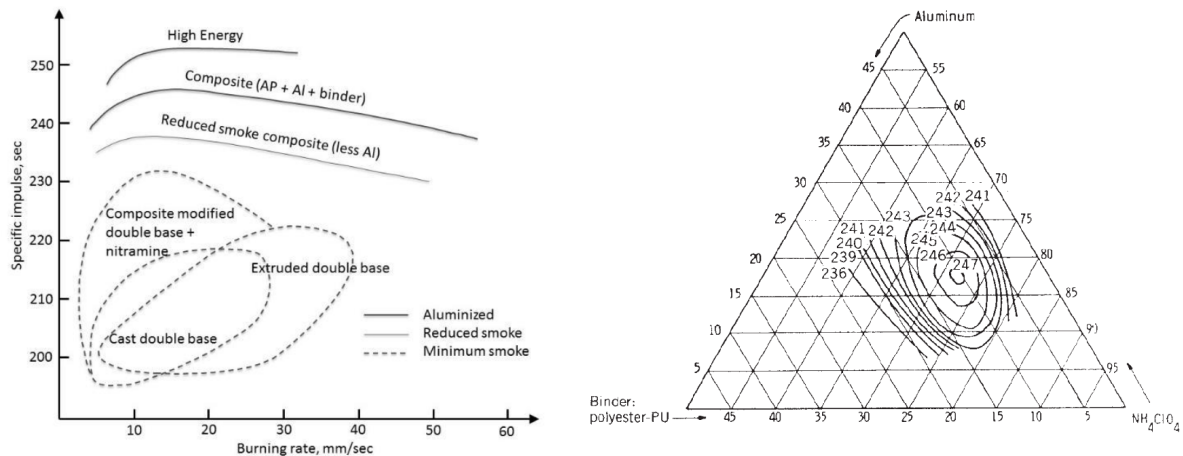


Figure 57: Performance against burn rate for different solid rocket propellents [Left], solid composite fuel performance [Right].

On the right of **Figure 57**, there is a graph which shows the performance of different percentage makeup of the oxidizer, fuel and binder for a composite fuel.

8.6. Real Solid Propellant Makeup

The realistic makeup of a double base, composite and hybrid double base composite solid fuel are shown in **Table 11**.

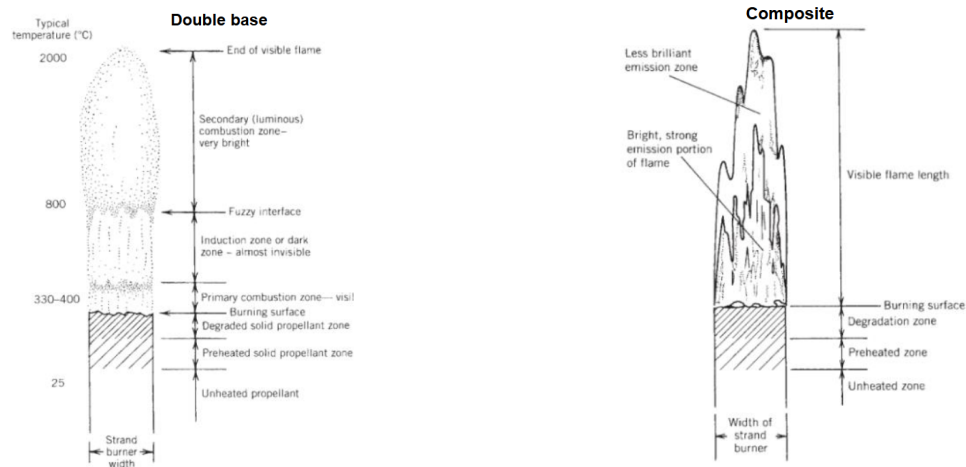
Double Base		Composite		Composite Modified Double Base	
Ingredient	Mass %	Ingredient	Mass %	Ingredient	Mass %
Nitrocellulose	51.4	Ammonium perchlorate	70.0	Ammonium perchlorate	20.4
Nitroglycerine	43.0	Aluminium powder	16.0	Aluminium powder	21.1
Diethyl phthalate	3.2	Polybutadiene acrylonitrile copolymer	11.78	Nitrocellulose	21.9
Ethyl centralite	1.0	Epoxy curative	2.22	Nitroglycerine	29.0
Potassium sulfate	1.2			Triacetin	5.1
Carbon black	< 1			Stabilizers	2.5
Candelilla wax	< 1				

Table 11: Makeup of different solid rocket fuels.

Note that **Diethyl phthalate** is a plasticizer which is added to the double base to allow for easier moulding. **Carbon black** is added in small quantities as an opacifier to make the grain darker and thus reduce radiative heating. **Candelilla wax** is added to make it easier for the grain to escape the mould.

8.7. Solid Propellant Flame Structure

Double base solid rocket fuels feature the fuel and oxidizer bound together on the same molecule allowing for a smokeless clean burn. However for composite fuels, the oxidizer is separate from the fuel leading to a much more chaotic and uncontrolled burn, these effects are depicted in **Figure 58**.



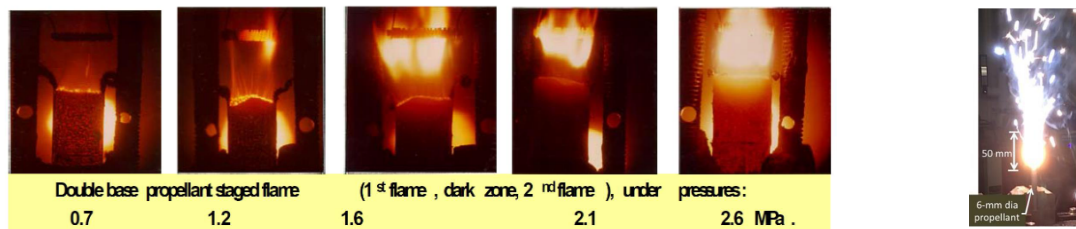


Figure 58: Double base fuel flame structure [Top Left], Composite fuel flame structure [Top Right], Real double base flame [Bottom Left], Real composite flame structure [Bottom Right]

8.8. Solid Rocket Ignition Systems

For different scales of solid rocket motor there exists two different types of ignition systems, these are explained below and shown visually in **Figure 59**.

- **Pyrotechnic Ignitor:** Generate a hot flame via explosives or energetic propellant-like formulations.
- **Pyrogenic Ignitor:** Essentially a small solid rocket motor optimized for heat not thrust.

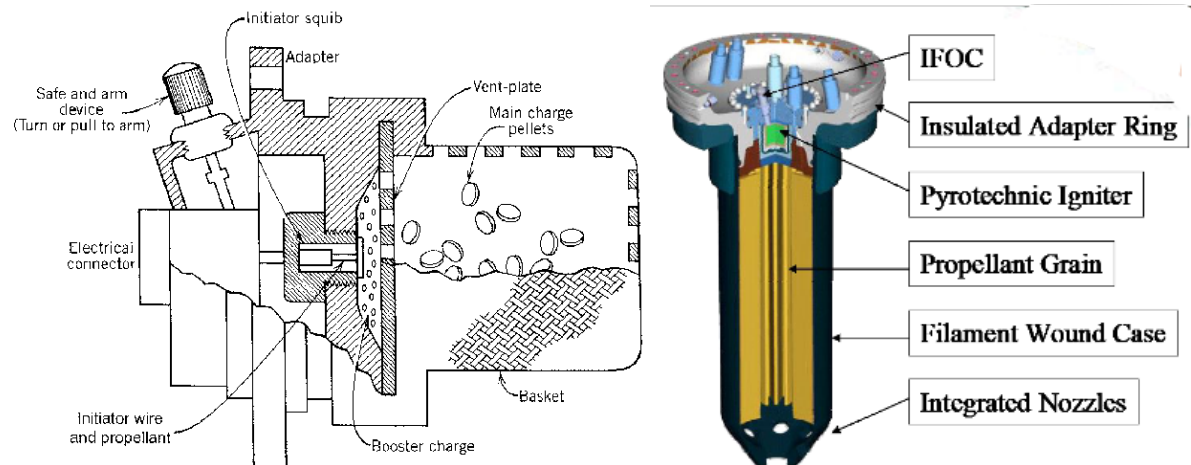


Figure 59: Pyrotechnic ignitor [Left], pyrogenic ignitor [Right]

For pyrotechnic ignitors, an initial arc may combust a squib, which then combusts a booster or intermittent charge (made from a excitable solid fuel formulation) which then ignites a basket of fuel (disks of solid rocket fuel) which is then vented into a solid rocket motor. for pyrogenic ignitors, a pyrotechnic ignitor first ignites a small solid rocket motor optimized for heat which is exhausted into the main solid rocket motor.

8.9. Hybrid rockets

A hybrid rocket is a combination of a bipropellant liquid and solid rocket. A typical hybrid rocket consists of a liquid oxidizer with a solid fuel. The inverse configuration does exist but is rarely used. An image depicting the key components of a solid rocket motor are shown in **Figure 60**.

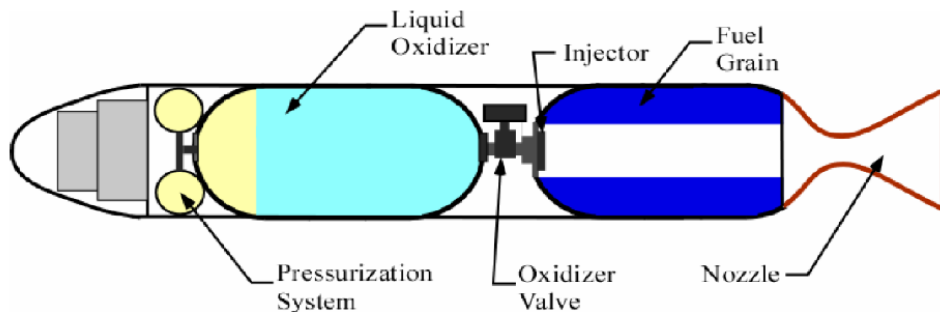


Figure 60: System level diagram of a hybrid solid rocket motor.

8.9.1. Advantages of Hybrid Rockets

Some key advantages of hybrid rockets over liquid bipropellant rockets and solid rockets are listed below. The performance of all three rocket motor types is shown in **Table 12**.

- Safer and relatively simpler than liquid bi-propellant and solid rockets.
- Has start, stop and throttling capabilities which are not present on solid rockets.
- Have a higher I_{sp} than solid rocket motors.

Type	I_{sp} at Sea Level	Thrust Range (N)
Solid	< 250s	$\leq 10^7$
Liquid bipropellant	H ₂ /LOX: 380s	$\leq 10^7$
	RP1/LOX: 300s	
Hybrid	300s	$\leq 10^6$

Table 12: Comparative performance of liquid bipropellant, solid and hybrid rockets.

8.9.2. Disadvantages of Hybrid Rockets

Some key disadvantages of hybrid rockets over liquid bipropellant rockets and solid rockets are listed below. Note that the biggest problem with hybrid rockets are the low fuel regression rates.

- No independent control of fuel mass flow rate which effects combustion.
- O/F mixture ratio (and performance) may vary due to variable **fuel regression rate** (typically $< 1\text{mm/sec}$, which limits thrust).
- Poorly known or understood due to small number of examples.
- Typically lower performance than for liquid bipropellant.
- Prone to large-amplitude, low-frequency pressure fluctuations (chugging) and higher frequency flame instabilities.

9. Lecture 9

9.1. Hybrid Rocket Combustion

Combustion within a solid rocket motor is much more complex than the combustion that takes place in solid or liquid rockets, as shown in **Figure 61**.

Fuel gasification and combustion

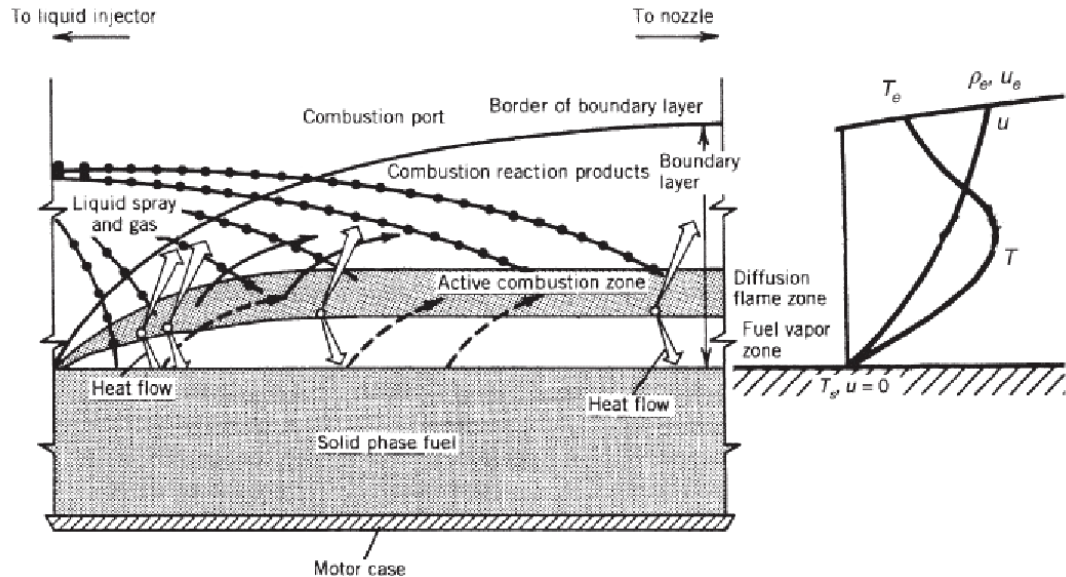


Figure 61: Combustion for hybrid rockets.

Note that there is a **highly turbulent boundary layer** which forms on the surface of the fuel grain. Heat is transferred through convection and radiation through the boundary layer into the fuel grain which evaporates it and allows for combustion to take place, due to this complex mechanism, the regression rates for the fuel grain are **typically one third of that of solid rockets**. The fuel surface regression rate against the flow rate of oxidizer is shown in **Figure 62**.

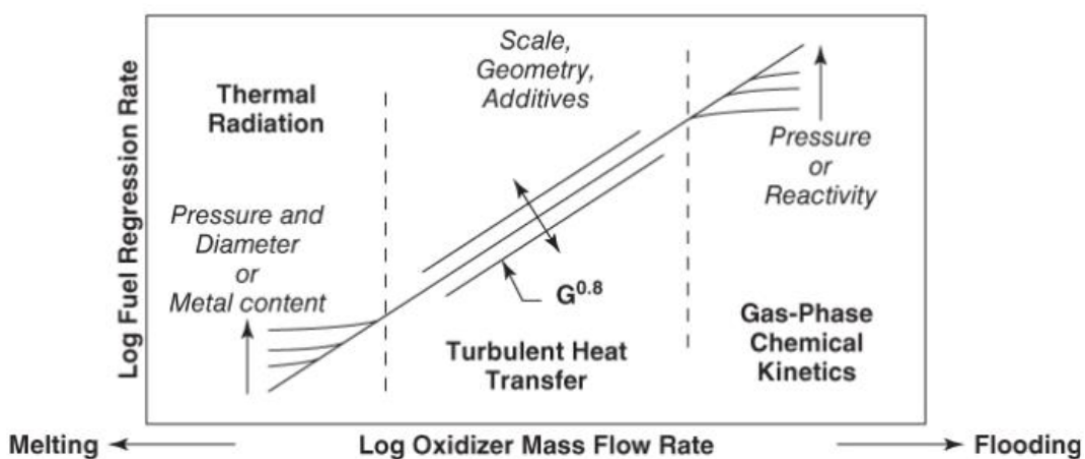


Figure 62: Plot of oxidizer flow rate against fuel regression rate.

For **low oxidizer flow rates** the heat transfer is **radiation dominated** and the fuel regression rate is low. For **intermediate values of oxidizer flow rate**, the heat transfer is **convection dominated** with the turbulent boundary layer behavior seen in **Figure 61**. Finally at very **high oxidizer flow rates** phase change and chemical kinetics take over.

9.2. Hybrid Rocket Equations

Using **Figure 62**, equations for the regression rate as well as the mass flow rate can be generated, the equation for regression rate is shown in **Eq. 45**.

$$\dot{r} = aG_{ox}^n = a \left(\frac{\dot{m}_{ox}}{N\pi R_p^2} \right)^n \quad (45)$$

Where:

- G_{ox} : Oxidizer mass flux (kg/m^2s)
- \dot{m}_{ox} : Oxidizer mass flow rate (kg/s)
- N : Number of circular ports
- R_p : Radius of circular ports (m)

Note that in **Eq. 45**, the empirical exponent n typically ranges between 0.4 - 0.8. **Eq. 45** can then be substituted into the equation for mass flow rate, **Eq. 42**, to yield **Eq. 46**.

$$\dot{m}_f = \rho_f A_p(t) \dot{r} = 2\pi^{1-n} \rho_f N^{1-n} a \dot{m}_{ox}^n R_p^{1-2n} L \quad (46)$$

Where:

- ρ_f : Fuel grain density (kg/m^3)
- A_p : Fuel grain surface area (m^2)
- L : Fuel grain length (m)

Note that the value of the empirical exponent n in **Eq. 46** effects the behavior of R_p in the following ways:

- for $n < 0.5$ fuel mass flow rate increases as R_p increases
- for $n > 0.5$ fuel mass flow rate decreases as R_p increases
- for $n = 0.5$ fuel mass flow rate remains constant as R_p increases

9.3. Hybrid Rocket Propellents

Typical hybrid rocket oxidizers are:

- Nitrous oxide, hydrogen peroxide, LOX, Hydroxyl ammonium nitrate

Typical hybrid rocket fuel grains are (parrafin wax used to increase regression rate):

- HTPB, PBAN, rubber, paraffin wax

Note that hybrid rockets are an area of on going research with exotic propellant and various embeddings being looked into.

An injector sits at the top of a combustion/decomposition chamber and has a few main purposes, these are:

- Introduce the liquid (fuel or oxidizer or both) into the combustion chamber and meter its flow rate.
- Cause the liquid to break up into smaller drops.
- Distribute and mix the propellants.
- Isolate the propellant tank from the thruster chamber through a suitable pressure drop across the injector.

Note that the pressure drop is very important, or combustion instabilities will cause upstream issues and effect flow rates. There are three main types of injectors that are used, and these are detailed in the following sections.

9.4.1. Orifice Injector

Also known as a hole injector, this class of injectors consist of holes through which the liquid is fed through. Typically these are designed with alternating holes of fuel and oxidizer and the spray from the holes is designed to impinge on adjacent holes. An image of a orifice injector is shown in **Figure 63**.

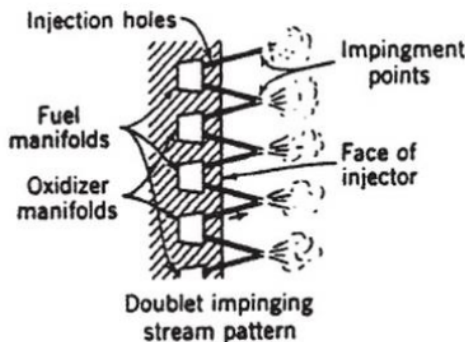


Figure 63: Image of an orifice injector.

9.4.2. Spray Injectors

This class of injectors inject the liquid into a cylindrical chamber where it swirls around and is then released into a conical jet shape **Figure 64**.

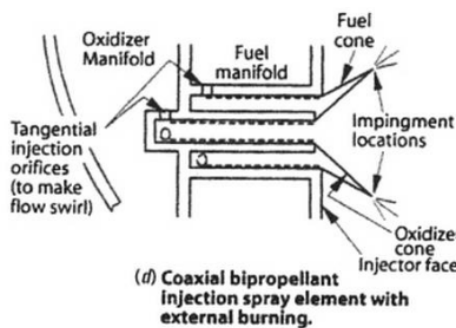


Figure 64: Image of a spray injector.

9.4.3. Pintle injectors

This class of injectors sprays one liquid into an internal channel with a 90 degree turn at the end. The other liquid is then sprayed on the outside of the channel, meaning when both liquids meet they mix and form a conical plume. This injector is shown in **Figure 65**.

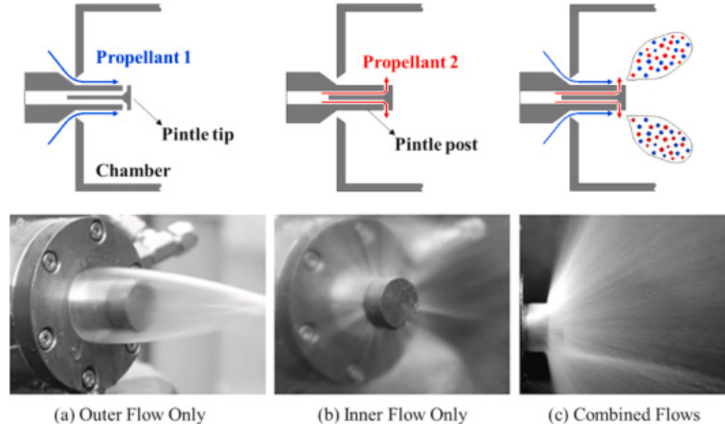


Figure 65: Image of a pintle injector.

9.4.4. Orifice Pressure Drop

The equation for the pressure drop across an orifice type injector can be calculated by considering the change in pressure being equal to the dynamic pressure and using the mass flow rate equation. This expression is shown in **Eq. 47**.

$$\dot{m} = C_d A \sqrt{2\rho \Delta P} \quad \rightarrow \quad \Delta P = \frac{1}{2\rho} \left(\frac{\dot{m}}{C_d A} \right)^2 \quad (47)$$

Where C_d is the coefficient of discharge and is present as $A_{\text{eff}} < A$. A typical range for the pressure drop is 0.2 - 0.3 P_c , any higher and **energy is being wasted**, any lower and **combustion oscillations will effect the upstream flow**. Typical values for $C_d \approx 0.65 - 0.7$. To determine C_d empirically, \dot{m} would be plotted against $\sqrt{\Delta P}$ for water flowing through the nozzle. This gives the gradient of the straight line (through the origin) as $C_d A \sqrt{2\rho}$, which allows for the calculation for C_d .

10. Lecture 10

10.1. Thrust Chambers

The thrust chamber is where combustion/burning occurs. Here liquid propellant is injected, atomized, vaporized, mixed and burnt. Chamber volume is typically maximized and depends on heat, propellant used, heating and manufacturing constraints. The key dimensions for a thrust chamber are shown in **Figure 66**.

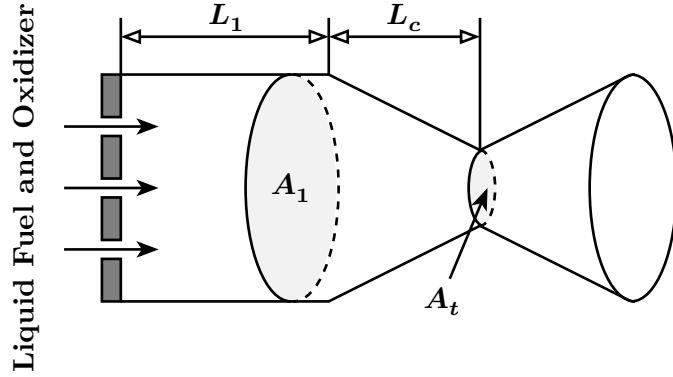


Figure 66: Thrust chamber dimensions.

Note that in **Figure 66**, the dimensions of the thrust chamber are simplified into conical sections. The volume of a combustion chamber is a key parameter and its formula is shown in **Eq. 48**.

$$V_c = A_1 L_1 + \frac{1}{3} A_1 L_c \left(1 + \sqrt{\frac{A_t}{A_1} + \frac{A_t}{A_1}} \right) \quad L * = \frac{V_c}{A_t} \quad (48)$$

Where:

- V_c : Combustion volume (m^3).
- L_1 : Cylindrical section length (m).
- A_t : Throat area (m^2).
- A_1 : Cylindrical section area (m^2).
- L_c : Converging section length (m).
- $L *$: Characteristic length (m).

For the characteristic length shown in **Eq. 48**, $L * \approx 0.8 - 3m$ and for monopropellants this value is even higher. The stay time for a droplet of fuel within the combustion chamber is shown in **Eq. 49**.

$$t_s = \frac{V_c}{\dot{m} V_1} \quad (49)$$

Where t_s is the stay time and V_1 is the the volume per unit mass of propellant within the chamber. The stay time defines the time for vaporization, mixing and combustion of the propellant and is experimentally determined with $t_s \approx 0.001 - 0.04s$.

10.2. Thrust Chamber: Heat Transfer

Thrust chambers can reach very high temperatures due to the combustion and compression that takes place within them (for monopropellant 1000K and for bipropellant 3000K). Nozzles must be designed to withstand this temperature as well as the associated stresses and

the pressure from the exhaust itself. The temperature variation across a nozzle is shown in **Figure 67**.

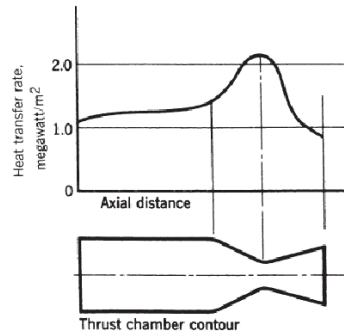


Figure 67: Temperature variation over a nozzle.

These high temperatures require some form of cooling in order to stop the nozzle and combustion chamber from melting.

10.2.1. Radiation Cooling

In this method of cooling, a material is chosen with a high emissivity which allows for heat to be radiated away from the nozzle. This method works well for small - medium engines as well as engines beyond a certain expansion ratio. The material used must be able to withstand high temperatures, some commonly used materials are Niobium, rhenium, and carbon-carbon composites.

10.2.2. Regenerative Cooling

This method of cooling is widely used in launch vehicles and large engines. In this method a liquid (typically the fuel) flows around the nozzle and thrust chamber before it is fed into the combustion chamber, cooling the nozzle and thrust chamber. In this method **no energy is lost** and specific cooling can be achieved by varying the diameter and number of cooling channels. An image of a regeneratively cooled nozzle is shown in **Figure 68** and the associated temperature variation across the wall is shown in **Figure 69**.

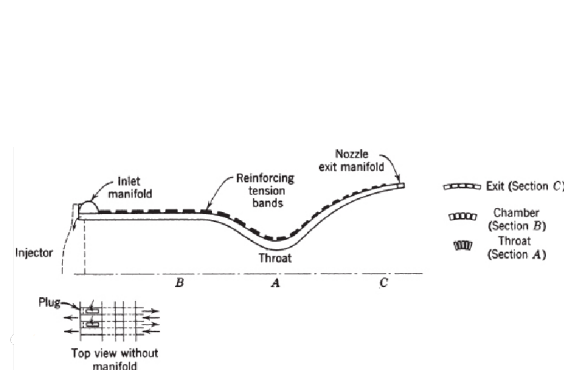


Figure 68: Cross sectional schematic of a nozzle with regenerative cooling.

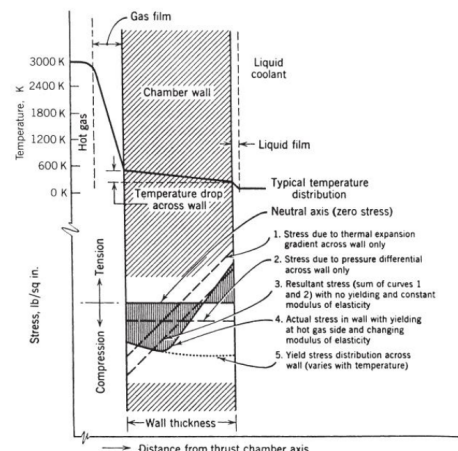


Figure 69: Temperature and stress variation across the nozzle wall of a regeneratively cooled engine.

Note that in **Figure 69**, the stress variation across the wall is dominated by the thermal expansion gradient and not the hoop stress, causing a high stress reversal and complex stress state.

10.2.3. Film Cooling

This method of cooling is where a small amount of liquid (typically fuel) is injected (using injectors at the wall or top of the chamber) along the wall to reduce the heat transfer. If fuel is injected, the oxygen/fuel ratio is altered, reducing the amount of combustion that takes place keeping the wall cool. However, film cooling is **only used as a secondary method** and it can also **cause significant performance reductions** due to the change on oxygen/fuel ratio. An image of film cooling is shown in **Figure 70**.

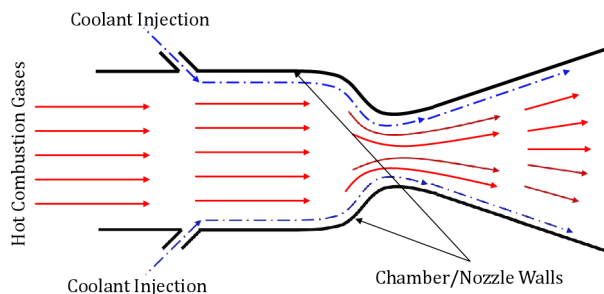


Figure 70: Film cooling employed

10.2.4. Ablative cooling

This method of cooling uses a layer of organic compound which at a certain temperature combusts and breaks away, removing heat energy with it. Typically, the liner consists of a fibre and resin (phenolics are used often) and can only be used as long as the ablative material exists within the engine. Ablative cooling is typically used **in solid rocket motors** where film and regenerative cooling cannot take place, an image of an ablatively cooled combustion chamber and nozzle are shown in

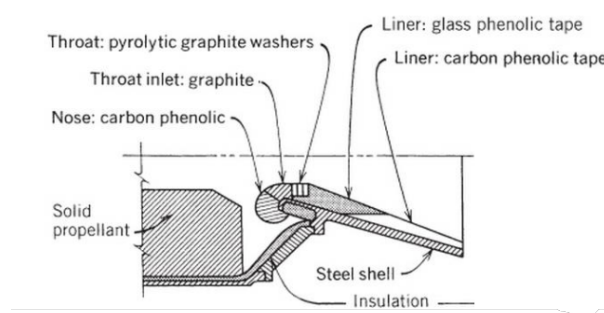


Figure 71: Ablative cooling on a solid rocket motor's nozzle and thrust chamber

10.3. Monopropellant Bed Loading

For monopropellant systems, it is important that the amount of catalyst is optimized, too much and there is wasted mass, type little and the bed is flooded, stopping decomposition from taking place. For a given thruster, a bed loading parameter, G is known and using this parameter the area of the catalyst bed can be calculated using **Eq. 50**.

$$G = \frac{\dot{m}}{A_1} \quad (50)$$

Where:

- G : Catalyst bed loading (kg/sm^2)
- A_1 : Catalyst bed area (m^2)
- \dot{m} : Propellant flow rate (kg/s)

Typically for small thrusters $G \approx 1 - 10 kg/sm^2$ and for large rockets $G \approx 10 - 100 kg/sm^2$. Once the value of G is known for a thruster, the catalyst bed can be sized using this equation.

11. Lecture 11

11.1. Introduction to Electric Propulsion

Electric propulsion is the process of **accelerating propellant using electricity**. Typically electric propulsio systems feature **much higher exhaust velcoities** than comparable chemical and solid thrusters (and therefore **much higher I_{sp} s**) at the cost of **lower thrust** ($F_{max} \approx 5N$). As shown in **Figure 1**, there are three main groups of electric propulsion systems, electrothermal, electrostatic and electromagnetic.

11.1.1. Overview of Electrothermal Propulsion Systems

Electrothermal systems use electricity to heat up a gas which is then passed through a nozzle. The two main systems used to heat up the gas are resistors in **Resistojets** and electrical arcs in **Arcjets**.

11.1.1.1. Overview of Resistojets

Resistojets are a subset within electrothermal propulsion systems which use an electrical current running through knife-edge-like wires which heat up liquid propellant passing over them. Internal baffles and insulation are used to keep the temperature within the chamber high. A schematic drawing of a resistojet thruster is shown in **Figure 72**.

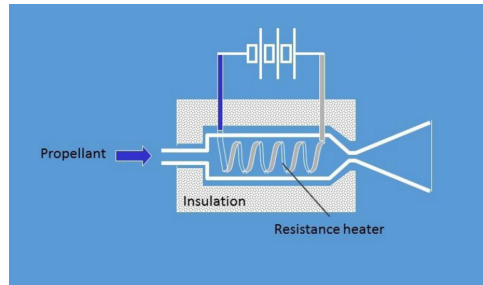


Figure 72: Schematic diagram of a Resistojet.

11.1.1.2. Overview of Arcjets

Arcjets are a subset within electrothermal propulsion systems which use a high potential difference between an anode and cathode to create a spark which then heats up a propellant. Although the spark is difficult to create and maintain, these systems can heat the propellant up to much higher temperatures than resistojet systems as the heating is no longer material limited. A schematic drawing of an arcjet thruster is shown in **Figure 73**.

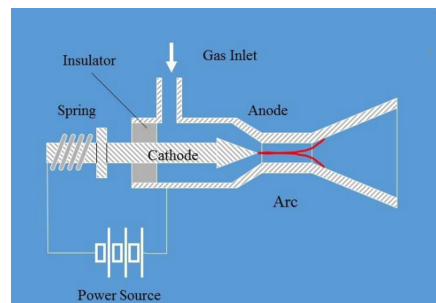


Figure 73: Schematic diagram of an Arcjet.

11.1.2. Overview of Electrostatic Propulsion Systems

Electrostatic propulsion systems make use of Coulombs force to accelerate and focus ions to generate thrust. The exhaust is then neutralized by introducing electrons into it. The two main electrostatic thrusters used are **gridded ion thrusters** and **electrospray/FEEP thrusters**.

11.1.2.1. Overview of Gridded Ion Thrusters

In this system, propellant is fed into a chamber where it is ionized (using either an electron gun, RF energy or a microwave system). The resulting plasma then sits at thousands of volts, eventually an ion will move towards the grid where it is rapidly accelerated due to the high negative charge creating thrust. An schematic image of a gridded ion thruster is shown in **Figure 74**.

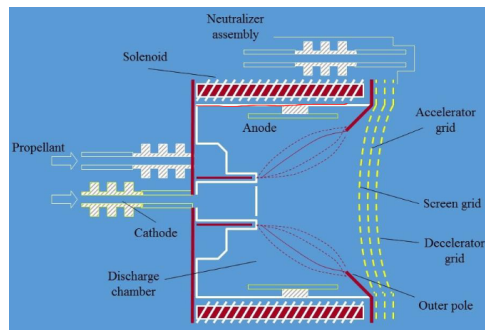


Figure 74: Schematic diagram of a gridded ion thruster.

11.1.3. Overview of Electrospray Thrusters

In this system, liquid is fed into a needle where it coalesces into a fluidic cone. A large voltage is then applied to the end of the needle and charged ions or ions are accelerated out into a spray. Although this system is simple, it is difficult to achieve and control. Organic liquids or metals can be used, an schematic diagram of an electrospray thruster is shown in

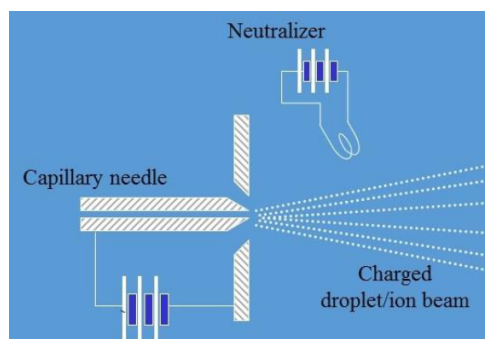


Figure 75: Schematic diagram of a electrospray thruster.

11.1.4. Overview of Electromagnetic Propulsion Systems

Electromagnetic propulsion systems use electricity to ionize a flow of propellant and then accelerate the resulting positive ions using a strong electric and magnetic field (utilizing the right hand rule to generate a force). The two main types of electromagnetic thrusters are **pulsed plasma thrusters** and **magneto plasma dynamic (MPD) thrusters**.

11.1.4.1. Overview of Pulsed Plasma Thrusters

Pulsed plasma thrusters are a simple form of electromagnetic thruster which creates an arc between a highly positively and negatively charged plate which then ablates away a small amount of a Teflon block. This is then accelerated out of the thruster using the Lorenz force. A schematic diagram of this thruster is shown in **Figure 76**.

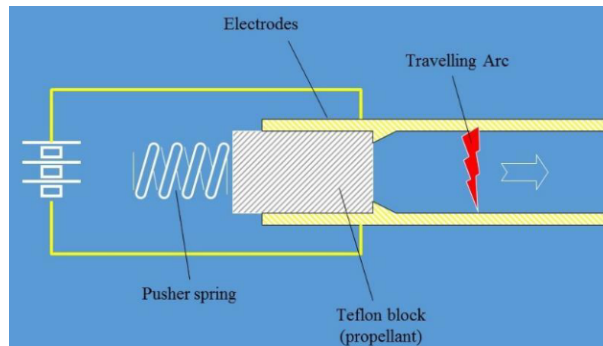


Figure 76: Schematic diagram of a pulsed plasma thruster.

11.1.4.2. Overview of Magneto Plasma Thrusters (MPDs)

MPDs are similar in design to arcjets however they operate at much higher currents. Whereas arcjets may operate at 10s of amps, MPDs may operate at 100k amps. This allows for much more ionization of the propellant into a plasma which can be further accelerated using the Lorenz force. A schematic diagram of a MPD is shown in **Figure 77**.

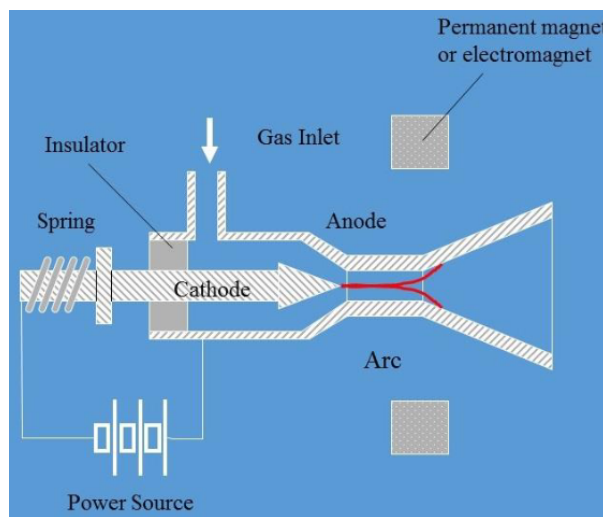


Figure 77: Schematic diagram of an MPD thruster.

11.2. Overview of Hall Effect Thrusters

These thrusters sit between electromagnetic and electrostatic thrusters, and are the dominant form of space propulsion. Whilst propellant does get ionized in a chamber and accelerated towards a negative grid, Hall effect thrusters also feature an annular chamber with a magnetic field also present. A schematic image of a Hall effect thruster is shown in **Figure 78**.

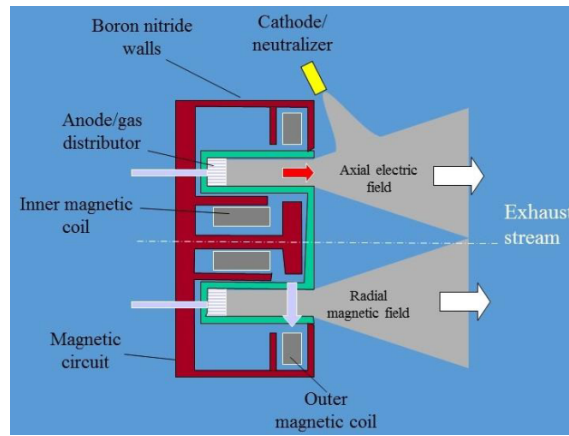


Figure 78: Schematic diagram of a Hall effect thruster.

11.3. Electric Propulsion Performance

Recall **Eq. 7**, **Eq. 8** and **Eq. 9** as well as **Figure 6** from lecture 2. These equations and figure have the following key takeaways:

- Electric propulsion exhaust velocity c and thrust F are **inversely proportional** to one another. A higher thrust means a lower exhaust velocity and performance and vice versa.
- Power input as well as power plant mass are **directly proportional** to thrust and acceleration. A higher thrust directly means a higher power input.
- In terms of values of the specific power plant mass:
 - $\alpha = 200 \text{ kg/kW}$ for a RTG
 - $\alpha = 20 \text{ kg/kW}$ for a solar panel
 - $\alpha = 2 \text{ kg/kW}$ for a nuclear reactor (note that the mass will have to be very big though.)

Note that the performance of the 7 different electrical propulsion systems mentioned above is shown in **Table 13**.

Type	Thrust Range (mN)	I_{sp} Range (s)	Thruster Efficiency	P_{in} Range (W)
Electrothermal Propulsion Systems				
Resistojet	200 - 300	200 - 350	65 - 90	50 - 1000
Arcjet	200 - 1000	400 - 1000	30 - 50	900 - 2200
Electrostatic Propulsion Systems				
Ion Thruster	0.01 - 500	1500 - 8000	60 - 80	100 - 4300
Electrospray	0.001 - 1	300 - 6000	15 - 70	1 - 50
Electromagnetic Propulsion Systems				
PPT	0.05 - 1	600 - 2000	≈ 10	50 - 500
MPD thruster	0.001 - 2000	2000 - 5000	30 - 50	2000 - 100,000
Misc Electrical Propulsion Systems				
Hall Thruster	0.01 - 2000	1500 - 3500	20 - 60	100 - 100,000

Table 13: Comparative performance of different electrical propulsion systems.

11.4. Why Electric Propulsion ?

Electric propulsion systems are the dominant form of in-space propulsion, to understand why consider the rearranged form of the rocket equation shown in **Eq. 51**.

$$\frac{M_0}{M_f} = \exp\left(\frac{\Delta V}{I_{sp}g_0}\right) = \exp\left(\frac{\Delta V}{c}\right) \rightarrow M_p = M_f \left(\exp\left(\frac{\Delta V}{c}\right) - 1\right) \quad (51)$$

Now consider an asteroid rendezvous mission with the following requirements:

- $M_{\text{Payload}} = 500\text{kg}$
- $c_{\text{Chemical}} = 3\text{km/s}$
- $\Delta V = 5\text{km/s}$
- $c_{\text{Electric}} = 30\text{km/s}$

For a chemical thruster, $M_p \approx 2000\text{kg}$ whereas for a electric thruster the $M_p \approx 90\text{kg}$. The downside here is the long burn time of electrical compared with chemical due to the very low thrust.

11.5. Uses of Electric Propulsion

Electric thrusters have seen wide spread use in space applications for both primary and secondary propulsion systems. These are:

- Primary propulsion systems
 - Interplanetary exploration.
 - Drag compensation in LEO.
 - Orbit raising.
 - Formation flying.
- Secondary Propulsion system
 - N-S station keeping.
 - E-W station keeping.

12. Lecture 12

12.1. History of Electric Propulsion

Some key points in the development of electric propulsion, from the initial development of EP to their widespread use, is shown in the timeline below:

- **20 July 1964** — SERT-1: First flight of an ion thruster
- **15 August 1991** — USSR Meteor-3: First in-space test of a Hall Effect Thruster.
- **24 October 1998** — NASA Deep Space 1 launch (first ion thruster on a science mission)
- **9 May 2003** — Hayabusa launch to asteroid Itokawa
- **13 June 2010** — Hayabusa sample return capsule to Earth
- **20 October 2018** — BepiColombo launch using UK T6 ion thruster
- **24 May 2019** — First SpaceX Starlink satellites launch (v0.9 batch)
- **13 October 2023** — NASA Psyche mission launch to asteroid Psyche
- **Mid-2025 (launch window)** — Lunar Gateway PPE + HALO first modules launch window

Note that there is a large gap between the first use of ion thruster and the first actual use on a mission, this was probably due to the following factors:

- **Lack of power production** (poor solar panel efficiency) on spacecraft.
- **Toxic propellants** that were chosen for the initial thrusters (mercury, cesium) and lack of safe propellants at the time (Xenon, Krypton).
- **Low number of launches**, due to this safe propellant options were prioritized.

12.2. Use of EP in Spacecraft

The number of satellites has grown incredibly over the last few decades, going from a few hundred to over 9000 (inflated due to constellations). A graph of the cumulative number of satellites is shown in **Figure 79**. A large majority of these satellites utilize electric propulsion.

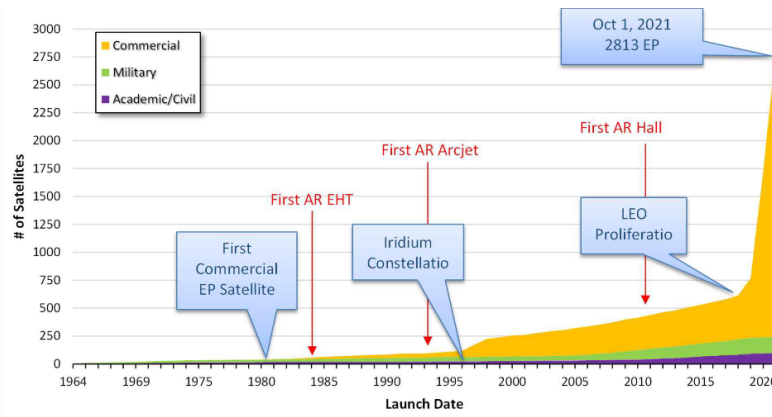


Figure 79: Cumulative number of satellites from 1964 - 2020.

12.3. EP Use-cases and Requirements

12.3.1. GEO Orbit Raising

For satellites which end up in a GEO, they are first inserted into a highly elliptical GTO (geostationary transfer orbit). From this an electric thruster is used to circularize the orbit and to then maintain the orbit (station keeping) over the lifetime of the mission. The key requirements of this mission type are shown below:

- **Thrust to power** defined by:
 - Time to do orbit transfer (current max is 6 months).
 - Power available per unit mass of satellite.
 - Due to these requirements, **30 - 70 mN/kW** is viewed as an acceptable value.
- The **power available** is defined by the available power on satellite, typically:
 - 1.5 tonne satellite: ~ 5 kW available.
 - 3 tonne satellite: ~ 10 kW available.
 - 6 tonne satellite: ~ 20 kW available.
- The **thruster lifetime** is based:
 - Transfer time: ~ 5000 hours
 - Station lifetime: 5000 - 10,000 hours.

On top of these requirements the $I_{sp} \approx 1000s$ for a good thruster.

12.3.2. LEO Orbit Raising

For many constellations as well as many other satellites, they are first dropped off in a LEO ($\approx 400km$) and need to then be raised to a higher LEO or even a MEO ($\approx 600 - 2000km$). Beyond this, some satellites also require some addition thrust for station keeping. The key requirements of this mission type are shown below: Requirements;

- **Thrust to power** defined by:
 - Time to do orbit transfer (current max is 1 year).
 - Due to this requirements, **40 - 60 mN/kW** is viewed as an acceptable value.
- The **power available** is defined by the available power on satellite, typically:
 - 200 kg satellite: ~ 500 W available.
 - 1.5 tonne satellite: ~ 5 kW available.
- The **thruster lifetime** is based:
 - Transfer time: $\sim 10,000$ hours
 - Station lifetime: dependant on satellite and mission.

On top of these requirements the $I_{sp} \approx 1000s$ for a good thruster.

12.3.3. Applicable Thrusters for Orbit Raising

Given the requirements for LEO and GEO rasing, there only exists a few electric thruster which can work in this regime. Consider **Figure 80**, the highlighted envelope shows the requirements for LEO and GEO raising. In reality only GITs, HETs and DCT(HEMPT) can be used, which type of thrusters are used for orbit raising are shown in **Figure 81**. As can be seen, HETs and GITs are most commonly used.

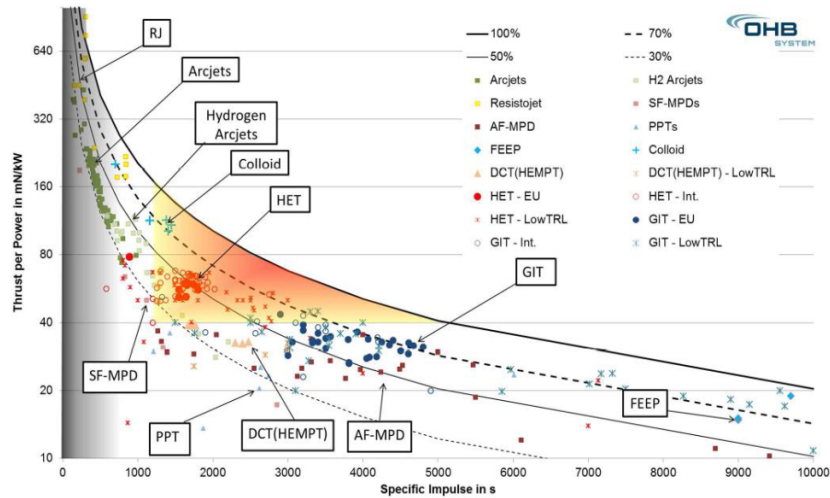


Figure 80: Plot of thrust per power against impulse for different electric thrusters, including low TRL and envelope for orbit raising.

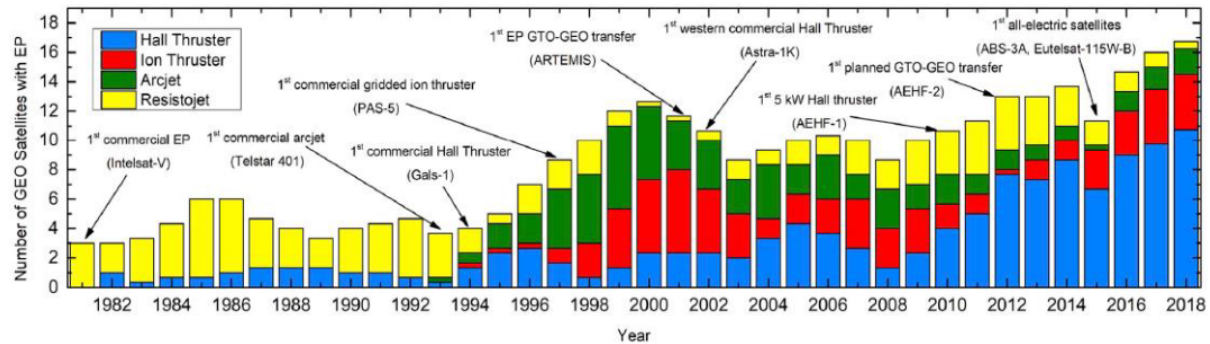


Figure 81: Plot showing which electric thrusters are used for orbit raising over time.

12.3.4. LEO and GEO Station Keeping

Many satellites require thrusters to maintain their orbit overtime. This equates to roughly **45 minutes of burning per day**. The requirements for these thrusters are different from orbit raising and are shown below:

- **Thrust to power** defined by:
 - Manoeuvre time.
 - Required thrust to power is low as the thruster operation does not interfere with the satellite operation.
 - Thus specific impulse can be maximized.
 - Due to this requirements, **30 - 200 mN/kW** is viewed as an acceptable value.
- The **power available** is defined by the available power on satellite, typically:
 - Only limited power available as thruster must operate during payload operation.
 - Therefore power is supplied by either increasing solar array area or switching off of payload load.
 - 1.5 tonne satellite: ~ 3 kW available.
- The **thruster lifetime** is based:
 - Dependent on thrust, mission, etc ($\sim 5,000 - 10,000$ h)

On top of these requirements the I_{sp} requirement is a bit lower than orbit raising.

12.3.5. Applicable Thrusters for Station Keeping

As the requirements for station keeping are more lax than the ones for orbit raising, there are more available thrusters, the envelope defined by the requirements in the previous section is imposed in **Figure 82**.

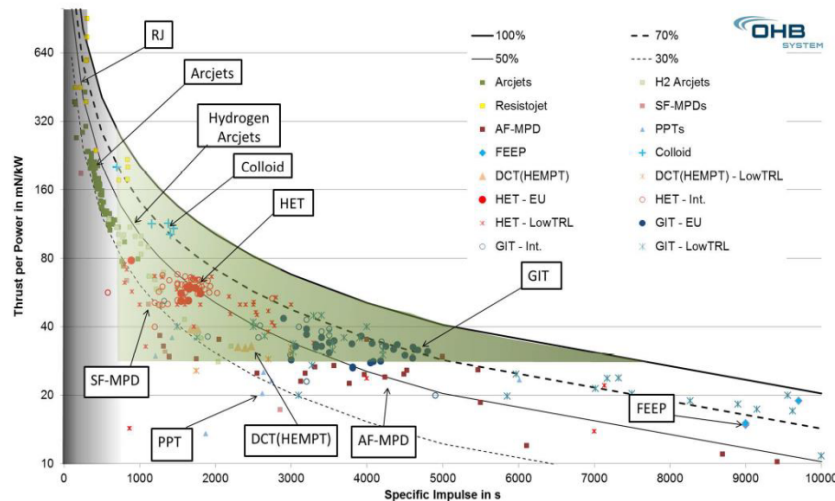


Figure 82: Plot of thrust per power against impulse for different electric thrusters, including low TRL and envelope for station keeping.

As is shown in **Figure 82**, some electrothermal propulsion methods become viable as well as some options augmented with hydrazine.

12.3.6. Interplanetary Missions

Interplanetary missions require a very large ΔV and so the main focus for the thruster is to have a very high I_{sp} . The full list of requirements for an interplanetary mission are shown below:

- **Thrust to power** defined by:
 - As the mission time is not a priority, the thrust to power is low meaning the mission time is very long (multiple years).
 - Due to this requirements, **> 20 mN/kW** is viewed as an acceptable value.
- The **power available** is defined by the available power on satellite, typically:
 - Defined by the final mission scenario.
 - Close to Earth, large power levels are available, further away lower power levels are available.
 - Only limited power available as thruster must operate during payload operation.
 - Therefore power is supplied by either increasing solar array area or switching off of payload.
 - 1.5 tonne satellite: ~ 3 kW available.
- The **thruster lifetime** is based:
 - Dependent on transfer time, typically $\sim 40,000 - 80,000$ h.

On top of these requirements the I_{sp} requirement is very high ($I_{sp} \gg 3000s$).

12.3.7. Applicable Thrusters for Interplanetary Missions

Due to their high I_{sp} and low thrust-to-power requirement, the envelope for available thrusters is pushed to the right. This means that only GITs and some high performance HETs can be used, this is shown in **Figure 83**.

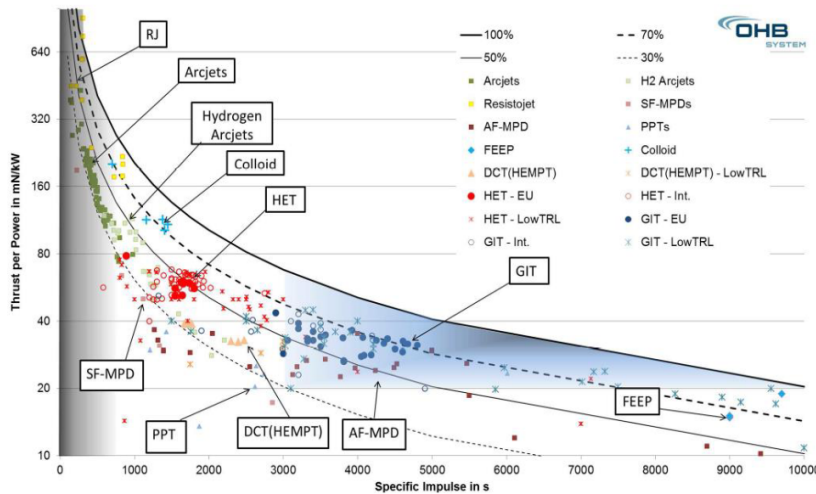


Figure 83: Plot of thrust per power against impulse for different electric thrusters, including low TRL and envelope for interplanetary missions.

12.4. Derivation of an Electric Thruster Rocket Equation

Consider a simple spacecraft consisting of the following subsections which all have the following masses (assuming spacecraft structural mass to be negligible):

- M_{Pay} : Mass of the payload (kg)
- M_{Pow} : Mass of the power plant (kg)
- M_P : Mass of the propellant (kg)

With these three sections being connected to a thruster. The initial mass of the spacecraft is therefore defined by **Eq. 52**.

$$M_0 = M_{Pay} + M_{Pow} + M_P \quad (52)$$

An expression for the mass of the power plant can be defined by substituting the equations defined in **Eq. 53** into **Eq. 52**.

$$M_P = \dot{m}t_b \quad \eta_T = \frac{\dot{m}c^2}{2P_{in}} \quad P_{in} = \frac{M_{Pow}}{\alpha} \quad (53)$$

The equation for the power plant mass is therefore defined in **Eq. 54**, where v_c is the characteristic velocity, not to be confused with c^* .

$$M_{Pow} = \frac{M_0 - M_{Pay}}{1 + \left(\frac{2\eta_T t_b}{\alpha c^2}\right)} = \frac{M_0 - M_{Pay}}{1 + \frac{v_c^2}{c^2}} \quad v_c = \sqrt{\frac{2\eta_T t_b}{\alpha}} \quad (54)$$

Utilizing **Eq. 54**, rearranging it and substituting in to the rocket equation yields **Eq. 55**.

$$\Delta V = c \ln \left(\frac{1 + \frac{v_e^2}{c^2}}{\frac{M_{pow}}{M_0} + \frac{v_e^2}{c^2}} \right) \quad (55)$$

As **Eq. 55** is an unintuitive equation, it has been plotted out with ΔV against increasing exhaust velocities in **Figure 84**.

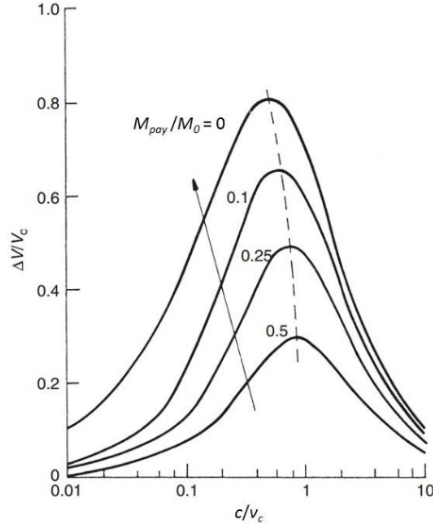


Figure 84: Plot of normalized ΔV against normalized exhaust velocities.

Note that as the exhaust velocity increases, the ΔV does not continually increase, instead it starts to eventually decrease and this is because after a point the mass of the power plant needed to produce the power to accelerate the exhaust outweighs any ΔV gain. Another way of thinking about this is that $M_{pow} \propto I_{sp}$ and $M_P \propto 1/I_{sp}$, meaning that there is an optimal mass of the spacecraft. **Figure 84** also has the following takeaways:

- For high I_{sp} s, if the system is operating at conditions to maximize performance, then t_b will be high.
- For an optimum burn time $t_{b_{Max}} \approx (\Delta V)^2$
- An optimum I_{sp} is roughly equal to the required change in velocity, $I_{sp_{Optimum}} \approx \Delta V$

13. Lecture 13

13.1. Introduction to Plasma

A useful definition for plasma is a **quasineutral gas of charged and neutral particles which exhibits collective behavior**. A plasma is formed when atoms gain enough energy (through heating or through other means) to be stripped of their electrons. As the plasma is a “soup” of ions, electrons and particles, the plasma as a whole will be **quasineutral**. The plasma itself will exhibit a **collective behavior** as ions and electrons will all experience electrostatic forces between one another.

13.2. Debye Length

One Fundamental property of a plasma is the **Debye length** shown in **Eq. 56**.

$$\lambda_D = \sqrt{\frac{\epsilon_0 k T_e}{n e^2}} \quad (56)$$

Where:

- ϵ_0 : Permittivity of free space = $8.85 \times 10^{-12} m^3 kg^{-1} s^4 A^2$
- k : Boltzmann's constant = $1.38 \times 10^{-23} JK^{-1}$
- e : Electron charge = $1.6 \times 10^{-19} C$
- T_e : Electron temperature (K)
- n : Plasma density (Number of Particles/m³)

Note that as the plasma is quasineutral, the density of ions and electrons must be the same. Further note that the electron temperature will be higher than the ion and particle temperature as the electrons are able to reach higher temperatures. To understand what the Debye length is, consider the scenario shown in **Figure 85**.

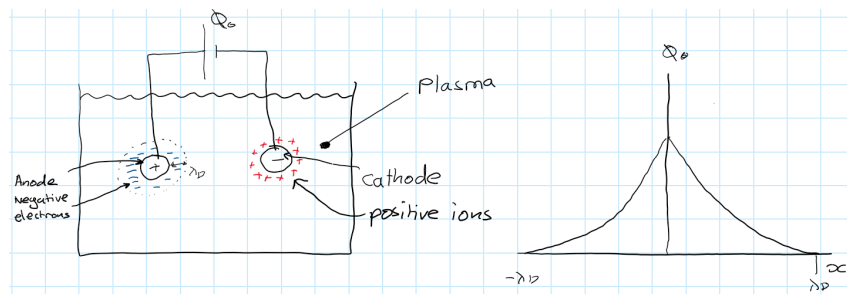


Figure 85: Figure of potential applied across a plasma with a plot of the potential difference against the distance away from the anode/cathode.

As a potential is applied across a plasma, the ions and electrons form a sheath around the cathode and anode respectively. This acts to neutralize the effect of the potential difference applied to the plasma. One key point is that the **debye length must be smaller than the size of the container** for the substance within it to be considered a plasma.

14. Lecture 14

14.1. Charged Particle Motion in Magnetic Fields

A charged particle subjected to a constant magnetic field will undergo circular motion, this is because the force on the charged particle will be centripetal towards the center of rotation (called the **guiding centre**). The force on a charged particle is given by the Lorenz force shown in **Eq. 57**.

$$\vec{F} = q\vec{v} \times \vec{B} \quad (57)$$

Where:

- \vec{F} : Force vector (N)
- q : Magnitude of charge of the particle (C)
- \vec{v} : velocity vector (m/s)
- \vec{B} : Force vector (T)

The angular velocity at which the charged particle rotates with is given by the **cyclotron frequency** and is shown in **Eq. 58**.

$$\omega_c = \frac{q\vec{B}}{m} \quad (58)$$

Where:

- ω_c : Cyclotron frequency (rad/s)
- m : Particle mass (kg)

The radius of the circle that the charged particle rotates through is called the **Larmor radius** and is shown in **Eq. 59**.

$$r_L = \frac{v_\perp}{\omega_c} = \frac{mv_\perp}{q\vec{B}} \quad (59)$$

Where:

- r_L : Larmor radius (m)
- v_\perp : Perpendicular velocity (m/s)

14.2. Charged Particle Motion in Electric Fields

A charge particle within an electric field will experience a constant force given a uniform electric field strength. The force on a charged particle in an electric field is given by the Lorenz force shown in **Eq. 60**.

$$\vec{F} = \vec{E}q \quad (60)$$

Where \vec{E} is the electric field strength with units N/C .

14.3. Charged Particle Motion in Magnetic and Electric Fields

In a space where there is an electric field and a magnetic field perpendicular to one another, a charged particle that enters that field will travel in a spiral pattern, this is shown in **Figure 86**.

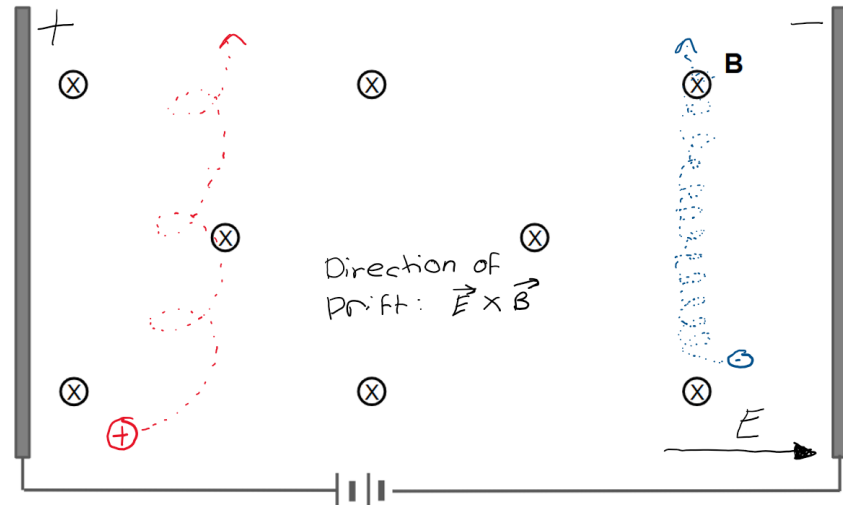


Figure 86: Path taken by an ion and electron in a magnetic and electric field.

Note that in **Figure 86**, regardless of the polarity of the magnet or direction of the electric field, an electron and positive ion will drift in the same direction, the only difference would be how tight their radii were. Note that the direction of the drift is obtained by $\vec{E} \times \vec{B}$. Note that this motion is similar to a charged particle in a varying magnetic field, shown in **Figure 87**.

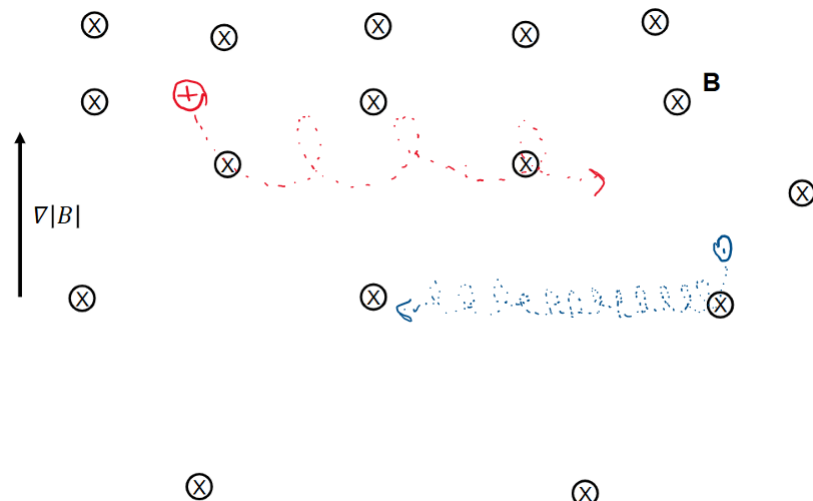


Figure 87: Path taken by an ion and electron in a non-constant magnetic.

Note that in **Figure 87**, whether the particle is an ion or electron dictates the direction it will drift in.

14.4. Magnetic Mirroring

Consider a charged particle moving in a spiral along a magnetic field line. If the magnetic field density increases, then the particle will start to spiral faster ($v_{\perp} \uparrow$) and the Larmor radius will tighten, this is shown in **Figure 88**.

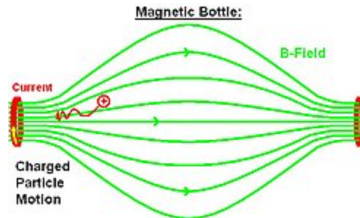


Figure 88: Magnetic mirroring.

As the perpendicular speed increases, there must be a decrease in the parallel speed to conserve energy, this means that eventually the parallel velocity goes to zero and inverts, causing magnetic mirroring. This can also be seen in the magnetic moment of a gyrating particle equation shown in **Eq. 61**.

$$\mu = \frac{1/2mv_{\perp}^2}{B} = \text{const} \quad (61)$$

As μ must remain constant and B increases, v_{\perp} decreases in proportion, increasing the speed at which the particle rotates.

14.5. Working Principle Behind Hall Effect Thrusters

Hall Effect Thrusters (HETs) utilize many of the physical concepts mentioned previously to ionize and accelerate a gas. An image showing the major components of a HET is shown in **Figure 89**.

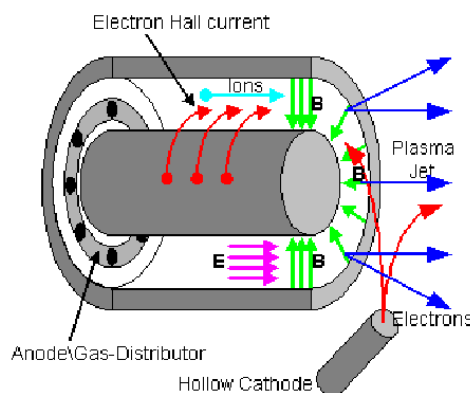


Figure 89: Basic components of a Hall Effect thruster.

To better understand the working principle behind a HET, we will consider the lifecycle of an electron, this is shown below:

1. Electrons are produced in the hollow cathode (some of the produced electrons ionize the ionized plasma jet).
2. Electrons are attracted towards the anode at the bottom of the annular channel.

3. Electrons see a strong magnetic force at the mouth of the annular channel where they start to rapidly spiral around (this creates a strong negative charge at the mouth accelerating ions).
4. The electrons are still attracted to the positive anode and very slowly drift down to the anode.
5. Closer to the anode, neutrals are ionized, producing ions which are accelerated out.
6. Electrons collide with the anode completing the circuit.

In reality the movement of electrons is more complex with wall collisions and magnetic mirroring occurring. Furthermore, it is still not understood why electrons eventually break away from the magnetic confinement area. The real motion of the particles is shown in **Figure 90**. Also shown is a plot of electric field strength and magnetic field strength, it can be seen that at the mouth where there is the strongest magnetic field, is where the strongest electric field is due to the magnetic confinement.

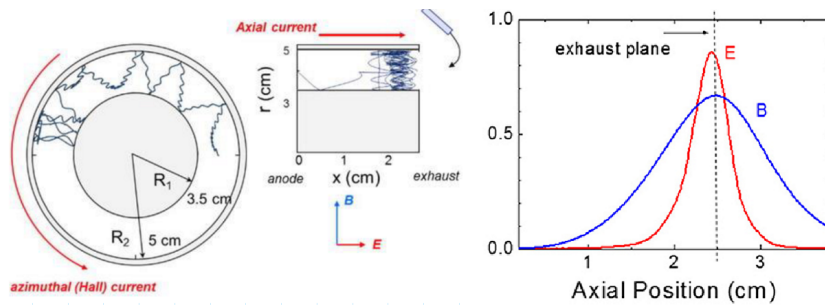


Figure 90: Simulated movement of electrons in a Hall effect thruster.

14.6. HET Performance and Improvement Areas

HETs sit at almost a goldilocks zone of performance, having much better performance than chemical or electrothermal thrusters whilst having higher thrust than GITs. A table comparing the performance of GITs to HETs is shown in **Table 14**

Type,	Thrust Range (mN)	Isp Range (s)	Thruster Efficiency	Input Power Range (W)
Gridded Ion Thruster	0.1 - 300	1500 - 5000	60 - 80	400 - 4300
Hall Thruster	5 - 2000	1000 - 2000	30 - 60	1000 - 50,000

Table 14: HET vs GIT performance.

However HETs do have drawbacks when compared to other electrical thrusters, some of the main drawbacks are:

- **Large beam divergence** (30 - 40 degrees), this is caused by non-uniform electric and magnetic fields as well as the rotation that the ions experience when in the magnetic field. This **reduces thrust**.
- **Electromagnetic interference** which is caused by plasma oscillations. This is due to the predator prey relationship between electrons, neutrals and ions.
- **Poor lifetime**, however this may be fixed through magnetic shielding.

14.7. HET Lifetime and Magnetic Shielding

HETs struggle with performance over their lifetime due to the magnetic confinement eroding the material near the mouth, this effect is shown in **Figure 91**.

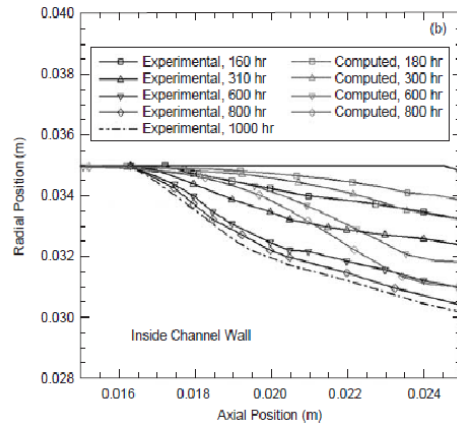


Figure 91: Erosion rate of HET near at the mouth.

One new method of mitigating this is by using a shielded magnet, this has the effect of moving the magnetic confinement region away from the walls, decreasing the erosion rate. A figure of magnetic shielding as well as the erosion rate with and without it (red and dashed red line) are shown in **Figure 92**.

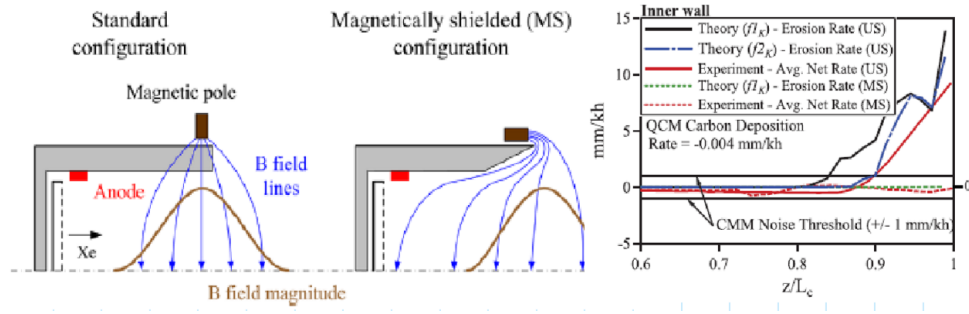


Figure 92: Magnetic shielding implemented on a HET with the new and old erosion rates.

14.8. HET Propellants

Xenon and Krypton are mostly used as HET propellants due to their high atomic weight and relative ease of obtaining. Various different propellants are shown in **Figure 93**.

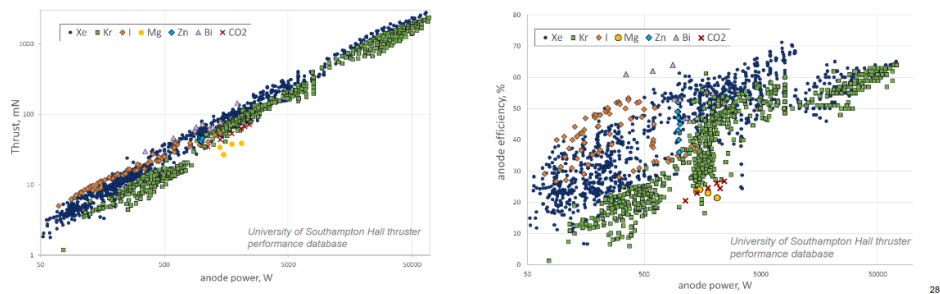


Figure 93: HET propellant performance

15. Lecture 15

15.1. Calculating Larmor Radii in HETs

For a HET, the ions should have a large Larmor radius so they are not bent out of shape and stay straight and the electrons should have a small Larmor radius so they stay within the confinement zone. To calculate the radii, **Eq. 59** can be used in combination with the equations defined in **Eq. 62**.

$$v_{(\perp)\text{electron}} = v_{th} = \sqrt{\frac{8kT_e}{\pi m_e}} \quad v_{(\perp)\text{ion}} = v_i = \sqrt{\frac{2qV_b}{m_i}} \quad (62)$$

Where the first equation is the thermal velocity as this is dominating for the electrons and the second is the energy gained due to the electrostatic attraction. Note that m_i is the ion mass and V_b is the beam voltage.

15.2. Hall Effect

The Hall effect itself is the **perpendicular potential difference experienced as a charged particle moves through a magnetic field**. Hall effect thrusters use this to confine the electrons within the magnetic field at the mouth of the thruster. These electrons can be thought of as a current (a Hall current). Therefore due to the Hall effect, a potential difference is created which counteracts the upstream potential difference, keeping the electrons in place and causing them to act as a pseudo-grid. The drift velocity of an electron can be calculated using the equation shown in **Eq. 63**.

$$\vec{v}_{E \times B} = \frac{\vec{E} \times \vec{B}}{B^2} \quad \rightarrow \quad v_{E \times B} = \frac{E_z}{B_r} \quad (63)$$

Where the first equation is the general vector form and the second equation is a simplified form taking into account the geometry of the Hall thruster. E_z is the axial electric field and B_r is the radial magnetic field. The Hall current which is the azimuthal current generated by the stream of electrons can be calculated using **Eq. 64**.

$$I_H = n_e e \left(\int_0^L v_{E \times B} dz \right) w = n_e e \left(\int_0^L \frac{E_z}{B_r} dz \right) w \approx n_e e w \frac{V_d}{B} \quad (64)$$

Where:

- n_e : Electron density (electrons / m^3)
- e : Electron charge = $1.6 \times 10^{-19} C$
- w : Annular channel width (m)
- L : Length of Hall current in the channel (m).
- V_d : Discharge voltage (V_d).

Note that $\frac{V_d}{B} \approx 1$ meaning that the hall current is mostly driven by the electron density and annular width.

16. Lecture 16

16.1. Electromagnetic and Electrostatic Thruster Thrust

The thrust of a HET or GIT or any electric thruster which accelerates ions using a potential difference is given by the expression shown in **Eq. 65**.

$$T = \dot{m}c \approx \dot{m}_i v_i \quad (65)$$

Where \dot{m}_i is the mass flow rate of the ions and v_i is the velocity of the ions. The mass flow rate of the ions can be calculated using **Eq. 66**.

$$\dot{m}_i = \frac{I_b M_{\text{ion}}}{q} \quad (66)$$

Where I_b is the ion beam current. Finally a full expression for the thrust can be generated by substituting **Eq. 66** and **Eq. 62** into **Eq. 65**, yielding **Eq. 67**.

$$T = \sqrt{\frac{2M_{\text{ion}}}{e}} I_b \sqrt{V_b} \quad (67)$$

Often Xenon is used as the propellant, meaning the equation can be simplified as many of the parameters are known, this simplified expression is shown in **Eq. 68**.

$$T = 1.651 I_b \sqrt{V_b} \quad [mN] \quad (68)$$

Note that the input power can be calculated as $P_{in} = I_b V_b$.

16.1.1. Efficiency Parameters

Eq. 68 assumes that the thruster is 100% efficient, there are a few efficiency parameters which can be applied to make the equations more realistic, the first parameter for the beam divergence is shown in **Eq. 69**.

$$\eta_{cos} = \frac{1}{2}(1 + \cos^2(\theta)) \quad (69)$$

Where theta is θ . The second parameter is the loss in efficiency due to ions which have been doubly ionized, this is shown in **Eq. 70**.

$$\alpha = \frac{1 + \frac{1}{\sqrt{2}} \frac{I^{++}}{I^+}}{1 + \frac{I^{++}}{I^+}} \quad (70)$$

16.2. Electromagnetic and Electrostatic Real Thruster Thrust

The actual thrust produced by a GIT or HET is given by substituting **Eq. 69** and **Eq. 70** into **Eq. 65**, yielding **Eq. 71**.

$$T = \alpha \eta_{cos} \sqrt{\frac{2M_{\text{ion}}}{e}} I_b \sqrt{V_b} \rightarrow T = \alpha \eta_{cos} 1.651 I_b \sqrt{V_b} \quad [mN] \quad (71)$$

16.3. Electromagnetic and Electrostatic Thruster I_{sp} and Efficiency Terms

The efficiency of a HET or GIT or any electric thruster which accelerates ions using a potential difference is given by **Eq. 72**, note that **Eq. 62** has been substituted in.

$$I_{sp} = \frac{c}{g_0} \approx \frac{v_i}{g_0} = \frac{1}{g_0} \sqrt{\frac{2qV_b}{M_{ion}}} \quad (72)$$

Similar to the thrust, there exists efficiency parameters. The real I_{sp} equation makes use of the same parameters with the addition of the thruster mass utilization efficiency which is a measure of how much of the propellant is ionized, this is shown in **Eq. 73**.

$$\eta_m = \frac{\dot{m}_i}{\dot{m}} = \frac{I_b}{q} \frac{M_{ion}}{\dot{m}} \quad (73)$$

where \dot{m} is the mass flow rate of the propellant. The real I_{sp} with the efficiency applied is therefore shown in **Eq. 74**.

$$I_{sp} = \frac{\alpha \eta_{cos} \eta_m}{g_0} \sqrt{\frac{2qV_b}{M_{ion}}} \rightarrow I_{sp} = 123.6 \alpha \eta_{cos} \eta_m \sqrt{V_b} \quad (74)$$

16.4. Electromagnetic and Electrostatic Thruster Efficiencies

Another useful efficiency parameter for ion accelerating thrusters is the electrical efficiency shown in **Eq. 75**.

$$\eta_e = \frac{I_b V_b}{I_b V_b + P_0} \quad (75)$$

Where P_0 is the other power input to the thruster required to create the thrust beam such as but not limited to electrical cost of producing the ions, cathode heater or keeper power, grid currents. The total efficiency can be written in terms of all of the defined efficiencies shown in **Eq. 76**.

$$\eta_{th} = \frac{\frac{1}{2} \dot{m} c^2}{P_{in}} = (\alpha \eta_{cos})^2 \eta_e \eta_m \quad (76)$$

Another useful efficiency parameter is the discharge loss shown in **Eq. 77**. Note that this parameter is not technically as it has units of W/A .

$$\eta_d = \frac{P_d}{I_b} \quad (77)$$

An interesting property is shown if the discharge loss is plotted against the mass utilization efficiency, this plot is shown in **Figure 94**. At higher propellant utilization efficiencies, the discharge loss increases, this is because at high η_m s, there are less neutrals within the exhaust which have a passive effect of cooling the exhaust. This therefore means operating at high η_m s leads to a high electron temperature increasing η_d .

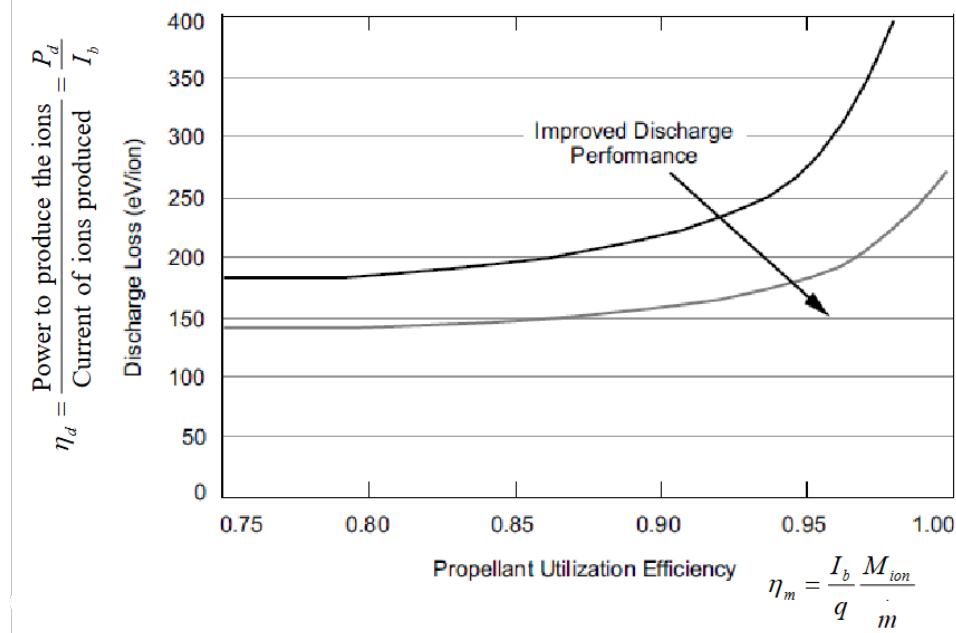


Figure 94: Plot of discharge loss against mass utilization efficiency.

16.5. Difficulties in Estimating HET Performance

There are some key parameters that have been mentioned for calculating key performance metrics that are difficult or not possible to experimentally measure. One key parameter that is difficult to measure is the **coupling voltage** shown in **Eq. 78** and **Figure 95**.

$$V_C = V_{\text{Plasma}} + V_{\text{Cathode}} \quad (78.1)$$

$$V_C = V_d - V_b \quad (78.2)$$

$$\therefore V_b = V_d - V_C = V_d - (V_{\text{Plasma}} + V_{\text{Cathode}}) \quad (78.3)$$

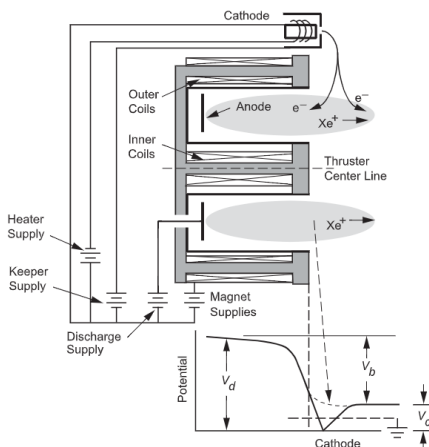


Figure 95: Plot of voltage applied across a HET

V_d can be experimentally measured however V_{Plasma} cannot be measured V_{Cathode} , this means that a thrust stand must be used to calculate key performance parameters. Another key parameter that is cannot be measured is the **beam current** I_b , the equation including it is shown in **Eq. 79**.

$$I_d = I_b + I_{ec} \quad (79)$$

Simply measuring the anode current doesn't allow for calculation of I_b as the backstreaming electron current I_{ec} cannot be measured and the physics behind why this happens is still unknown. Another key efficiency parameter is the current discharge efficiency shown in **Eq. 80**.

$$\eta_b = \frac{I_b}{I_d} \quad (80)$$

Which is a measure of how much I_{ec} there is, a good thruster will keep I_{ec} as low as possible. Another aspect to note is that the P_{in} and \dot{m} terms in η_{th} contain all of the contributions shown in **Eq. 81**.

$$\dot{m} = \dot{m}_{\text{anode}} + \dot{m}_{\text{cathode}} \quad P_{in} = P_{\text{anode}} + P_{\text{cathode}} + P_{\text{electromagnets}} \quad P_{\text{anode}} = I_d V_d \quad (81.1)$$

$$\eta_{th} = \frac{\frac{1}{2} \dot{m} c^2}{P_{in}} = \frac{\frac{1}{2} (\dot{m}_{\text{anode}} + \dot{m}) c^2}{P_{\text{anode}} + P_{\text{cathode}} + P_{\text{electromagnets}}} = \frac{\frac{1}{2} (\dot{m}_{\text{anode}} + \dot{m}) c^2}{I_d V_d + P_{\text{cathode}} + P_{\text{electromagnets}}} \quad (81.2)$$

One quick way of approximating the total efficiency when certain parameters cannot be accurately calculated is by utilizing the anode efficiency shown in **Eq. 82**.

$$\eta_{\text{anode}} = \frac{F^2}{2 \dot{m}_{\text{anode}} I_d V_d} \quad (82)$$

16.6. Closing Remarks on HETs

HETs stand out as the most dominant type of electric propulsion method used in space in the modern day, with their development being a key area of focus. They set poised for use in wider and wider mission requirements and sit in the goldilocks zone for space missions (good I_{sp} and good thrust). There are some drawbacks and lack of understanding present, some key areas of development are:

- Smaller HETs see much lower total efficiencies.
- Larger HETs come with the penalty of much greater power requirements.
- Operating on different propellants without large performance loss.
- The specific mechanisms behind Bohm diffusion and why electrons fall back to the anode.

It is also important that the domination of Hall thrusters in the EP sector mean that R&D is taken away from other forms of EP.

16.7. Magnetoplasmadynamic (MPD) Thrusters

These thrusters utilize both an electric field and an induced magnetic field to ionize and accelerate propellant. An image of such a thruster is shown in **Figure 96**.

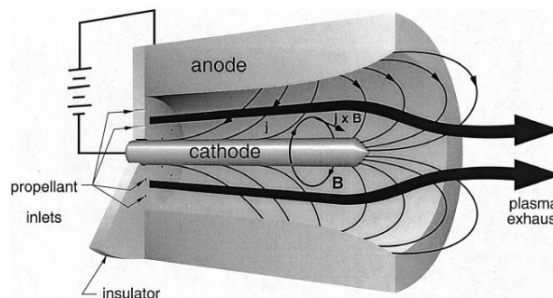


Figure 96: Image of the anatomy of a MPD thruster.

Note that an MPD is very similar to an arcjet, the main difference is the size of the current applied. MPDs feature much higher currents which produce a self field which is not true in arcjets. MPD thrusters generate thrust through the following mechanism:

- A very large current is applied between the anode and cathode ($10 - 100kA$).
- The applied voltage between the anode and cathode cause the propellant which is fed into the annular channel to break down into a plasma.
- The high plasma current generates a strong magnetic field, and the resulting Lorentz force ($F = J \times B$) electromagnetically accelerates the plasma along and out of the channel, producing thrust.

There exists two types of MPD, these are **self field** where the magnetic field is solely generated via the high current flow and **applied field** which generate a magnetic field using a solenoid magnet to create the magnetic field. A cross sectional image showing these two types is seen in **Figure 97**.

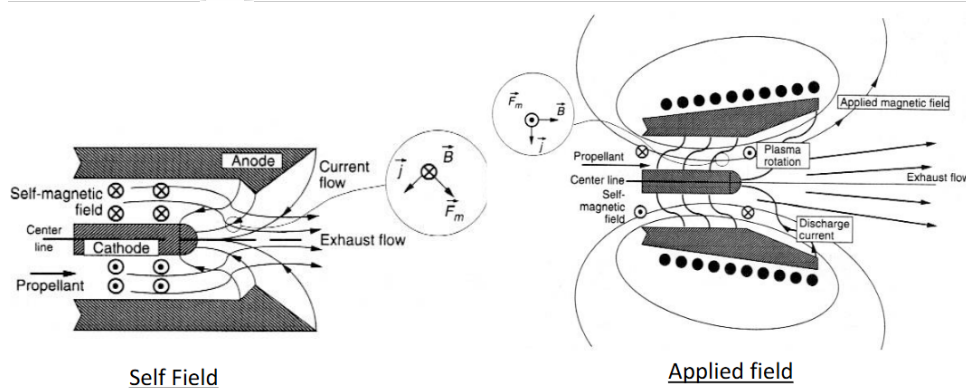


Figure 97: Image of a self field MPD vs an applied field MPD.

MPDs can achieve high efficiencies and high thrusts but require an incredibly high power draw. A comparison between MPDs ion thrusters and Hall effect thrusters is shown in **Table 15**.

Type,	Thrust Range (mN)	Isp Range (s)	Thruster Efficiency	Input Power Range (W)
MPD	0.001 - 20,000	2000 - 5000+	30 - 50	2000 - 100,000+
Ion Thruster	0.01 - 500	1500 - 8000	60 - 80	400 - 4300
Hall Thruster	0.01 - 2000	1500 - 2000	30 - 50	1000 - 4500

Table 15: MPD vs HET vs GIT performance.

MPDs do have some issues however, which limits their widespread use, these are:

- Require very high power inputs to achieve high thrust and efficiencies. Electrode erosion.
- Very large electrical components.
- Low efficiencies result in huge heat losses.
- ‘Onset’ phenomena where instabilities occur at higher currents.

16.8. Pulsed Plasma Thrusters

These are a simpler form of electromagnetic thruster in comparison to a HET or an MPD, an image of such a system is shown in **Figure 98**.

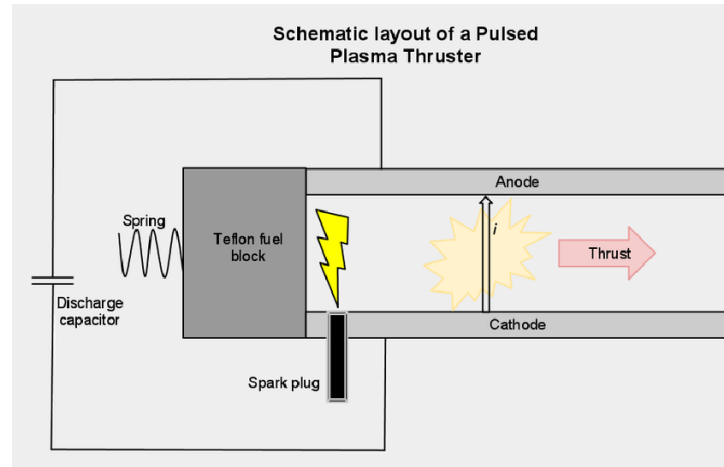


Figure 98: Schematic image of a PPT.

PPTs produce thrust through the following mechanism:

- The spark plug ablates a thin layer of the propellant block (Usually made of Teflon or PTFE).
- The partially ionized ablated propellant flows between the two channels where a large current is applied.
- The large current further ionizes the propellant as well as producing a strong self magnetic field.
- The ionized plasma is then accelerated through the channel through electromagnetic acceleration ($F = J \times B$).

Due to their simplicity and low voltage requirements, PPTs have very low thrusts and efficiencies. A comparison of PPT performance is shown in **Table 16**

Type,	Thrust Range (mN)	Isp Range (s)	Thruster Efficiency	Input Power Range (W)
Resistojet	200 - 300	200 - 350	65 - 90	50 - 500
PPT	0.05 - 10	600 - 2000	10	10 - 100
MPD thruster	0.001 - 20,000	2000 - 5000	30 - 50	2000 - 100,000

Table 16: PPT performance.

16.9. Into to Electrostatic Propulsion

START OF WEEK 9

Electrostatic thrusters accelerate electrons solely through an electric field, driven by a potential difference. The types of electrostatic thrusters covered in this section are:

- Gridded Ion Thrusters (GIT)
 - Radiofrequency Ion Thruster (RIT)
 - Microwave Ion Thruster
 - Electron Bombardment Ion Thruster (AKA Kaufman Ion Thruster)
- Electrospray / FEEP thruster

16.10. Radiofrequency Ion Thruster

In this type of ion thruster, the electrons are imparted energy via a radio frequency coil wrapped around the discharge chamber. A schematic diagram of such a thruster is shown in **Figure 99**.

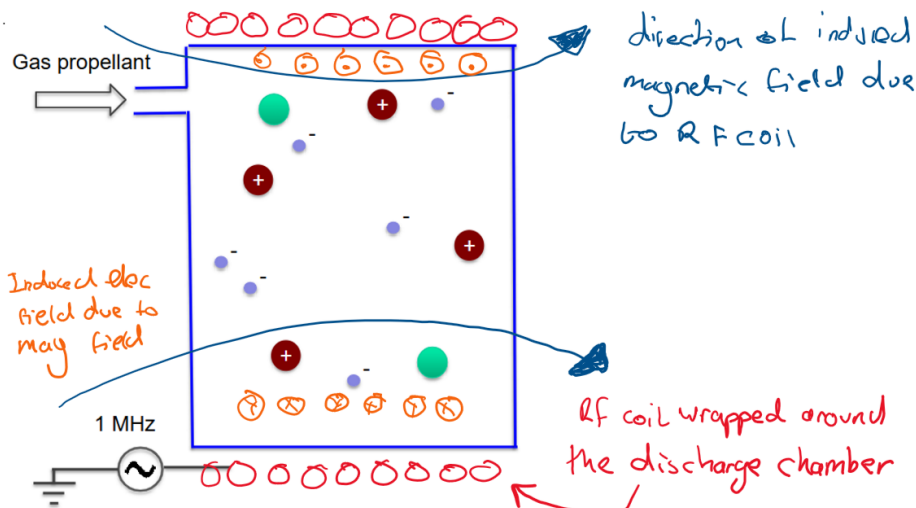


Figure 99: Schematic image of a RIT.

In a RIT a plasma is produced via the following mechanism:

- An alternating current in the RF coil (frequency $\approx 1 - 30$ MHz) induces an **axial time varying magnetic field** in the discharge chamber.
- Due to Faraday's law, this changing magnetic field induces an **azimuthal electric field** in the discharge chamber.
- This induced electric field acts on the electrons, causing them to oscillate azimuthally with collisions converting the oscillatory motion into thermal energy through ohmic heating.
- Hot electrons collide with neutrals ionizing them and increasing plasma density.
- When the RF polarity is reversed, the direction of the electron movement is reversed which means the net effect on the electrons is heating not drift.

An expression for the induced axial magnetic field can be derived and is shown in **Eq. 83**

$$B_Z = \frac{NI}{\mu_0} e^{i\omega t} \quad (83)$$

Where:

- B_Z : Strength of the axial magnetic field (T).
- N : Number of coils in the RF coil.
- I : The current flow through the RF coil (A).
- μ_0 : The permeability of the vacuum = $4\pi \times 10^{-7} H/m$
- t : Time (s)

Utilizing Faraday's law and rearranging the resulting expression, an equation for the azimuthal electric field can be derived, this is shown in **Eq. 84**.

$$\nabla \times \vec{E} = -\frac{\partial \vec{B}}{\partial t} \rightarrow E_\theta = -\frac{i\omega r}{2} B_{Z_0} e^{i\omega t} \quad (84)$$

Where r is the radius of the discharge chamber and B_{Z_0} is the initial axial magnetic field.

16.11. Microwave Ion Thrusters

Also known as electron cyclotron resonance ion thrusters, this type of thruster uses some of the same principles as a RIT but with the added benefit of cyclotron resonance. A schematic image of such a thruster is shown in **Figure 100**.

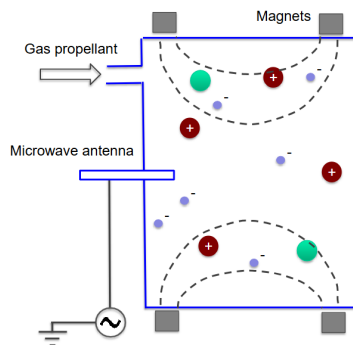


Figure 100: Schematic image of a Microwave Ion Thruster.

Microwave ion thrusters generate a plasma through the following mechanism:

- A microwave antenna injects microwaves (frequency $\approx 2.4 - 2.8$ GHz) into the discharge chamber.
- As microwaves are an EM wave, an alternating magnetic and electric field are introduced.
- The azimuthal electric field causing ohmic heating of the electrons in the same manner as a RIT just at a much higher frequency.
- Due to a static magnetic field which produces a B at a specific value corresponding to the Lamor radius, the electrons undergo Electron Cyclotron Resonance (ECR).
- ECR means that:
 - Electrons absorb energy very efficiently meaning low power plasma ignition.
 - Plasma production is much easier meaning high plasma density.
 - No internal electrodes needed.
 - Longer lifetime and excellent efficiencies.

16.12. Electron Bombardment Ion Thruster

This type of ion thruster utilizes a different mechanism to the RIT to generate a plasma. A schematic diagram showing an example of an electron bombardment ion thruster is shown in **Figure 101**.

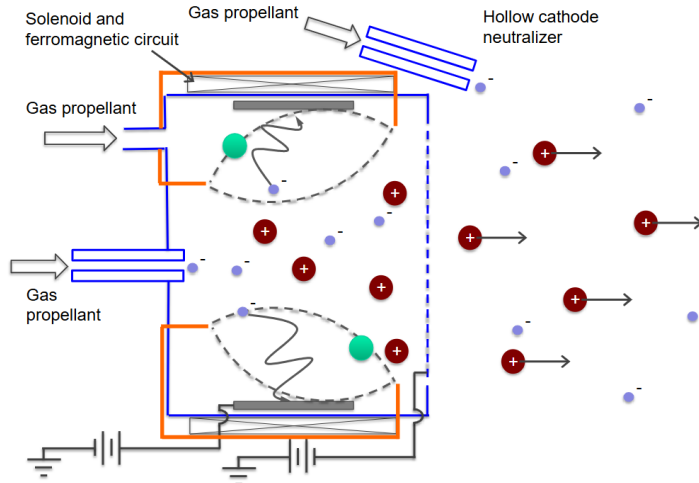


Figure 101: Schematic image of an electron bombardment ion thruster.

Electron bombardment ion thrusters generate a plasma utilizing the following mechanism:

- A hollow cathode (electron gun) uses a small amount of propellant to introduce hot electrons into the discharge chamber.
- These electrons then ionize neutrals forming a plasma.
- As the ions accelerate out of the discharge chamber there develops a build up of electrons, therefore an anode is required on the walls to remove electrons.
- As the electrons are very mobile they quickly get attracted to the anode and the potential is lost, to combat this a magnetic field is used to impeded the motion of the electrons as they approach the anode.

16.13. Ion Thruster Grids

All of the types of ion thrusters mentioned require grids to accelerate the ions within the plasma. Typically GITs consist of three grids, these are:

- **Screen Grid:** Has a very high positive potential ($\approx +1000V$). The plasma sits on the left side of the screen grid meaning that electrons are attracted to it forming a sheath ($width = \lambda_D$). This sheath occludes the effect of the high positive potential to the rest of the plasma.
- **Accelerator Grid:** This grid sits at a negative potential ($\approx -200V - -500V$) and accelerates the ions forward when they enter the region between the screen grid and the accelerator grid.
- **Decelerator Grid:** This grid sits at a neutral charge in order to repel or decelerate back-flowing positively charged plume ions which would have otherwise collided with the accelerator grid and eroded it.

17. Lecture 17

17.1. Ignition of Radiofrequency Ion thrusters

With electron bombardment it is easy to see that starting electron flow will cause the engine to ignite but with Radiofrequency Ion thrusters the process of ignition is not as clear.

By default, any gas will have some free electrons within it. The chance that the electrons will undergo a collision increases with the pressure that the gas is at. Therefore to ignite a Radiofrequency Ion thruster a **minimum pressure** must be achieved before there are enough electrons to sustain interactions. The probability that a given electron will collide with a neutral is given by **Eq. 85**.

$$Pr = 1 - e^{-\frac{x}{\lambda}} = 1 - e^{-n_0 \sigma x} \quad (85)$$

Where:

- **Pr**: The probability of an electron colliding with a neutral.
- **x**: Length of the interaction region near the wall (m).
- **λ** : Mean free path (m).
- **n_0** : The density of the neutrals (kg/m^3)
- **σ** : Neutral cross sectional area (m^2)

Note that the mean free path is the distance an electron travels before it interacts with a neutral and is equal to $\lambda = 1/n_0 \sigma$. An expression for the pressure can be extracted by rearranging this expression for density and then utilizing the ideal gas law, this is shown in **Eq. 86**.

$$Pr = 1 - e^{-n_0 \sigma x} \quad P = nkT \quad \rightarrow \quad P_{\min} = -\frac{kT}{\sigma x} \ln(1 - Pr) \quad (86)$$

Where n is the number of particles per unit volume, T is the temperature in kelvin and k is Boltzmann's constant. An example plot with $x = 5cm$ and Xenon as the propellant is shown in **Figure 102**.

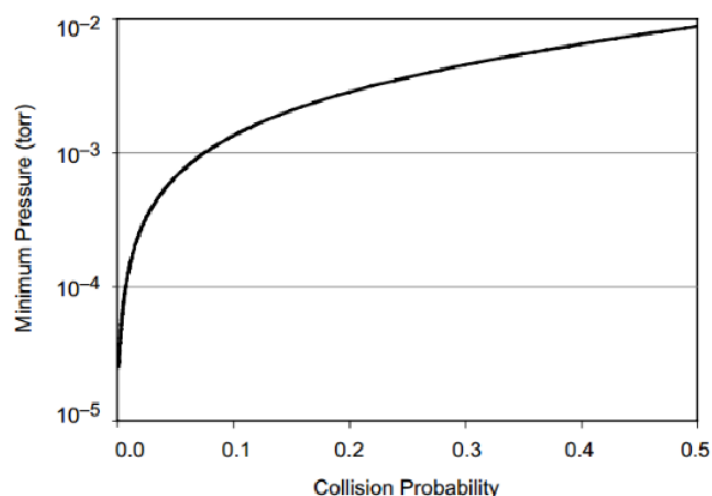


Figure 102: Plot of electron collision probability against pressure.

18. Lecture 18

18.1. Space Charge Limitations

The main limitation on GITs (aside from the low mass flow rate of ions) is the space charge limitation. This is explained below:

- As more and more positive ions flow through the screen grid, the gap between the screen grid and the accelerator grid starts to develop a positive charge
- When this reaches a maximum, the positive ions will occlude the effect of the accelerator grid.
- This chokes the thruster as new ions no longer see the voltage difference between the screen and accelerator grids.

To calculate the current density in a space charge limited scenario the Child-Langmuir Law can be used, shown in **Eq. 87**.

$$J_i = \frac{4\epsilon_0}{9} \left(\frac{2e}{M} \right)^{\frac{1}{2}} \frac{V^{\frac{3}{2}}}{d^2} \quad (87)$$

Where:

- J_i : The current density (A/m^2)
- ϵ_0 : Permittivity of free space = $8.85418782 \times 10^{-12} m^{-3} kg^{-1} s^4 A^2$
- e : Charge of an electron = $1.60217663 \times 10^{-19} C$
- M : Mass of an ion (kg)
- V : Voltage between the screen and the accelerator plate (V).
- d : Distance between the screen and the accelerator plate (m).

Note that the area referenced in J_i is roughly the area of one hole in the screen grid. The voltage distribution between grids for a free space limited case is shown in **Figure 103**.

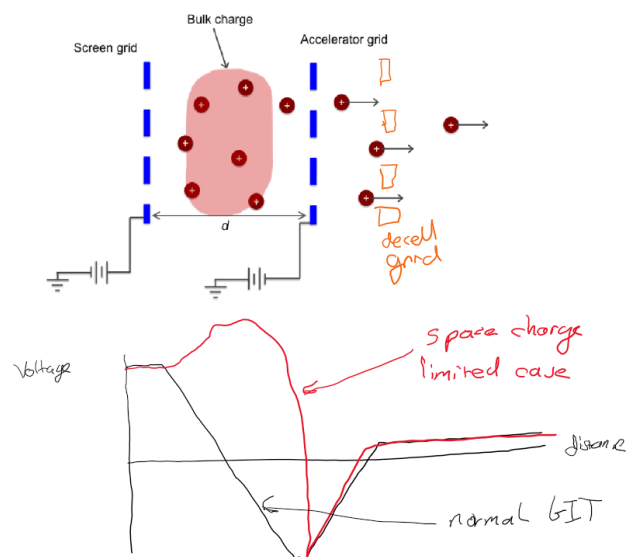


Figure 103: Plot of voltage over distance for space charge limited case.

18.2. Grid Erosion and Charge Exchange Ions

Ideally a GIT will ionize all of the neutral propellant atoms within the discharge chamber, however some neutrals will pass through into the grids as well as into the plume. When this happens a charge exchange ion (CEX ion) will be created, this process is detailed below:

- Neutral passes into the gap between screen and accelerator grid or into the plume.
- The neutral then collides with a fast moving positive ion.
- In the collision the neutral ion donates an electron to the positive ion neutralizing it and it itself becomes a low energy positive ion (CEX ion).
- As it has low energy and almost no momentum, it is immediately attracted to the negative accelerator plate where it hits and erodes it.

There are two types of erosion that occur due to CEX ions, this is **barrel erosion** and **pits and grooves erosion**. These two types of erosion are explained below as well as shown in **Figure 104**.

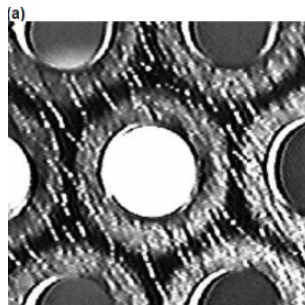


Fig. 5-22. NSTAR thruster accelerator grid at (a) 125 hours and (b) 30,352 hours.

Barrel erosion

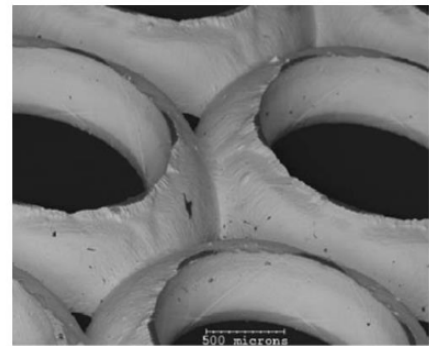
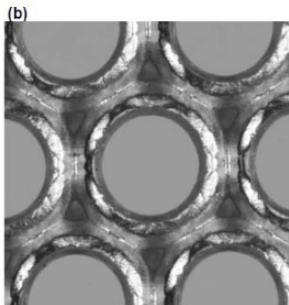


Fig. 5-23. SEM photograph shows that sputtering in the webbing between the holes had almost destroyed the structural integrity of the NSTAR grids.

Pits and grooves erosion

Figure 104: Image of barrel and pit and groove erosion.

- **Barrel Erosion:** Occurs when CEX are created between the screen and accelerator grids. CEXs collide with the inner orifice of the accelerator grid widening it overtime.
 - **Fix:** Ensure that the discharge chamber is ran at a pressure where all neutrals are eliminated.
- **Pit and Groove Erosion:** Occurs when CEX are created far beyond the engine in the plume. CEXs then collide with a high kinetic energy into the accelerator grid creating a complex erosion pattern.
 - **Fix:** Use a decelerator grid in order to ensure CEXs are not accelerated towards the accelerator plate.

18.3. Closing Remarks on GITs

Although they were the first EP method used in space their modern day use is diminishing as more missions and spacecraft opt for HETs. Their added mechanical and electrical complexity outweigh the I_{sp} gains on top of their thrust being half of that of a HET.

18.4. Heated Filament

Before hollow cathodes were used as an electron source, a heated filament was the go to option. It consists of an exposed wire which emits electrons through **thermionic emission**. The filament was typically made from thoriated tungsten which had a low work function and so could emit many electrons. The main issue with heated filaments were:

- Needed high temperatures ($\approx 2600K$) to release enough electrons.
- Filament would quickly erode through bombardment meaning the lifetime was very short.

18.5. Hollow Cathodes

Hollow cathodes are the go to option to create a stream of electrons. An image showing the anatomy of a hollow cathode is shown in **Figure 105**.

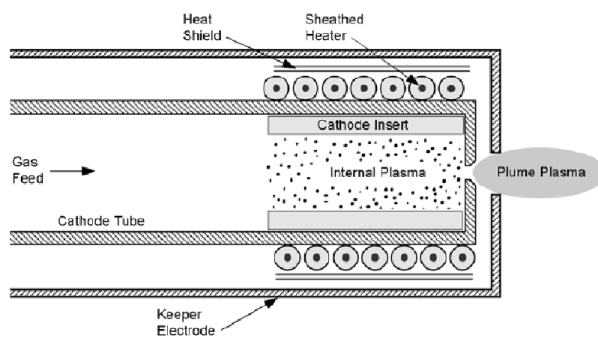


Figure 105: Schematic image of a hollow cathode.

A hollow cathode consist of:

- An **insert material** with a very low work function (tungsten, barium oxide, lanthanum hexaboride)
- A **hollow cathode tube** which is a cylindrical metal cavity with a small orifice at the end.
- A **resistive heater** that is wrapped around the cathode.
- A **keeper electrode**.
- A **gas feed** (typically 1-10% of total thruster flow).

To start up and use a hollow cathode the following is done:

1. Warm up the insert using the heater to initiate thermionic emission.
2. This can only release so many electrons as eventually negative charge density prevents further electron emission.
3. Start flowing gas over the hot insert which drives up the pressure in the cathode as the orifice is small.
4. The keeper electrode is positively charged which attracts electrons out of the hollow cathode.
5. Electrons collide with gas atoms forming a plasma. The plasma is quasineutral meaning no more occlusion on the surface of the insert and more electron emission.
6. Once a dense plasma forms the heater can be turned off as ion bombardment heats the insert sustaining emission.
7. Ions mostly remain within the plasma and electrons are still attracted out of the orifice (no longer due to positive keeper electrode but due to positive plume).

The number of electrons emitted via thermionic emission off of a surface is given by the Richardson-Dushman equation shown in **Eq. 88**.

$$J = AT^2 e^{\frac{-e\phi}{kT}} \quad (88)$$

Where:

- J : Beam current density (A/cm^2)
- A : Empirical constant $\approx 120 A/cm^2 K$
- T : Temperature K
- e : Elementary charge $= 1.60217663 \times 10^{-19} C$
- ϕ : Work function eV
- k : Boltzmann's constant $\approx 1.38 \times 10^{-23} J/K$

In reality the work function itself is effected by temperature, this relationship is given by the equation shown in **Eq. 89**.

$$\phi = \phi_0 + \alpha T \quad (89)$$

Where:

- ϕ : Temperature corrected work function eV
- ϕ_0 : Normal work function eV
- α : Experimental material constant eV/K
- T : Temperature K

Eq. 89 can be substituted into **Eq. 88** to yield a temperature corrected form of the Richardson-Dushman equation shown in **Eq. 90**

$$J = DT^2 e^{\frac{-e\phi_0}{kT}} \quad D = A e^{\frac{-e\alpha}{k}} \quad (90)$$

Where D is the material specific modification term to the Richardson-Dushman equation. Some common hollow cathode insert materials are shown in **Table 17** and a plot of their performance is shown in **Figure 106**.

Material	$D [A/cm^2 K]$	$\phi [eV]$
Barium oxide + tungsten matrix	1.5	1.56
Lanthanum hexaboride	29 - 110	2.8
Molybdenum	55	4.2
Tantalum	37	4.1
Tungsten	70	4.55

Table 17: PPT performance.

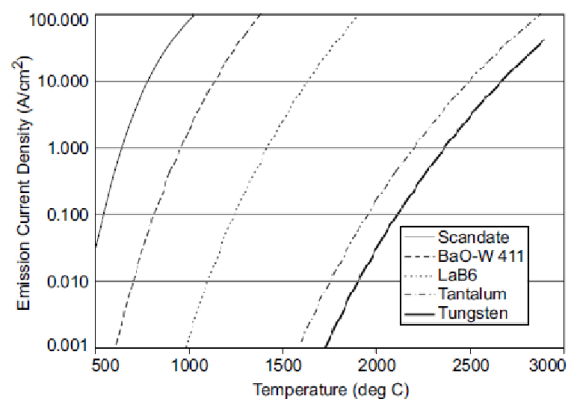


Figure 106: Work function vs temp for different hollow cathode insert materials.

Hollow cathodes do have some key drawbacks, these are mainly:

- They are difficult to initially start up.
- Insert is sensitive and can get contaminated.
- Insert can overheat.
- The tip of the keeper can erode due to constant bombardment.
- Difficult to scale down to smaller sizes.

18.6. Alternative Electron Sources

One alternative for very small thrusters is a **field emission cathode**. This method emits electrons from a solid surface via quantum tunneling driven by an extremely strong electric field at a sharp emitter tip (tip material can be carbon nanotubes).

Another option that has been tested is by using a small gridded ion thruster which has an inverted polarity so that electrons are removed not ions and this stream is directed into the plume.

19. Lecture 19

19.1. FEEP and Electrospray Thrusters

Field emission electric propulsion (FEEP) and electrospray thrusters differ from GITs as they do not need a discharge chamber and do not fundamentally create a plasma. A schematic image of this type of thruster is shown in **Figure 107**.

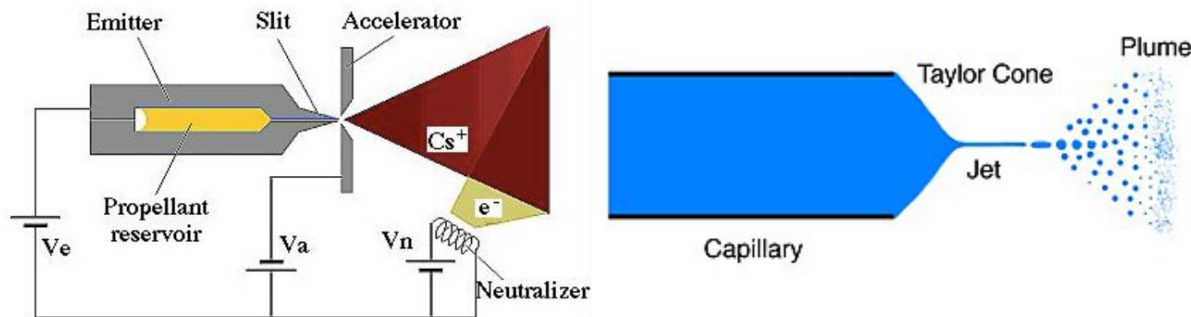


Figure 107: Schematic diagram of a FEEP or electrospray type thruster.

Figure 108: Diagram of the formation of a Taylor cone.

FEEP and electrospray thrusters use the following principles to generate thrust:

- A liquid metal (FEEP) or ionic liquid (electrospray) is held in a reservoir and fed into a needle where capillary action (surface tension) hold it in place.
- A strong electric field is induced via an accelerator/extractor forming a Taylor cone which the surface binding energy.
- For a FEEP thruster:
 - Individual ions are then directly pulled from the liquid metal Taylor cone forming a jet which eventually expands into a plume.
- For an electrospray thruster:
 - Either ions, charged droplets, or a mixture of both are pulled from the Taylor cone, forming a jet which eventually expands into a plume.
- Either way the positive plume must be neutralized, often achieved through a heated filament.

FEEP thrusters use liquid metals such as Indium, Caesium, Rubidium, Gallium as their propellents. Electrospray thrusters use ionic liquids such as 1-ethyl, 3-methylimidazolium tetrafluoroborate (EMIB₄).

19.1.1. Electrospray Thrusters

Electrospray thrusters do have some benefit over FEEP thrusters. Conceptually a neutralizer may not be needed as the polarity of the extractor grid can be reversed pulling out either the positive or negative ion. Furthermore the ionic liquids are safer to use than the liquid metals. There are three forms of electrospray thrusters shown in **Figure 109**. These three types are:

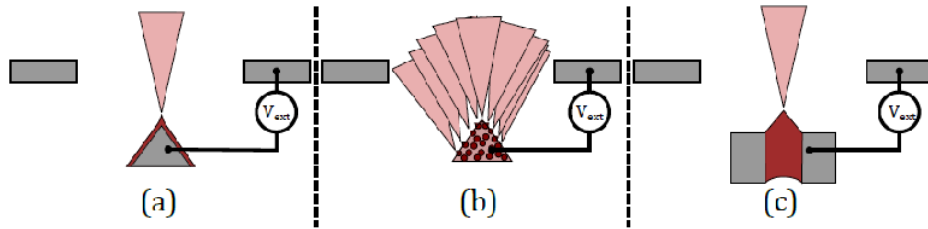


Figure 109: Different types of electrospray thrusters.

- [a] **Externally Wetted**: Liquid flows over a cone .
- [b] **Porous**: A porous material is used for the nozzle and shaped into a cone, forming multiple Taylor cones.
- [c] **Capillary**: A needle head where a Taylor cone can form off.

19.2. FEEP and Electrospray Onset Voltage

To find the minimum voltage that ions or droplets can be pulled out of the Taylor cone an equation is needed. This derivation starts from considering the surface tension and the electrostatic force, both of these expressions are shown in **Eq. 91**.

$$P_E = \frac{\epsilon_0}{2} E_n^2 \quad P_{ST} = \gamma \left(\frac{1}{R_1} + \frac{1}{R_2} \right) \quad (91)$$

Where:

- **P_E** : Electrostatic Pressure (Pa).
- ϵ_0 : Permittivity of free space = $8.85418782 \times 10^{-12} m^{-3} kg^{-1} s^4 A^2$.
- E_n : Electric field strength normal to the cone (N/C).
- **P_{ST}** : Surface pressure (Pa).
- γ : Surface tension (N/m).
- R_1 : 1st radii of curvature (m).
- R_2 : 2nd radii of curvature (m).

These two equations can be equated to one another and the resulting equation can be simplified using the geometry of the Taylor cone ($R_2 \gg R_1$ and α = cone half angle), yielding **Eq. 92**.

$$E_n = \sqrt{\frac{2\gamma}{\epsilon_0 r \tan(\alpha)}} \quad (92)$$

Where:

- α : Cone half angle = 49°
- r : Distance from cone tip (m)

Another equation can be derived for the electric field strength given the geometry of the cone in a parallel plate capacitor, this yields **Eq. 93**.

$$E_T = \frac{2\phi}{r_e \ln\left(\frac{4Z_0}{r_e}\right)} \quad (93)$$

Where:

- E_T : Electric field strength (N/C).
- ϕ : Electric potential (V)
- r_e : Radius of needle end (m)
- Z_0 : Distance between cone end and accelerator plate (m)

Both **Eq. 93** and **Eq. 92** can be substituted into one another yielding **Eq. 94**.

$$V_{on} = \left[\frac{2\gamma r_e \cos(\alpha)}{\epsilon_0} \right]^{\frac{1}{2}} \ln\left(\frac{4Z_0}{r_e} \right) \quad (94)$$

Some different onset voltages for different propellant materials are shown in **Table 18** ($r_e = 0.25\text{mm}$, $Z_0 = 0.5\text{mm}$).

Type	Propellant	γ [mN/m]	V_{on} [V]
FEEP	Caesium	71	3363
FEEP	Indium	556	9411
Electrospray	Ionic liquid	40	2524

Table 18: Onset voltages for different fuel types.

19.3. FEEP and Electrospray Performance, Uses and Drawbacks

FEEP and electrospray thrusters provide very low amounts of thrust but can provide that thrust incredibly accurately and at very high efficiencies. The performance of FEEP and electrospray thrusters is detailed in **Table 19**.

Type	Thrust range [mN]	I_{sp} [s]	Applied Voltage [V]	Efficiency	P_{in} [W]
FEEP	0.001 - 0.4	6000 - 12,000	$\approx 10,000$	50 - 90	< 30
Electrospray	0.001 - 0.2	150 (droplets) 3000 (ions)	≈ 3000	10 - 90	< 30

Table 19: Onset voltages for different fuel types.

Due to their small thrust they are not well suited for large missions, but have found their niche for precise attitude control and Cubesat propulsion. The main issue with these type of thrusters is their lifetime performance, specifically the constant bombardment that the accelerator sees.

